Strategies for Understanding and Treating Osteoarthritis

A thesis

submitted by

Averi Gibson

In partial fulfillment of the requirements
for the degree of

Doctor of Philosophy

in

Cell, Molecular and Developmental Biology

TUFTS UNIVERSITY

Sackler School of Graduate Biomedical Sciences

May 2016

Advisor:
Dr. Li Zeng

Abstract

Osteoarthritis (OA) is a disease characterized by articular cartilage degeneration. It causes chronic, debilitating pain, and as it is associated with aging and obesity, it is a continually expanding issue. Under OA conditions, mechanical stress and an increase in inflammatory cytokines such as IL-1β cause a disruption in joint homeostasis. As a result, metabolic and structural changes occur in multiple joint tissues, including the induction of catabolic enzymes that degrade articular cartilage matrix (such as MMPs) and the formation of ectopic bone spurs. Ultimately these changes lead to progressive and irreversible joint degeneration. However, current therapies are mostly focused on pain relief, rather than slowing down joint destruction. This thesis presents two independent but inter-related projects that aim to identify and facilitate the investigation of novel disease-modifying therapeutic targets for OA.

A major hurdle in OA research is the lack of sensitive detection and monitoring methods, which hampers the evaluation of potential therapeutics. The aim of my first study was to investigate if metabolic imaging of the joint using a near infrared fluorescence (NIRF) probe activated by MMPs (MMPSense680) could visualize *in vivo* OA progression. Using MMPSense680, I assessed the IL-1β induced upregulation of MMP activity in human chondrocytes *in vitro*. MMP activity was then evaluated *in vivo* in the destabilization of the medial meniscus (DMM) OA mouse model. The *in vitro* studies confirmed that NIRF imaging could identify enhanced MMP activity in IL-1β-treated human chondrocytes. *In vivo* imaging showed significantly higher fluorescence in OA knees compared to sham (control) knees of the same mice and the emitted fluorescence

intensity steadily increased over the entire course of OA examined. Therefore, imaging of MMP activity *in vivo* provided sensitive and consistent visualization of OA progression, beginning from early time points post OA inducing surgery.

The aim of my second study was to examine Wnt7a as a potential disease-modifying reagent for OA development, as Wnt signaling has been implicated in OA pathogenesis, but with unclear and controversial results. I first examined Wnt7a gene expression in cartilage samples from healthy subjects and OA patients. The effect of lentiviral Wnt7a ectopic expression was then investigated *in vitro* using human articular chondrocytes under pro-inflammatory cytokine IL-1β treatment and *in vivo* using the DMM OA mouse model. Wnt7a mRNA expression was reduced in human OA cartilage and displayed an inverse correlation with MMP and IL-1β expression. *In vitro*, lentiviral Wnt7a ectopic expression inhibited IL-1β-induced gene expression in human chondrocytes. *In vivo*, lentiviral Wnt7a strongly attenuated articular cartilage damage and chondrocyte cell loss induced by DMM surgery. In addition, joint Wnt7a ectopic expression inhibited the progressive upregulation of NIRF MMPSense680 signals in the DMM animals. I also found that Wnt7a induced mediators of multiple Wnt pathways in chondrocytes. An NFAT inhibitor impaired Wnt7a's activity in inhibiting MMPs, and blockage of Wnt canonical signaling with NFAT inhibition further increased IL-1β-induced MMP expression. These results indicate that Wnt7a signaling inhibits inflammatory-induced catabolic gene expression in human chondrocytes and requires NFAT for this activity. In experimental OA, Wnt7a is sufficient to attenuate MMP activities in the joint and promote joint cartilage integrity.

Acknowledgements

Foremost, I would like to thank my thesis advisor, Dr. Li Zeng, for her support and guidance. With much enthusiasm and patience, she has constantly pushed me to grow in all aspects of my training. She has been an incredible role model and mentor over the last four years and I am truly fortunate to have studied with her.

I also want to thank many past and present members of the Zeng lab, namely Andrea Foote, Roshni Rainbow, Heenam Kwon, Tomoya Uchimura, Daisy Nakamura and Carrie Hui Mingalone, for their camaraderie and unending willingness to answer all of my many questions. I am honored to have had the opportunity to work and grow with all of you.

Many additional thanks to my thesis committee members, Dr. James Schwob, Dr. Pamela Yelick, and Dr. Alexander Poltorak and my outside examiner Dr. Vicki Rosen, for their expertise, encouragement, and helpful critiques. I truly appreciate the time you have invested to help me develop and refine these projects, as well as my skills as a researcher.

I would also like to acknowledge the Tufts CMDB, MSTP, and Sackler faculty and students. All of you have been an exceptional resource and support system over these many years. I'd like to extend a particular thank you to Dr. Albert Tai for all of his help with my microarray and Dr. Gary Sahagian and Dr. Min Fang at the Tufts Small Animal Imaging Facility for their help with my NIRF and micro-CT imaging.

Finally, but by no means least, thank you to my wonderful husband and family for being so supportive and understanding over these many years. I couldn't have done this without you. This thesis is dedicated to you.

Table of Contents Page

List of Tables

List of Figures

List of Abbreviations

ACL: Anterior cruciate ligament
ACS: Articular cartilage structure
ANOVA: Analysis of variance
AP-1: Activator protein 1
APC: Adenomatous polyposis coli
BMI: Body mass index
BSA: Bovine serum albumin
BV: Bone volume
CamKII: Calmodulin kinase II
CK1: Casein kinase 1
DMM: Destabilization of the medial meniscus
DKK-1: Dickkopf-related protein 1
Dvl: Disheveled
ECM: Extracellular matrix
FZD: Frizzled
GDF5: Growth/differentiation factor 5
GSK3: Glycogen synthase kinase 3
GWAS: Genome-wide association study
hMSCs: Human mesenchymal stem cells
IF: Immunofluorescence
IHC: Immunohistochemistry
IL-1β: Interleukin-1 beta
iNOS: Inducible nitric oxide synthase
IPA: Ingenuity pathway analysis
JNK: c-Jun N-terminal kinase
LRP: Low-density lipoprotein receptor-related protein
MAPK: Mitogen-activated protein kinase
MCP1: Monocyte chemotactic protein 1
MEK: MAPK kinase of the extracellular signal-related kinase
Micro-CT: Micro-computed tomography
MIG: Monocline induced by gamma interferon
MMP: Matrix metalloproteinase
MMTL: Medial meniscotibial ligament
MRI: Magnetic resonance imaging
NFAT: Nuclear factor of activated T-cells
NF-κB: Nuclear factor kappa-light-chain-enhancer of activated B cells
nHACs: Normal human articular chondrocytes
NIRF: Near infrared fluorescence
OA: Osteoarthritis
PI3K: Phosphatidylinositol 3-kinase
PKC: Protein kinase C
PMM: Partial medial meniscectomy
qPCR: Real-time polymerase chain reaction
RLU: Relative luciferase units

ROI: Region of interest
SEM: Standard error of the mean
SDS-PAGE: Sodium dodecyl sulfate polyacrylamide gel electrophoresis
sFRP3: Secreted frizzled-related protein 3
SNP: Single-nucleotide polymorphism
TBP: TATA binding protein
Tcf/Lef: T-cell factor/lymphoid enhancer factor
TGF-β: Transforming growth factor-β
TIMPs: Tissue inhibitors of metalloproteinases
TMJ: Temporal mandibular joint
TV: Tissue volume
UTR: Untranslated region

Copyrighted Material Permission

JOHN WILEY AND SONS LICENSE
TERMS AND CONDITIONS

This Agreement between Averi Gibson ("You") and John Wiley and Sons ("John Wiley and Sons") consists of your license details and the terms and conditions provided by John Wiley and Sons and Copyright Clearance Center.

License Number	3832130449731
License date	March 18, 2016
Licensed Content Publisher	John Wiley and Sons
Licensed Content Publication	Arthritis & Rheumatology
Licensed Content Title	Analysis of the Trajectory of Osteoarthritis Development in a Mouse Model by Serial Near-Infrared Fluorescence Imaging of Matrix Metalloproteinase Activities
Licensed Content Author	Averi A. Leahy, Shadi A. Esfahani, Andrea T. Foote, Carrie K. Hui, Roshni S. Rainbow, Daisy S. Nakamura, Brian H. Tracey, Umar Mahmood, Li Zeng
Licensed Content Date	Jan 28, 2015
Pages	12
Type of use	Dissertation/Thesis
Requestor type	Author of this Wiley article
Format	Print and electronic
Portion	Full article
Will you be translating?	No
Title of your thesis /dissertation	Strategies for Understanding Osteoarthritis
Expected completion date	May 2016
Expected size (number of pages)	125

Chapter 1: Introduction

Section 1.1 Introduction to Articular Cartilage

Articular cartilage is a unique connective tissue that lines joint surfaces. It functions as a shock absorber and friction minimizer to protect the underlying bone during movement. It is made up of individual chondrocyte cells that are surrounded by a widespread extracellular matrix (ECM). This ECM is made up of collagen II, proteoglycans, and water [1]. Collagen II provides tensile strength to the ECM by creating a tightly knit fibrous network within the tissue. The proteoglycans, the most plentiful of which is aggrecan, are highly constrained within this collagen II framework. As proteoglycans are negatively charged, forcing them in such close proximity to one another creates electrostatic repulsion, thus conferring compressive stiffness to the cartilage tissue [2]. This ECM is so pivotal to the function of cartilage that it comprises 95% of the cartilage volume; chondrocytes themselves only account for the remaining 5% [3]. Cartilage is also avascular, aneural, and alymphatic, making it very vulnerable to injury [1].

Chondrocytes regulate the ECM by secreting both catabolic factors and ECM components. However, the ECM components and the catabolic factors are secreted at very low rates, as the turnover rate for collagen II in articular cartilage is estimated to be 117 years [4] and 3-25 years for aggrecan subfractions [5]. Any process that skews this delicate balance towards an increase in catabolic enzymes production would lead to cartilage ECM degradation and thus cartilage tissue loss. Due to the slow release of ECM

proteins and cartilage's avascular, aneural, and alymphatic nature, cartilage has very limited intrinsic regenerative capabilities.

Section 1.2 Osteoarthritis

1.2.1 Introduction to Osteoarthritis

Osteoarthritis (OA) is the most common joint disease. OA is characterized by gradual destruction of joint articular cartilage, which ultimately results in chronic joint pain, stiffness, and instability. OA is a heterogeneous disorder that is associated with a variety of risk factors that can lead to disease. The strongest risk factor for OA development is aging. Other risk factors include female sex, obesity, joint injury, malalignment of the joint, and family history [6].

OA is a large and expanding problem. In the United States, OA was estimated to affect 26.9 million adults in 2005 [7]. With our aging population, this number is only growing. OA is also a global problem, as worldwide knee OA had an estimated worldwide prevalence of 3.8% in 2010 [8]. That equates to approximately 261.5 million people. This comes at a cost, both socially and economically. Knee OA is one of the top 5 leading causes of impaired mobility and long-term disability in non-institutionalized adults in the United States due to the chronic pain associated with the disease [9]. Despite OA's continued burden, treatment options focus primarily on pain relief and symptom

management. Currently, there is no treatment available to actually slow disease progression.

1.2.2 Risk Factors for Osteoarthritis Development

OA is often considered a classic disease of the elderly. That is because OA is rare in adults under 45 years old, but is common in those over 65 years old. Calculated prevalence varies between studies, but it is estimated that by the age of 65, up to 50% of adults in the United States will show signs of OA [6, 7]. In addition, women are generally at a greater risk for OA development, although this occurs in a joint-dependent manner. Specifically, women show significantly higher rates of knee and hip OA compared to men. Women also tend to have more severe knee OA, especially after menopause [10].

Another well documented risk factor for OA development is obesity. A variety of studies have shown that a higher body mass index (BMI) correlates with an increased risk for OA development [11-13]. A study examining the trend in correlation between different BMI levels and knee OA development even demonstrated that the risk for knee OA development increases almost exponentially as BMI increases [13]. Obesity was traditionally believed to contribute to OA development solely through an increase in mechanical joint loading. Recently, increasing evidence suggests that the adipokines produced by adipose tissue may also play a role in OA pathogenesis [14].

Traumatic joint injury is also associated with an increased risk for OA development. For example, one report demonstrated that knee injury during adolescence increased the risk for knee OA development later in life [15]. In this study, the reported knee injuries included ligament tears, meniscal tears, bone fractures and other traumatic events. Another study also demonstrated specifically that anterior cruciate ligament (ACL) tears are associated with an increased risk for early OA development, even if the ACL is surgically repaired [16]. It is believed that traumatic joint injuries lead to OA development by long-term alteration of joint mechanics and articular cartilage loading. Impact to the articular cartilage during the traumatic injury can also cause direct damage to the tissue, leading to chondrocyte cell death and structural damage [17].

Joint malalignment caused by anatomic abnormalities can also cause alterations to joint mechanics and increase the risk for OA damage to the joint. An example of this can be seen with varus and valgus knee deformities, which result in improper angulation of the knee joint and bowing of the legs. Varus knee deformities cause inward angulation of the knee joint, leading to increased stress in the medial portion of the knee and decreased stress in the lateral portion. Accordingly, varus knee deformities increase the risk for OA development in the medial portion of the knee, where increased stress is being applied to the joint, and actually decrease risk in the lateral portion. On the other hand, valgus knee deformities cause outward angulation of the knee joint, leading to increased stress in the lateral portion of the knee and decreased stress in the medial portion. Interestingly, it has been shown that valgus knee deformities do not increase the risk for OA development, but do increase the risk for progression of already present OA in the lateral compartment

of the knee while decreasing the risk for OA progression in the medial compartment [18]. Additionally, anatomic abnormalities in other joints can also predispose patients to OA development. For example, anatomic abnormalities of the hip that cause hip malalignment, such as congenital hip dysplasia and Legg-Perthes disease, are associated with an increased risk for later OA development in the hip and the knee [19, 20].

Genetic risk factors are also important in the development of OA. In fact, heritability studies using twins and other family-based methods have estimated genetic factors to account for approximately 40-70% of the risk for developing OA, depending on the joint site [21]. As OA is a very complex disease, it is believed that the genetic architecture of OA involves multiple variants of varying effect sizes. There are specific genetic abnormalities that have been identified that result in a large increased risk for familial OA. For example, dominant inheritance of severe, early OA in one family was mapped to an inherited mutation in the collagen II gene [22]. However, single mutations that result in severe, familial OA are relatively rare.

Recently, extensive efforts using candidate gene studies and large-scale genome-wide association studies (GWASes) have been performed in hopes of identifying more common genetic loci associated with OA development. Currently, these studies have identified 18 OA-associated genetic variants [23-31]. Most of these loci are common single-nucleotide polymorphisms (SNPs) whose calculated odds ratios are relatively low (~ 1.1 to 1.3), suggesting that their singular effect on OA development is small. Currently, the best replicated genetic variant associated with OA development is the rs143383

polymorphism of growth/differentiation factor 5 (GDF5). GDF5 is a member of the transforming growth factor-β (TGF-β) family that affects chondrogenesis and joint formation during development [32]. The rs143383 SNP is in the 5'-untranslated region (UTR) of GDF5 and results in decreased GDF5 expression in chondrogenic cells [33]. Originally, rs143383 was shown to increase the risk for hip OA development in a Japanese population with a relatively high odds ratio (1.79) compared to that of other established OA-associated loci [33]. This locus was then shown to also be associated with an increased risk for knee OA development in both Asian and European populations [23].

Interestingly, many of the genetic variants identified to be associated with OA development have varying effects depending on ethnicity, sex, and the joint involved. This suggests that OA pathogenesis is not uniform across populations and that there may be joint-specific risk factors for disease development. Additionally, most of the identified loci map to genes that have not been previously linked to musculoskeletal biology [34]. Thus this information may help to identify new factors or processes involved in OA pathogenesis. It is estimated that the currently identified OA-associated genetic variants only account for approximately 11% of OA heritability [35], demonstrating that this area of study is just beginning and that there are still many more OA-associated loci that have yet to be identified.

1.2.3 The Pathogenesis of Osteoarthritis

The pathogenesis behind OA is still being elucidated. It has been shown that wear and tear of cartilage plays a critical role in OA development. This can be seen in OA's association with aging and risk factors which alter joint mechanics, such as ligament tears [3]. Inflammation also plays a key role. Inflammatory cells are present in the joint during OA, although in smaller numbers than in rheumatoid arthritis [1]. These inflammatory cells do not directly damage the cartilage, but release cytokines such as interleukin-1 beta (IL-1β) which alter the metabolism of articular cartilage chondrocytes [36].

OA involves a metabolic shift in chondrocytes towards catabolism. This metabolic shift results in a reduction of anabolic activity and a corresponding induction in catabolic enzymes such as matrix metalloproteinase (MMPs) that degrade the cartilage ECM. Specifically, MMP13 is the main degrader of collagen II in articular cartilage. This shift towards catabolism increases the rate of ECM degradation, leading to the loss of articular cartilage tissue over time [2]. Additional studies have shown that OA can also involve an increase in chondrocyte hypertrophy, which results in a decrease in the production of the normal cartilage ECM component collagen II and an increase in the production of collagen I and collagen X [36, 37]. Furthermore, chondrocyte cell death is also induced by OA. Currently, the exact mechanisms involved in these chondrocyte changes and the signaling pathways that govern them are not well understood.

Ultimately, OA development results in articular cartilage destruction. This tissue damage begins as patchy, localized areas of ECM loss and chondrocyte cell death. Sporadic areas of cartilage damage can increase focal stress on the cartilage during movement, thus further altering joint mechanics [38]. Several ECM breakdown products produced by articular cartilage damage have also been shown to induce inflammatory cytokine production on their own [39-41]. Thus, localized articular cartilage damage can induce further articular cartilage destruction through an increase in altered joint mechanics and inflammation, creating a self-perpetuating cycle of articular cartilage loss (Fig. 1.1).

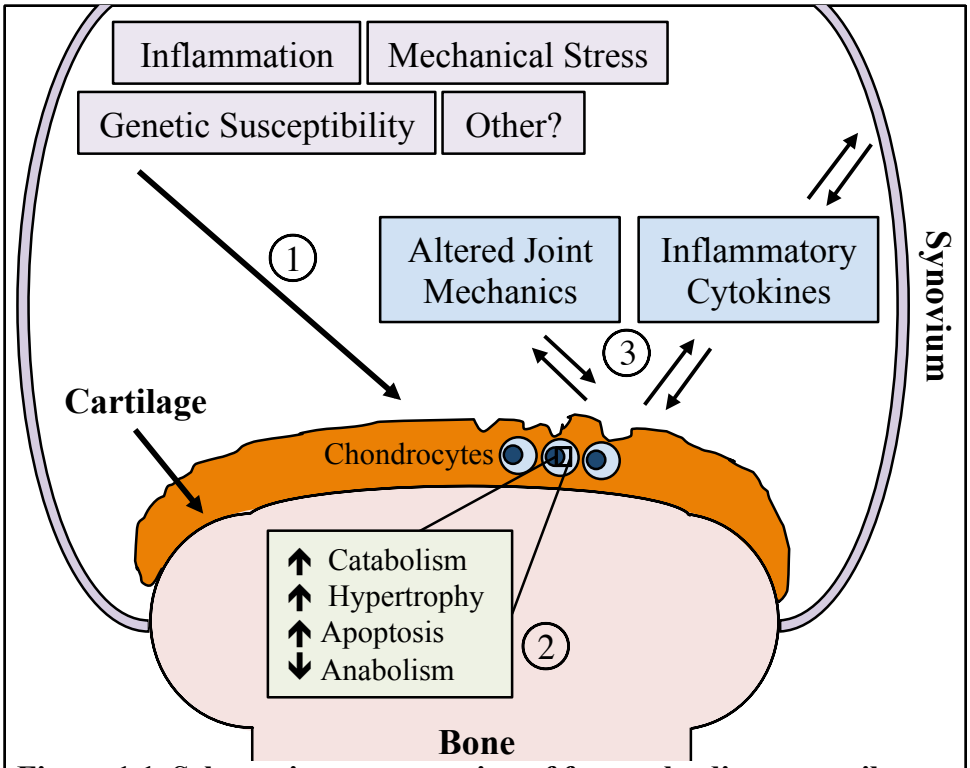

Figure 1.1. Schematic representation of factors leading to cartilage destruction in OA. OA pathogenesis is a complicated, multifaceted process. Many factors can contribute to OA development and cartilage destruction, including mechanical stress, genetic susceptibility, and inflammation (1). These stimuli ultimately lead to a shift in chondrocyte metabolism towards catabolism of the ECM, as well as an increase in chondrocyte hypertrophic differentiation and chondrocyte apoptosis (2). As OA develops, altered joint mechanics and inflammatory cytokines produced in the synovium and the cartilage further stimulate these catabolic processes and accelerate joint destruction (3).

1.2.4 Osteoarthritis as a Whole Joint Disease

While OA is characterized by the loss of articular cartilage in the joint, it has become increasingly recognized that other joint tissues are also altered by OA and may play a role in disease development [42]. For example, it has been well established that patients with OA often develop bone spurs called osteophytes along the margin of their affected joint. This is the result of ectopic bone formation at the interface between the joint cartilage and the underlying bone. Sclerosis of the subchondral bone is also commonly seen with OA [2]. These joint changes are also replicated in mouse models of the disease [43]. Additionally, it has been shown that manipulations of a specific joint tissue in OA can impact the disease's effects on other joint tissues. For instance, several studies have demonstrated that alterations to gene expression specifically in the subchondral bone can affect the rate of cartilage tissue degradation in mouse *in vivo* surgical OA models [44, 45]. Accordingly, the importance of monitoring disease progression in multiple joint tissues has been recognized.

1.2.5 Clinical Care of Osteoarthritis

Currently, treatment options for OA center on symptom management. The mainstay of treatment is the use of NSAIDs, which reduce inflammation and pain. Physical therapy has also been shown to reduce pain and increase physical function in patients [46]. However, physical therapy and NSAID treatment are only efficacious up to a point; end stage treatment for the disease is total knee placement surgery [2]. Since the pathogenesis

of OA is still being understood, there are no pharmacologic options currently clinically available that can slow disease progression. Preventative efforts for patients almost certain to develop OA, such as those with ligament tears, also do not exist.

As more details of OA pathogenesis are uncovered, new potential drug targets for clinical trials have been identified. For example, inhibition of IL-1 looked very promising as a possible therapeutic strategy, as several pre-clinical studies demonstrated that inhibition of IL-1 prevented experimentally induced OA cartilage degeneration *in vivo* [47-49]. This was also an attractive strategy because anti-IL-1 clinical treatments were already FDA approved for use in patients with other diseases, such as rheumatoid arthritis. However, multiple randomized control studies in OA patients concluded that anti-IL-1 treatment did not result in any significant clinical benefit to the patients, even after several months of treatment [50, 51]. At this time, multiple clinical trials targeting other cytokines or using growth factors in OA patients have also reported negative results [52]. This has been disappointing and underscores the need for a much better understanding of the mechanistic complexities of this disease.

1.2.6 Identifying Novel Treatment Options for Osteoarthritis

There is still much to learn about OA pathogenesis. This thesis presents two independent but inter-related projects that aim to address important areas of knowledge that are still lacking in our current understanding of OA. My first project focuses on using metabolic imaging of the joint to track OA progression over time. My second project investigates

Wnt7a as a potential disease-modifying reagent for OA development. The Wnt project also includes experiments that use the metabolic imaging technique validated in my first project, confirming the utility of this system. The goal of these projects is to advance our current understanding of the control of cartilage homeostasis under pathological conditions and to facilitate the identification of new potential therapeutic strategies for OA treatment.

Section 1.3 Metabolic Imaging of Osteoarthritis

1.3.1 Current Options for Imaging Osteoarthritis

A major hurdle in developing treatment options for OA is the lack of optimal detection and monitoring methods, especially for early disease time points [53, 54]. Imaging is commonly used to diagnose and monitor OA; however, none of the imaging options currently available are ideal for early detection or sensitive monitoring. For example, radiographs are the most commonly used imaging modality for clinical detection of OA. However, articular cartilage cannot be directly visualized on a radiograph. Instead, joint space narrowing is used as a marker for articular cartilage loss and OA damage [55]. In fact, joint space narrowing is considered reliable enough to serve as the only structural endpoint approved by the FDA to evaluate the efficacy of OA therapeutics [56]. However, joint space narrowing is neither sensitive nor specific for OA articular cartilage damage because without direct visualization of the articular cartilage surface, it cannot be proven that any observed joint space narrowing is due specifically to articular cartilage loss. In

fact, it has been shown that both meniscal position and meniscal degeneration account for a large proportion of joint space narrowing observed on radiographs [57].

Arthroscopy, magnetic resonance imaging (MRI), and ultrasonography are imaging modalities that are able to visualize articular cartilage and identify surface defects. However, all of these modalities rely on the identification of morphological joint changes. By the time these defects are visible, the OA disease process is already in its late stages [58]. As early diagnosis may help to ensure earlier intervention and potentially better clinical outcomes, there is a strong need to develop imaging modalities for early OA detection and sensitive monitoring of disease progression. This would also highly benefit preclinical identification and testing of possible therapeutic strategies, as tracking OA progression *in vivo* currently relies almost exclusively on histological examination of the joint. This makes it difficult to detect small changes over time and requires sacrificing the animals. A more sensitive method to monitor OA progression *in vivo* from its beginning stages that did not require animal sacrifice would help us to more efficiently assess the efficacy of different treatment options in preclinical testing [59].

Early OA detection and sensitive monitoring of disease progression may be better accomplished by moving away from imaging modalities that only analyze morphological joint changes, and instead exploring modalities that can detect other changes that occur in the joint tissues during OA. As a defined metabolic shift towards matrix catabolism occurs early in OA [58], one promising alternative would be to develop a real-time report of the metabolic status of the joint.

1.3.2 Matrix Metalloproteinases (MMPs) in Osteoarthritis

One key feature of joint destruction in OA is the induction of MMPs that cleave cartilage matrix proteins [60, 61]. However, the exact pattern of *in vivo* MMP induction is still unknown. For example, while MMP2 and MMP13 proteins were detected in synovial fluid from OA patients [62], MMP3 expression was shown to be downregulated in late stage OA human femoral cartilage compared to controls [63]. Furthermore, a mouse model of mild injury-induced OA caused by destabilization of the medial meniscus (DMM) [64, 65], demonstrated increased MMP3 and MMP13 mRNA expression in OA knees compared to sham controls, but did not exhibit a consistent change over time [43, 66]. It is also likely that MMP protein expression and activity would differ from mRNA expression at different stages of OA development, as MMP inhibitors known as tissue inhibitors of metalloproteinases (TIMPs) are also induced in OA [66]. As many of these MMPs have overlapping functions, the dynamics of the net MMP activity that shapes the landscape of matrix degradation throughout early and later OA stages is still not clear. However, this is an important area of investigation as a change in overall MMP activity may sensitively reflect metabolic changes in the OA joint prior to gross structural damage.

1.3.3 Near Infrared Fluorescence (NIRF) Imaging

Near infrared fluorescence (NIRF) imaging is an emerging technology that can non-invasively reflect real-time metabolic, enzymatic, and physiological tissue states. To do so, NIRF probes are conjugated with enzyme-specific substrates so that fluorescence only

occurs upon enzymatic activation. Therefore, the intensity of the fluorescent signal indicates the activity level of the enzyme [67]. The enzymatic substrate link can be varied for different targets. NIRF probes that measure the activity level of various proteases upregulated in OA are already commercially available. For example, MMPSense680 is a NIRF probe made by PerkinElmer that is specifically activated by tissue MMP activity.

There are several characteristics of NIRF imaging that make it advantageous for *in vivo* preclinical testing and for clinical use. Near infrared photons are able to penetrate both tissue and bone, display low autofluorescence, and present a low risk to patients or animals as they utilize non-ionizing radiation [68]. Due to these desirable attributes, NIRF imaging is already currently being investigated for a variety of clinical uses. For instance, human studies are already underway to investigate the use of NIRF probes for imaging the lymphatic system, nodal staging of breast cancer, and differentiating malignant breast masses from benign ones [69].

NIRF imaging's use in the detection of joint disease has also begun to be investigated. Several studies have successfully used NIRF probes measuring protease activity to identify rheumatoid arthritis development in mouse models [70-76]. As protease activity has also been shown to be upregulated in the joint during OA [58], this is a promising strategy for OA detection as well. However, it is currently unknown if NIRF imaging of protease activity in the joint can detect incremental changes in joint metabolism as OA progresses that could be used to monitor disease severity. This is complicated by the fact that the trajectory of protease activity during OA progression is not well understood. It is

also unknown if NIRF imaging could identify metabolic changes associated with OA *before* morphological joint changes occur. Further study using NIRF imaging in OA mouse models is necessary to determine the sensitivity of this technique and its utility in the early detection and monitoring of OA.

1.3.4 Near Infrared Fluorescence (NIRF) Imaging of MMP Activities in a Mouse Model of Osteoarthritis

As NIRF imaging of protease activity in the joint holds much promise**,** I aimed to investigate if NIRF imaging specifically of MMP activity could be used for real-time detection of OA development in a mouse wear and tear *in vivo* OA model (the DMM model), with a special focus on the *early* stages of OA, and to correlate the NIRF results with damage visible through histology. This line of questioning could help to determine if NIRF imaging could potentially be used for early detection and sensitive disease monitoring in preclinical models of OA, something that is currently lacking in the field. This could open the door for the development of more efficient and sensitive *in vitro* and *in vivo* screening methods for testing the efficacy of OA therapeutics. In addition, studying the trajectory of protease activity over disease development could enhance our knowledge of the early metabolic changes that occur in OA.

To investigate these questions, I used an MMP-activatable NIRF probe to examine the trajectory of MMP activity in the knee joint of the DMM mouse model (a model of injury-induced OA) from the early stages of disease development [64]. The NIRF

imaging results were correlated with histologically observed OA joint damage. I found that the NIRF detected MMP activity steadily increased starting from early OA development to the end time point of my investigation, suggesting that NIRF can be used as a sensitive and minimally invasive measure for joint degeneration in a real-time fashion. The results of this study were published in *Arthritis and Rheumatology* in February of 2015 [77].

Section 1.4 Wnt Signaling in Osteoarthritis

1.4.1 Introduction to Wnt Signaling

Wnt signaling is a group of highly conserved signaling pathways that play a crucial role in development and disease [78, 79]. The Wnt proteins are a diverse family of secreted glycoproteins that bind to Frizzled (FZD) receptors to activate the Wnt signaling pathways. There are 19 specific Wnt proteins that exist in humans and mice. These different Wnt proteins are highly conserved across species [80].

Wnt proteins are known to activate two types of signaling pathways: the canonical and non-canonical pathways [81]. The balance of these two types of pathways may shift during development or aging [82]. To activate the Wnt canonical pathway, Wnts bind FDZ receptors with the low-density lipoprotein receptor-related protein (LRP) 5/6 co-receptor, which leads to accumulation of β-catenin in the cytoplasm (Fig. 1.2). This is through inhibition of the destruction complex, made up of Axin, adenomatous polyposis

coli (APC), glycogen synthase kinase 3 (GSK3), and casein kinase 1 (CK1), which normally tags β-catenin for degradation. With the destruction complex inhibited, β-catenin can accumulate in the cytoplasm and translocate into the nucleus, where it interacts with the T-cell factor/lymphoid enhancer factor (Tcf/Lef) transcription factors to stimulate transcription of downstream target genes such as Axin2 [83].

The non-canonical Wnt pathways include activation of calcium signaling, the planar cell polarity (PCP) pathway, and Akt signaling [84-86] (Fig. 1.3). The calcium pathway increases intracellular calcium and activates calmodulin kinase II (CamKII) and calcineurin, subsequently promoting the translocation of nuclear factor of activated T-cells (NFAT) into the nucleus [86]. The PCP pathway activates JNK signaling through the small GTPases Rac and Rho. This pathway is traditionally thought to control cytoskeletal remodeling and planar cell polarity; however it can also affect gene transcription in the nucleus through effects on the transcription factor activator protein 1 (AP-1) [87, 88]. The canonical and non-canonical Wnt signaling pathways may also antagonize one another. For example, Wnt activated calcium signaling can stimulate β-catenin degradation and thus inhibit Wnt canonical pathway signaling [81, 89].

Traditionally, specific Wnt proteins have been divided into two classes, canonical and non-canonical activating Wnts. The original classifications were based upon which Wnt proteins could induce β-catenin-dependent signaling in *Xenopus* embryos and mouse

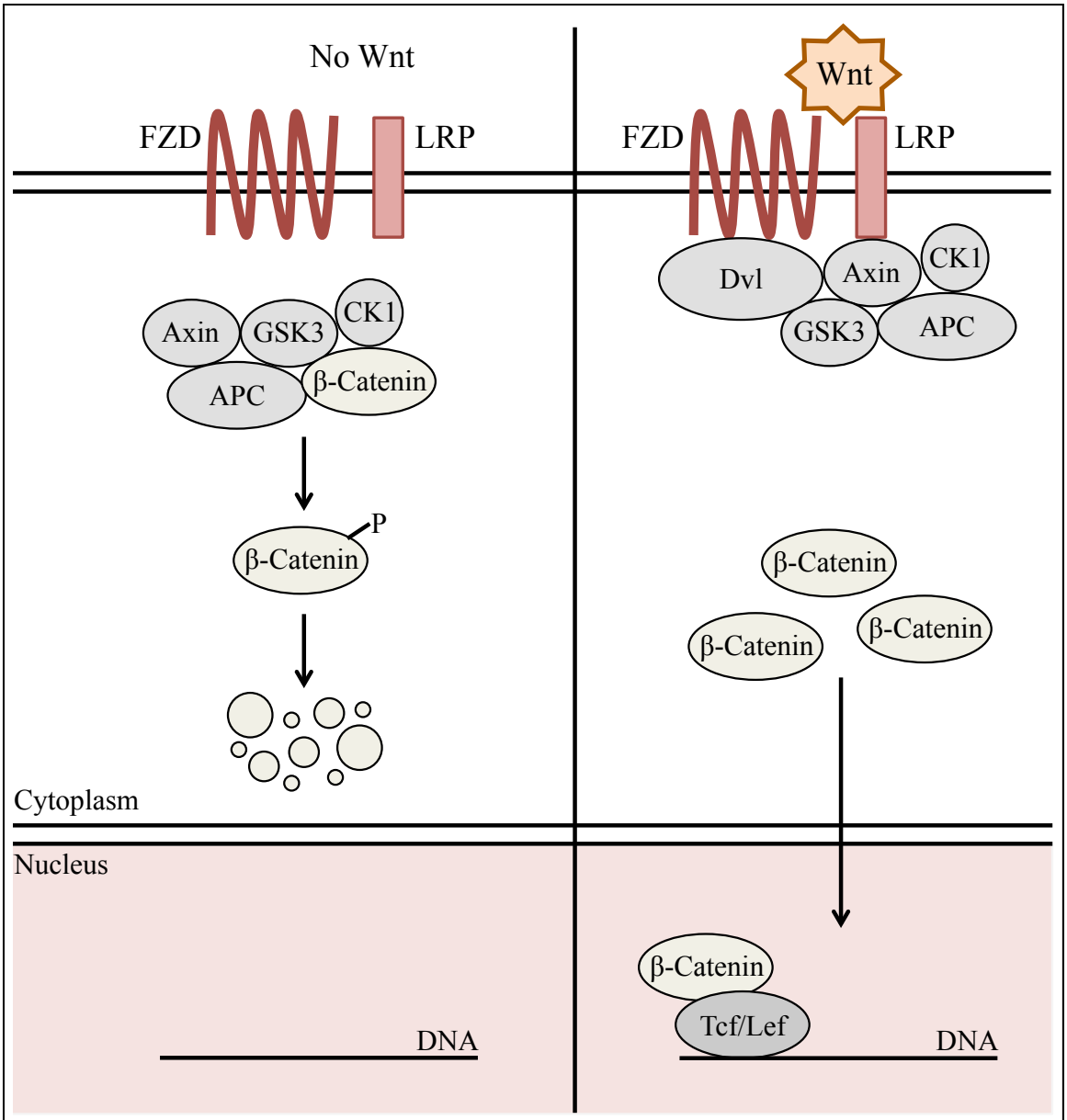

Figure 1.2. Schematic representation of canonical Wnt signaling. In the absence of Wnt, the destruction complex (Axin, APC, GSK3, and CK1) phosphorylates β-catenin. This targets β-catenin for ubiquitination and destruction by the proteasome. When Wnt binds to FZD and LRP, Dvl is activated, which then inhibits the destruction complex and thus inhibits β-catenin degradation. β-catenin then can accumulate in the cytoplasm and enter the nucleus to cause activation of target gene transcription through association with Tcf/Lef. APC: Adenomatous polyposis coli. CK1: Casein kinase 1. Dvl: Disheveled. FZD: Frizzled receptor. GSK3: Glycogen synthase kinase 3. LRP: Low-density lipoprotein receptor-related protein. Tcf/Lef: T-cell factor/lymphoid enhancer factor.

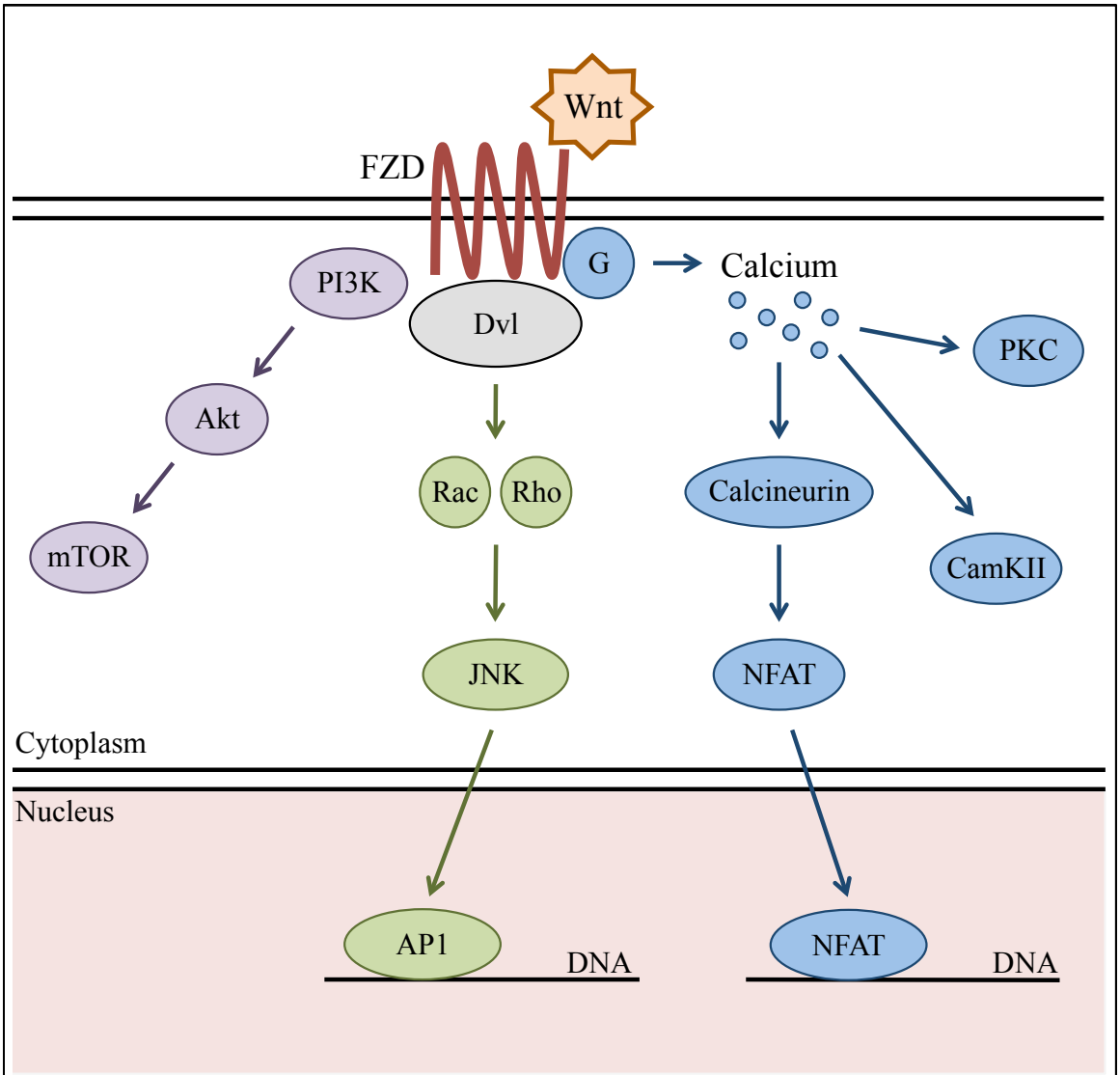

Figure 1.3. Schematic representation of non-canonical Wnt signaling. Several non-canonical Wnt signaling pathways have been proposed. For the Wnt calcium pathway (blue), Wnt binding to FZD activates heterotrimeric G proteins (G), which in turn increase intracellular calcium levels. Intracellular calcium activates CamKII, PKC, and Calcineurin. Calcineurin then activates NFAT, which translocates to the nucleus to activate transcription of target genes. In the Wnt/JNK or planar cell polarity (PCP) pathway (green), Wnt binding to Fzd and Dvl activates JNK signaling through the small GTPases Rac and Rho, which ultimately can lead to cytoskeletal remodeling and/or nuclear translocation of AP-1. Wnt binding to FZD can also activate Akt and mTOR signaling (purple). AP-1: Activator protein 1. CamKII: Calmodulin kinase II. Dvl: Dishevelled. FZD: Frizzled receptor. JNK: c-Jun n-terminal kinase. NFAT: Nuclear factor of activated T cells. PI3K: Phosphatidylinositol 3-kinase. PKC: Protein kinase C.

mammary cells [90-92]. However, it has become clear that these classifications do not hold true for all cell types. For example, Wnt5a is traditionally considered a non-canonical Wnt protein and is still very commonly used in experiments as an example of non-canonical signaling. Nevertheless, it has been demonstrated that Wnt5a can induce β-catenin signaling in *Xenopus* embryos, mouse embryos, and human 293 cells [93-95]. Several of these studies showed that Wnt5a can both induce or repress β-catenin signaling in the same cell type depending on which receptors are present on the receiving cells [94, 95]. In fact, many Wnt proteins have now been shown to activate both canonical and non-canonical signaling in a cell type dependent manner [89, 96-101]. These results demonstrate that Wnt protein activation of Wnt signaling is highly context dependent and that canonical and non-canonical activation are not mutually exclusive.

1.4.2 Current Understanding of Wnt Signaling in Osteoarthritis

Human studies demonstrating changes in Wnt signaling in OA patients have spurred investigation into whether Wnt signaling plays a role in OA development [102-108]. For example, several studies of patient data have determined that a specific genetic polymorphism in secreted frizzled-related protein 3 (sFRP3), a Wnt signaling antagonist, is associated with an increased risk for OA development in women [102, 105, 109]. It was later demonstrated that sFRP3 null mice develop normally, but show increased articular cartilage damage compared to control mice after OA induction via collagenase induced joint instability, papain induced enzymatic digestion of joint cartilage matrix, and methylated bovine serum albumin (BSA) induced inflammatory arthritis. The sFRP3

null mice also demonstrated increased β-catenin levels, suggesting that sFRP3 normally downregulates Wnt canonical signaling in the joint [110]. This is supported by a separate *in vitro* study showing that the sFRP3 genetic polymorphism that is associated with increased susceptibility to OA in patients results in an sFRP3 protein that has a reduced ability to inhibit Wnt canonical signaling compared to wild type sFRP3 [102]. This combination of studies demonstrated a possible role for Wnt canonical signaling in OA development.

Indeed, many additional studies have shown an increase in β-catenin levels in both human and animal OA samples [101, 111, 112]. Nevertheless, how Wnt canonical signaling affects joint destruction in OA is still controversial. For example, while ablation of β-catenin *in vivo* resulted in degeneration of articular cartilage [113, 114], overexpression of β-catenin *in vivo* also caused an OA-like phenotype [111]. On the other hand, separate studies examining the canonical Wnt pathway inhibitor Dickkopf-related protein 1 (DKK-1) demonstrated that both overexpression and antisense knockdown of DKK-1 both instead inhibited OA articular cartilage damage [115, 116]. Furthermore, two other genetic analyses performed after the original identification of the genetic polymorphism in sFRP3 did not find a significant association between polymorphisms in sFRP3 and the development of OA in patients [117, 118]. These studies highlight the plethora of inconsistent results related to the role of Wnt canonical signaling in OA. It is also unclear how non-canonical Wnt signaling is involved, as similarly inconclusive results have been seen related to calcium signaling in OA [119-122]. Perhaps such seemingly contradictory data indicate that an intricate balance in Wnt signaling must be

maintained for optimal cartilage homeostasis. Such a balance is likely to be delicately maintained by multiple Wnt molecules. However, despite the *in vivo* studies of downstream Wnt signaling components, no Wnt ligands have been tested in an *in vivo* experimental OA setting.

In vitro experiments showed that Wnt3a, Wnt5a, Wnt7a, and Wnt7b induced MMP expression in rodent chondrocytes under normal, non-pathological conditions [123-127]. However, further studies using human articular chondrocytes demonstrated that Wnt3a and Wnt7b had the opposite effect as in rodent cells; they decreased MMP expression under both control and IL-1β treatment [128]. Thus, it is important to investigate the effect of Wnts in both human and rodent systems, and under normal and pathological conditions. However, at this time no Wnts have been comprehensively evaluated both *in vitro* and *in vivo* in chondrocytes under normal or pathological conditions. Additional studies systemically examining *in vitro* and *in vivo* OA conditions are necessary to help clearly define the role of specific Wnts and Wnt signaling in OA.

1.4.3 The Effect of Wnt7a on IL-1β Induced Catabolic Gene Expression In Vitro and Articular Cartilage Damage in Experimental Osteoarthritis In Vivo

Wnt7a is an intriguing molecule that acts through both the canonical and non-canonical Wnt pathways in a cell type-dependent manner [85, 99, 100]. While Wnt7a has been shown to be expressed in articular cartilage [83], the effect of Wnt7a in OA or on human chondrocytes under pathological conditions has not been examined. In this study, I

investigated the expression of Wnt7a in human OA cartilage and found an intriguing non-linear inverse correlation between the expression of Wnt7a and several catabolic genes. I then examined the effect of Wnt7a ectopic expression in human primary articular chondrocytes under inflammatory conditions, as well as in the DMM mouse model of OA. My results indicate a beneficial effect of Wnt7a on chondrocytes *in vitro* and *in vivo*, and suggest collaboration between the canonical and non-canonical Wnt signaling pathways that mediate the activity of Wnt7a.

Chapter 2: Near Infrared Fluorescence (NIRF) Imaging of MMP Activities in a Mouse Model of Osteoarthritis

2.1 Materials and Methods

In Vitro **Chondrocyte Cultures.** Primary normal human knee articular chondrocytes (nHACs, Lonza) were redifferentiated in alginate beads according to Lonza's established protocol. For 2D cultures, redifferentiated nHACs were cultured for 4 days in chondrogenic differentiation media (Lonza) that contained 0, 1, or 4 ng/mL IL-1β (Peprotech). For 3D cultures, nHACs were seeded into the silk scaffolds (graciously provided by David Kaplan, pore size of 100-200μm generated with solvent evaporation using HFIP) at a density of $0.5x10^6$ cells/scaffold and cultured for 4 days with chondrogenic differentiation media (Lonza) that contained 0, 5 or 10 ng/mL IL-1β.

Experimental Animals. All animal care and experimental procedures were approved by the Institutional Animal Care and Use Committees at Tufts University and Massachusetts General Hospital. Wild-type CD1 male mice were purchased from Charles River Laboratories. All mice were caged in groups under standard conditions with a 12-hour light/dark cycle.

Surgical Model of OA in Mice. Destabilization of the medial meniscus (DMM) surgery was performed on 7 week old CD1 male mice according to the established protocol [64]. Briefly, under isoflurane anesthesia, the right knee joint was opened along the medial

border of the patellar ligament and the medial meniscotibial ligament (MMTL) was severed. Sham surgery, where the MMTL was visualized but not severed, was performed on the left knee of the same mice as an internal control. Mice were monitored for pain and infection post surgery and allowed unrestricted cage exercise.

NIRF *in vitro* imaging. For *in vitro* NIRF imaging on cultured chondrocytes, 0.4μM of the NIRF probe MMPSense680 (PerkinElmer) was added to the culture medium for 4 hours for 2D cultures and 16 hours for 3D cultures. Live cultures were then examined using a LSM 510 confocal microscopy system (Zeiss) for NIR fluorescence (633nm excitation, 700nm emission). Hoechst dye (Invitrogen) was added to localize the cells.

NIRF *in vivo* imaging and data analysis. For *in vivo* imaging, the hair of the mouse hind limb was removed to reduce autofluorescence. Under isoflurane anesthesia, MMPSense680 (4 μL of 13.3 nmol) was directly injected through the patellar ligament into the knee joint cavity using a 30G needle. Unless otherwise noted, immediately before imaging an approximately 1.5 cm skin incision was created directly over the patellar ligament of each knee to allow imaging without skin overlying the joint. Images were acquired using the Multispectral Imaging System (In Vivo Pro; Carestream, CT, USA) in the following sequence 1) white light 2) X-ray 3) near infrared scanning with 530-680 nm excitation filters and 700 nm emission filter. At least 4 mice were used for the serial imaging and single time point imaging experiments. The number of mice used for imaging at each time point are: n=7, 8, 7, 8, 4, 8, 4, 8, for weeks 1-8 respectively, with a total of 54 mice used.

Fluorescence signal intensity of the NIRF data was measured by Shadi Esfahani using the standard analysis software from Carestream. A region of interest was drawn over each knee joint to quantify the mean fluorescent signal intensity and the area of increased signal within the raw image. The fluorescence signal intensity of the mouse skin was measured as the background signal and subtracted from the raw data for each knee joint to internally calibrate each image. Total signal intensity ratio was calculated as (DMM knee mean fluorescence signal intensity x DMM knee area of increased signal) / (sham knee mean fluorescence intensity x sham knee area of signal). Using the 8-bit NIRF images in ImageJ (NIH), a straight line was placed over the regions of interest and the "plot profile" of the arbitrary signal intensity values was generated. Using the "surface plot" analysis, the arbitrary values of intensities over the whole raw images were shown in a three-dimensional plot.

Histological Analysis. Knee joints were isolated and fixed in 4% paraformaldehyde for 24 hours, decalcified in 10% EDTA for 1 week, and then embedded in paraffin. 5 μm serial sections were cut sagittally across the femorotibial joint. Sections every 40 μm were stained with 0.1% safranin O and counterstained with hematoxylin. Fast green counterstaining was also used when indicated. To quantify observed cartilage damage, 9 stained sections from each sample were pooled, randomized and blindly scored using the established articular cartilage structure and the safranin O scoring systems [129]. The femur and tibia were scored separately and added together to calculate a total joint score for each section. The sections were blindly analyzed for two additional OA histological

parameters, tibial chondrocyte cell loss and osteophyte maturity, with established methods [43, 129, 130].

Light microscopy imaging. Bright field images of chondrocytes were taken using an Olympus IX-71 microscope and an Olympus DP70 digital camera. The optical parameters and camera exposure time were kept constant between samples.

***In Vitro* MMPSense680 activation by MMPs.** 10 ng of pro-enzymes (MMP-1, 2, 9, and 13; Anaspec) were added to 0.4μM MMPSense680 and 100μM APMA (Sigma) in a 96-well black bottom plate and incubated at 37°C. In the enzyme combination experiment, 2.5ng/enzyme was used. For inhibiting MMP activities, 100μM of the pan MMP inhibitor PD166793 (Anaspec) dissolved in 0.5% DMSO was used. As a positive control, 0.1ng of trypsin was incubated with 0.4μM of MMPSense680. For negative controls, pro-enzymes, APMA or MMPSense680 alone or pro-enzymes with MMPSense680 but without APMA were used. Plates were read in the IVIS-200 Imaging System (PerkinElmer) at 1, 5, and 24 hours post incubation, and signal intensities were analyzed using Living Image software (PerkinElmer). NIRF signals were calculated as the radiance from APMA activated MMPs subtracted by the radiance from the pro-MMP without APMA (baseline control).

RNA isolation and real-time polymerase chain reaction (qPCR). Total RNA from cultured redifferentiated nHACs was isolated with the Qiagen RNeasy Mini Kit (Qiagen) and cDNA was generated using M-MLV Reverse Transcriptase (Invitrogen). qPCR was

performed using the iQ5 Real-Time PCR Detection System (Bio-Rad). All qPCR analyses were normalized to TBP expression [131]. Primer sequences are available upon request.

Statistical Analysis. Data are shown as mean ± SEM. The semiquantitative histological scoring systems were evaluated using nonparametric statistical analyses. All other experiments were evaluated with a Student's t-test or analysis of variance (ANOVA) with post-hoc tests for pairwise comparisons. Normality of the data was tested using the Shapiro-Wilk normality test. Best-fit line equations and R^2 values were determined using a second order polynomial regression. Spearman correlation was used for correlation analyses. A p value of less than 0.05 was considered significant in all cases.

2.2 Results

2.2.1 MMP sensitive NIRF probe exhibits enhanced fluorescent signals in IL-1β-treated chondrocytes in vitro

With the help of Carrie Hui Mingalone, Roshni Rainbow, and Daisy Nakamura, we confirmed the ability of the NIRF probe MMPSense680 to detect MMP activity in chondrocytes *in vitro*. First, MMPSense680 was incubated with recombinant pro-MMPs and APMA, a known MMP activator [132], to confirm that MMPSense680 fluorescence was activated specifically by active MMPs. The resulting NIRF signal was measured after 1, 5, and 24-hour incubations. We found that the detected MMPSense680 signal

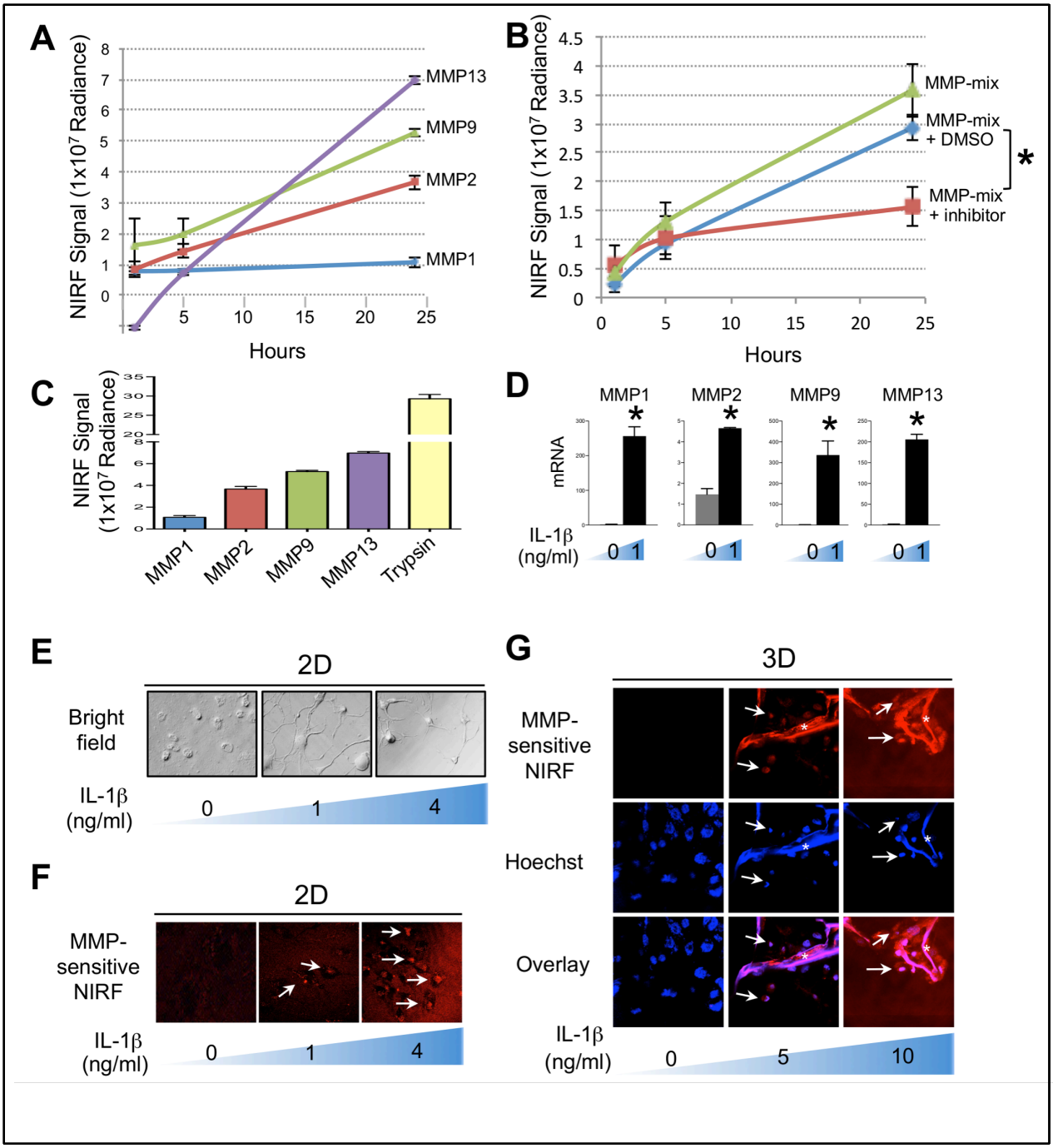
A
NIRF Signal (1x10⁷ Radiance)
Hours
MMP13
MMP9
MMP2
MMP1
B
NIRF Signal (1x10⁷ Radiance)
Hours
MMP-mix
MMP-mix + DMSO
MMP-mix + inhibitor
*
C
NIRF Signal (1x10⁷ Radiance)
MMP1
MMP2
MMP9
MMP13
Trypsin
D
MMP1
MMP2
MMP9
MMP13
mRNA
IL-1β (ng/ml)
0 1
E
2D
Bright field
IL-1β (ng/ml)
0
1
4
F
2D
MMP-sensitive NIRF
IL-1β (ng/ml)
0
1
4
G
3D
MMP-sensitive NIRF
Hoechst
Overlay
IL-1β (ng/ml)
0
5
10

Figure 2.1. MMP sensitive near infrared fluorescence (NIRF) probe detects enhanced MMP activities upon pro-inflammatory cytokine IL-1β treatment in 2D and 3D cultures of human primary articular chondrocytes (nHACs). A. Activation of MMPSense680 by active recombinant MMPs minus background fluorescence over 24 hours. **B.** MMPSense680 activation by recombinant MMPs plus the pan-MMP inhibitor PD 166793, demonstrating that PD166793 inhibits recombinant MMP activation of MMPSense680. **C.** MMPSense and trypsin activation of MMPSense680 after 24 hour incubation. **D.** qRT-PCR analysis of MMP expression in nHACs (Lonza) treated with or without 1 ng/μL of IL-1β for 3 days, confirming MMP induction with IL-1β treatment. **E.** Bright field images of IL-1β-treated nHACs in 2D cultures. **F.** Confocal images after 4 hours of MMPSense680 (0.2μM, PerkinElmer) addition, indicating IL-1β induced MMP activity in nHACs in a dosage-dependent way (arrows). **G.** Confocal images of HACs grown in 3D silk porous scaffolds (100-200μm pore size) after 16 hours of MMPSense680 (0.2μM) addition. MMP activity was induced by IL-1β in a dosage-dependent way (arrows). Hoechst dye labeling indicates the locations of live cells. Black * = $p < 0.05$ and white * indicates the presence of the silk scaffold.

increased over time, with the largest signal being detected at 24 hours (Fig. 2.1A). MMP13 resulted in the strongest MMPSense680 activation, followed by MMP9 and MMP2. A mixture of the recombinant MMPs (MMP-mix) demonstrated a comparable MMPSense680 fluorescence activation (Fig. 2.1B). MMP inhibition by the pan-MMP inhibitor PD 166793 significantly reduced MMPSense680 fluorescence signal, indicating that the observed fluorescence was specifically a result of the active MMPs (Fig. 2.1B). As a positive control, trypsin was used to confirm that MMPSense680 activation was caused by proteolytic cleavage of the probe (Fig. 2.1C).

We then tested whether MMPSense680 can reflect an induction in MMP activity when chondrocytes were treated with the pro-inflammatory cytokine IL-1β *in vitro* [58, 133-135]. Indeed, IL-1β treatment of normal human articular chondrocytes (nHACs) led to the induction of MMP1, MMP2, MMP9 and MMP13 expression (Fig. 2.1D). Furthermore, chondrocytes exhibited a more elongated morphology (Fig. 2.1E) and

enhanced MMP-activated NIRF signal by IL-1β treatment in a dosage-dependent manner (Fig. 2.1F). Similarly, nHACs grown in 3D silk porous scaffolds also demonstrated IL-1β dosage-dependency in the upregulation of the MMP-activated NIRF signal (Fig. 2.1G).

2.2.2 MMP sensitive NIRF probe exhibits enhanced signals in vivo in DMM OA mouse

To determine whether an MMP sensitive NIRF probe could be used *in vivo* to detect cartilage destruction in the OA knee, I performed destabilization of the medial meniscus (DMM) surgery on CD1 male mice. I chose the DMM surgery as an *in vivo* OA model because it has been shown to reliably cause mild injury-induced OA in mice [64]. To minimize potential differences in intrinsic MMP activities between individuals, I performed DMM surgery on the right knee of each mouse and sham surgery on the left knee of the same mouse as an internal control.

I injected the NIRF probe MMPSense680 intraarticularly to measure the current MMP activity level in the joint. Previous studies on MMP activities in the aorta and the brain have established that MMPSense680 is also activated specifically by MMPs *in vivo*, as mice treated with an MMP13 inhibitor and MMP9$^{-/-}$ mice demonstrated largely reduced MMPSense680 fluorescence [136, 137]. To determine the optimal time for fluorescence imaging in DMM mice, Andrea Foote and Shadi Esfahani imaged mice 7 weeks post DMM at several time points after probe injection. At all measured time points, the DMM knee demonstrated a higher fluorescent signal than the sham knee of each mouse (Fig. 2.2A). NIRF signals were quantified to calculate the mean fluorescence intensity for each

knee and the DMM:sham total signal intensity ratio (i.e. mean fluorescence x area of signal) for each mouse (Fig. 2.2B, 2.2C). Results of both types of analysis indicated significantly higher MMP activity in the OA knee compared to the sham knee and that the most significant difference between the two knee joints was observed at 2 hours post injection (Fig. 2.2A-C). Therefore, this time interval was used in all subsequent experiments. To delineate the location of the NIRF signal in the mouse joint after probe injection, NIRF images were overlaid with x-ray images. The x-ray overlay confirmed that the obtained fluorescent signal was localized to the knee joint (Fig. 2.2D).

As a control, I imaged mice that had not undergone DMM surgery before and after probe injection. Before probe injection, no NIRF signal was observed (Fig. 2.3A), suggesting that no endogenous or intrinsic fluorescence from the mice contributed to any of the detected NIRF signals. Following probe injection, mice demonstrated low NIRF signal intensities that were very similar between the right and left knees, indicating that the difference between DMM and sham knee NIRF signals was not due to intrinsic differences in MMP activity between the two knees at baseline (Fig. 2.3A). I also imaged mice 7 week post DMM before and after removal of the skin overlying the joint to confirm that the NIRF signal came specifically from the knee joint (Fig. 2.3B, 2.3C). I observed similar NIRF signal ratios between the DMM and sham knees with both transcutaneous and exposed joint imaging (Fig. 2.3B, 2.3C), which is suggestive of the potential for imaging the knees without skin excision in future translational applications. Since shaper images were obtained when the joint was directly exposed, I kept this practice in subsequent experiments.

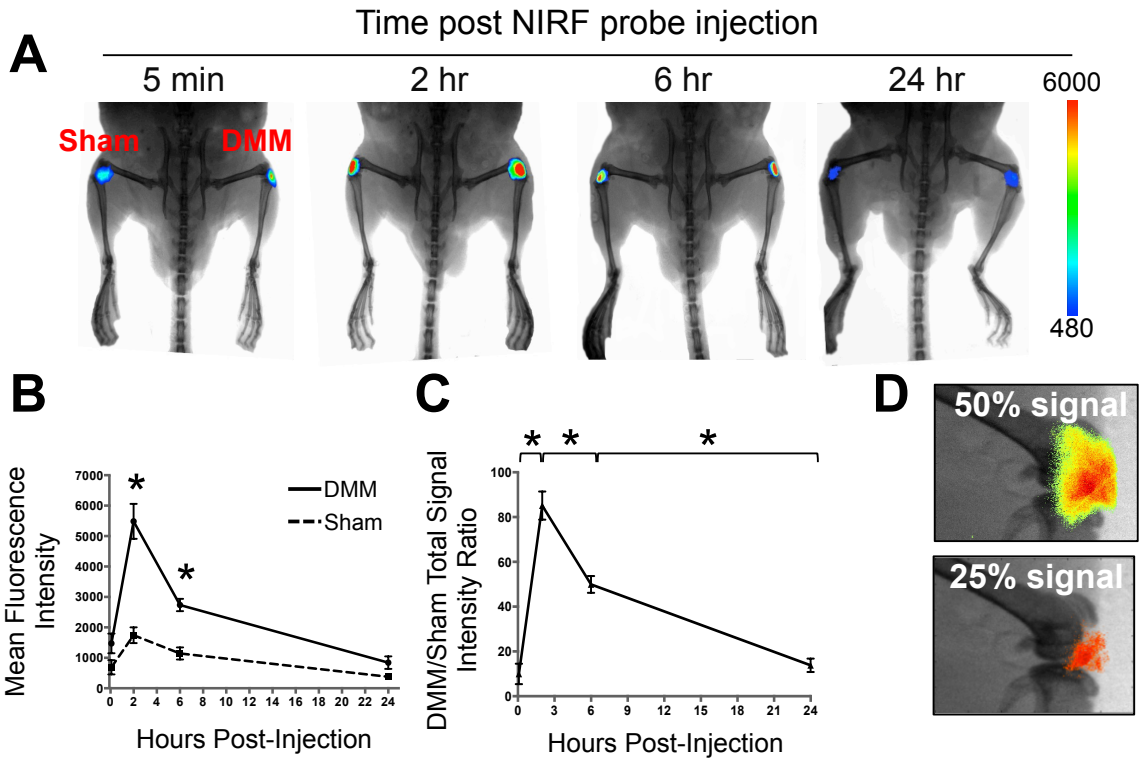

Figure 2.2. MMP sensitive NIRF probe exhibits enhanced signals *in vivo* in DMM OA mouse. A. *In vivo* NIRF images overlain on X-ray images from DMM mice after 4 µL intraarticular injection of MMPSense680 in each knee. Mice were imaged at multiple time points post probe injection, demonstrating enhanced fluorescent signal in the DMM knee as compared to sham knee of the same mouse, with two hours post probe injection showing the largest difference. **B.** Mean fluorescent intensity emitted from each knee was quantified from collected NIRF images. **C.** Total signal intensity was quantified for each knee from the collected NIRF images and the signal intensity ratio of DMM:sham was calculated for each mouse. **D.** NIRF signal overlain on X-ray from 7-week DMM mouse with plotting thresholds set so only the brightest 50% (left) or brightest 25% (right) of NIRF signal is shown, demonstrating that the NIRF signal comes specifically from the knee joint. * = $p < 0.05$ for groups at the same time point, unless otherwise indicated by brackets.

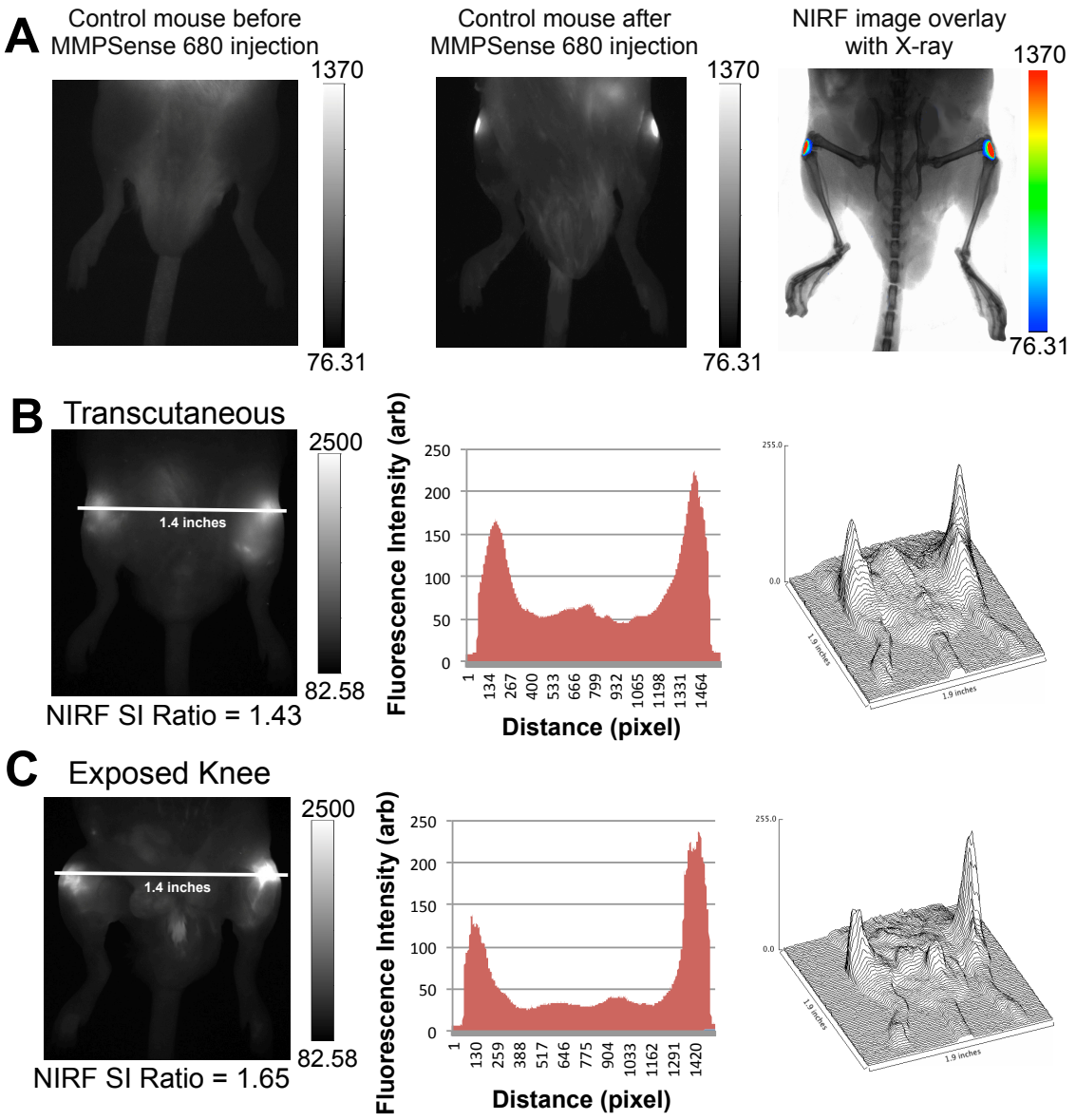

Figure 2.3. NIRF signals are derived from the joint instead of the overlaying skin. **A.** Raw images of a control mouse prior to and after MMPSense680 intraarticular injection and processed NIRF image overlain on X-ray image of the control mouse after probe injection. **B.** Transcutaneous NIRF image overlain on X-ray image from a DMM mouse taken 2 hours after 4 µL intraarticular MMPSense680 injection. ImageJ was used to quantify emitted fluorescence across the width of the image and to create a surface plot analysis to generate a three dimensional plot of the intensities of the whole raw transcutaneous NIRF image. **C.** NIRF image taken with the skin pulled open to expose the knee overlain on X-ray image from a DMM mouse taken 2 hours after 4 µL intraarticular MMPSense680 injection. ImageJ was used to quantify emitted fluorescence across the width of the image and to create a surface plot analysis to generate a 3D plot of the intensities of the whole raw exposed knee NIRF image.

2.2.3 MMP sensitive NIRF signal intensity steadily increases over OA progression in DMM mice

The observation that DMM surgery induced a significantly higher level of MMP sensitive NIRF signal compared to sham controls at 7 weeks post DMM (Fig. 2.2) led us to hypothesize that NIRF signal intensity would correlate with OA development as the joint degenerates. To test this hypothesis, I imaged individual mice serially every 2 weeks over 8 weeks post DMM. As the half-life of MMPSense680 is only 72 hours, I expected signals from the previous imaging session to have dissipated before subsequent imaging of the same mouse 2 weeks later. To confirm that the fluorescent signal from the previous imaging session was gone, I pre-imaged all mice immediately before new probe injection at each imaging session. Strikingly, the DMM knee exhibited a higher fluorescent signal than the sham knee of the same mouse at every examined time point (Fig. 2.4A). Signal quantification performed by Shadi Esfahani indicated that the mean fluorescent intensity of the DMM knee increased in a linear fashion from 2 to 8 weeks post surgery, while sham knee signals showed only a mild increase over time (Fig. 2.4B). When the DMM:sham total signal intensity ratios were calculated (i.e. mean fluorescence intensity x area of increase signal), they indicated a significant increase over the course of OA development that was studied (Fig. 2.4C). This data indicates that MMP activities in the OA joint were induced shortly after surgery and continuously rose from the very early stages of OA to moderate OA.

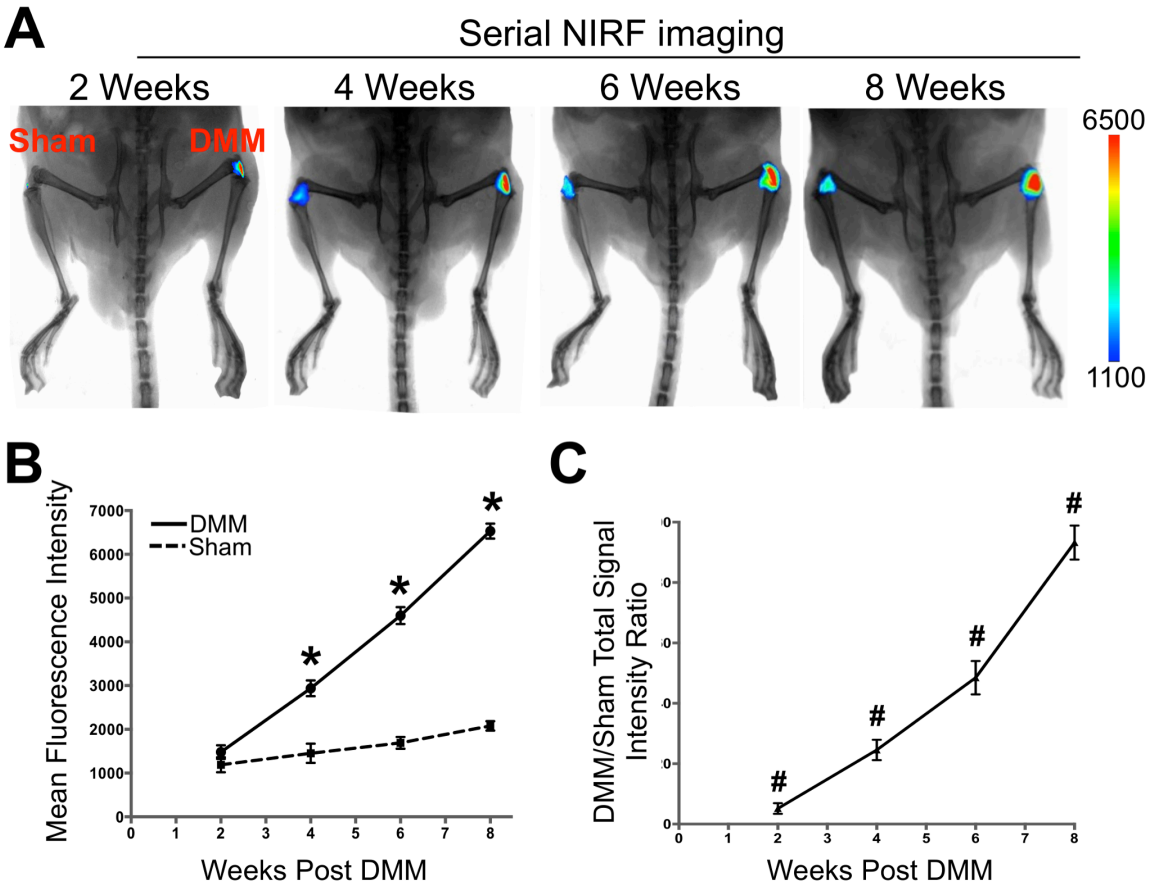

Figure 2.4. MMP-activatable NIRF signal intensity steadily increases over the course of OA progression in repeatedly imaged DMM mice. A. *In vivo* NIRF images overlain on X-ray images from DMM mice taken two hours after 4 µL intraarticular injection of MMPSense680 in each knee. The same mice were imaged repeatedly every 2 weeks for 8 weeks total. Representative images show the combined X-ray and NIRF image of one individual mouse at 2, 4, 6, and 8 weeks post DMM surgery. Increasing levels of MMP activities were observed over OA development. **B.** Mean fluorescent intensity emitted from each knee was quantified from collected NIRF images. * = $p < 0.05$ for groups at the same time point. **C.** Total signal intensity was quantified for each knee from the collected NIRF images and the signal intensity ratio of DMM:sham was calculated for each mouse. Data was fit with a best-fit line using a second order polynomial regression, equation: $y = 1.6x^2 - 1.42x + 2.5$, R^2 value: 0.9463. # = $p<0.05$ compared to all groups.

2.2.4 Correlation of NIRF signal intensity with cartilage histological analysis over OA progression in DMM mice

I performed histological analysis of NIRF imaged mice over 8 weeks post DMM to correlate the collected NIRF signals with histological parameters typically used to examine progressive OA joint degeneration over time. As it is not possible to evaluate joint histology at each time point in serially imaged mice, I performed additional surgeries and mice were sacrificed at multiple time points immediately after NIRF imaging (Fig. 2.5A). Again, the average NIRF signal intensities of the DMM knee rose consistently over time, while those from the sham knee remained relatively flat (Fig. 2.5B). As a result, the ratio of DMM:sham total signal intensity increased significantly over time (Fig. 2.5B). This confirms that the observed increase in NIRF detected MMP activity seen in the serially imaged mice was not due to the injection performed at each imaging session. When serial imaged animals were also included in the plot, it further confirmed the trend of increased MMP activity in the DMM knee compared to sham controls over the entire time-course studied and demonstrated the strong reliability and reproducibility of this trend (Fig. 2.5C).

Safranin O staining was performed for histological analysis of OA joint damage at the time of NIRF imaging (Fig. 2.6A-C). To quantify articular cartilage damage, histological images were randomized and blindly scored for changes in articular cartilage structure and safranin O staining based on published assessment methods [43, 129]. Cartilage structural damage and loss of safranin O staining were significantly higher in the DMM

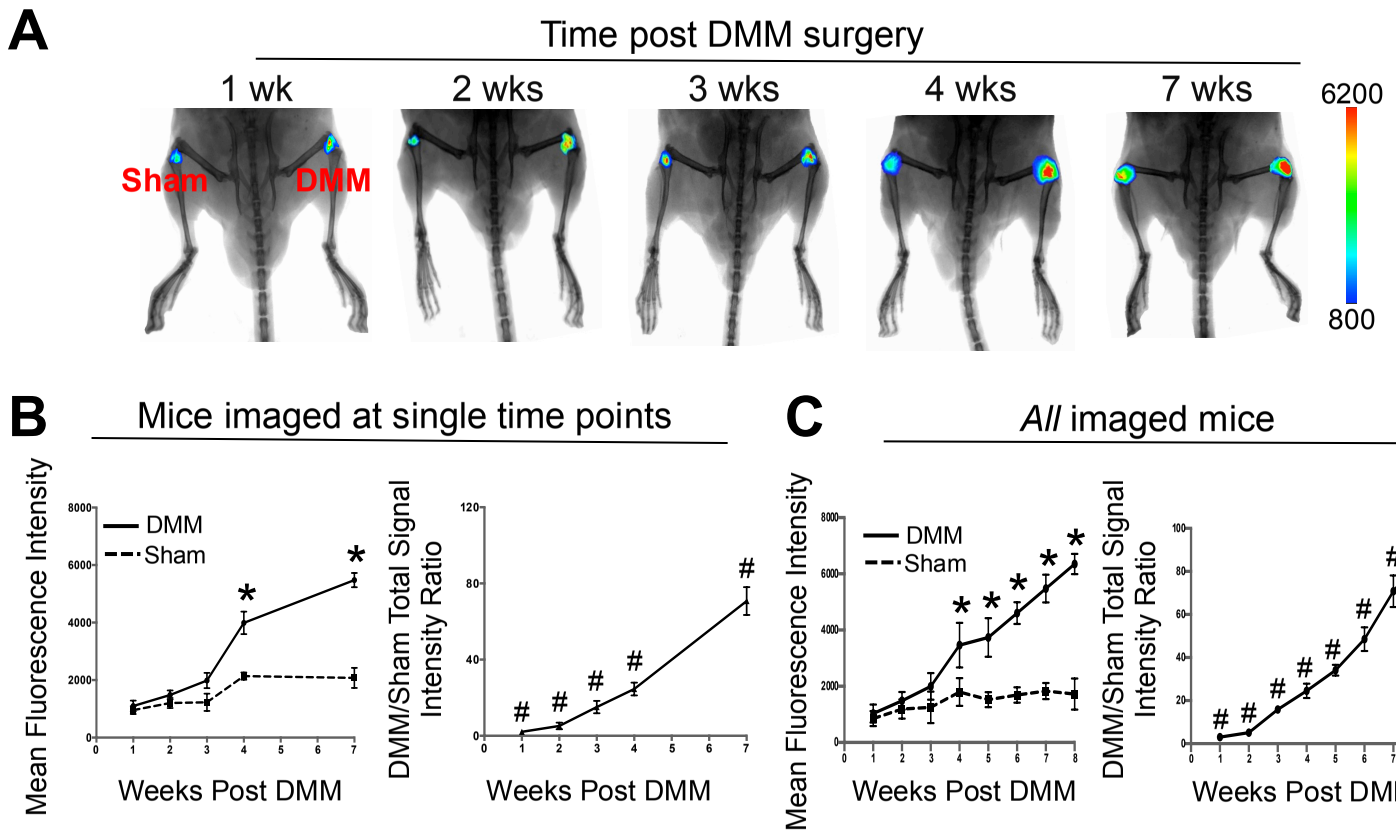

Figure 2.5. MMP-activatable NIRF signal intensity steadily increases over OA progression in DMM mice imaged at single time points. A. *In vivo* NIRF images overlain on X-ray images from DMM mice taken two hours after 4 µL intraarticular injection of MMPSense680 in each knee. Mice were imaged at a single time point (1, 2, 3, 4, or 7 weeks post DMM surgery). **B.** Mean fluorescent intensity and total signal intensity emitted from each knee were quantified from collected NIRF images. The total signal intensity ratio of DMM:sham was calculated for each mouse. Data was fit with a best-fit line using a second order polynomial regression, equation: $y = 2.5x^2 - 4.6x + 4.5$, R^2 value: 0.9595. **C.** All quantified imaging data, including serially imaged mice and mice imaged at only a single time point, were pooled. Mean fluorescence intensity and total signal intensity ratio from pooled data was plotted over OA development. Data was fit with a best-fit line using a second order polynomial regression, equation: $y = 0.31x^2 + 2.8x + 5.6$, R^2 value: 0.9401. * = $p < 0.05$ for groups at the same time point. # = $p<0.05$ compared to all groups.

knee as compared to the sham knee at all time points (Fig. 2.6A-E). Interestingly, fibrillation and clefts were consistently seen in the DMM samples 1-week post surgery, which resulted in a higher cartilage structure score (Fig. 2.6A, 2.6D). However, such changes became less pronounced in the following weeks and only became visible again as OA progressed to 8 weeks (Fig. 2.6A, 2.6D). Samples were also scored for loss of GAG matrix content with safranin O scoring. However, safranin O scores did not significantly change over time (Fig. 2.6E). This is consistent with a previous study examining C57 mice from 2 to 8 weeks post DMM surgery [43].

In addition to articular cartilage degeneration, chondrocyte cell loss and osteophyte development are also established indicators of OA joint damage in the DMM mouse model that progressively increase over time [43, 138]. In my histological analysis, I observed a significant increase in chondrocyte cell loss from 1 to 8 weeks post DMM (Fig. 2.6F). Furthermore, all mice at all time points demonstrated osteophyte formation in their DMM knee, while no osteophytes was observed in any of the contralateral sham knees (Fig. 2.6C, 2.6G). As osteophyte size does not progressively increase over time in the DMM model, osteophyte size was not assessed in these samples [43]. Rather, I examined the mineralization of the osteophyte. As expected in the DMM model, the observed osteophytes developed from being mostly cartilaginous at week 1 to mostly mature bone at 4 to 8 weeks post DMM (Fig. 2.6C, 2.6G). The joint synovium was also assessed; however no obvious synovitis was apparent at any of the time points examined. This is expected, as synovitis is not an appreciable part of mild surgical OA models such as DMM until very late stages of the disease [43, 64, 139]. In summary, most of the histological parameters of progressive OA joint damage that were examined positively

correlate with the NIRF signals obtained at the same time point (Fig. 2.6H). However, the only histological assessment with a statistically significant correlation was chondrocyte cell loss. This suggests that increased NIRF signals generally indicate increased joint destruction, but that the NIRF signal cannot be used on its own to definitively indicate histological damage at this time.

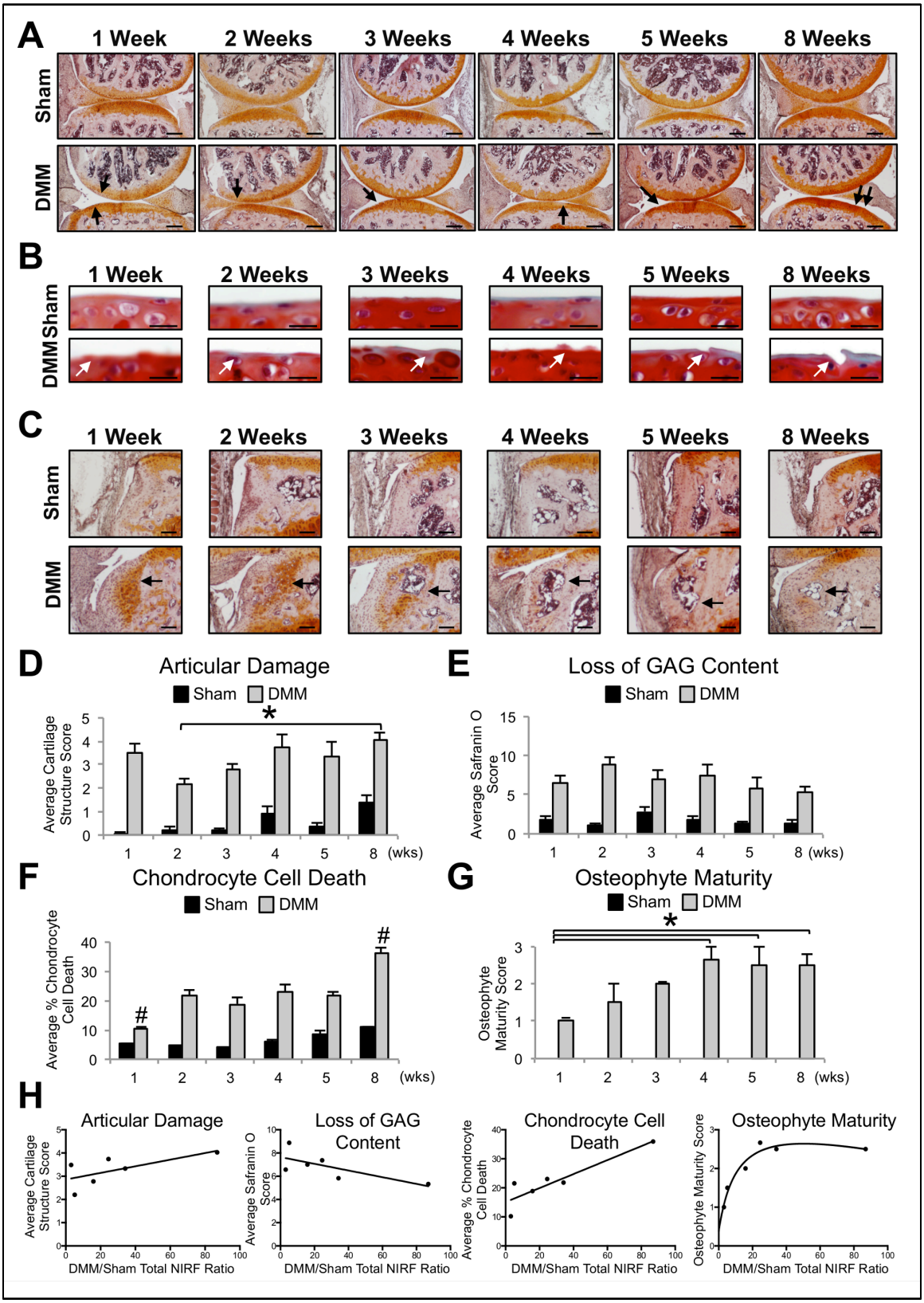
A
1 Week
2 Weeks
3 Weeks
4 Weeks
5 Weeks
8 Weeks
Sham
DMM
B
1 Week
2 Weeks
3 Weeks
4 Weeks
5 Weeks
8 Weeks
DMM Sham
C
1 Week
2 Weeks
3 Weeks
4 Weeks
5 Weeks
8 Weeks
Sham
DMM
D
Articular Damage
Sham DMM
Average Cartilage Structure Score
(wks)
E
Loss of GAG Content
Sham DMM
Average Safranin O Score
(wks)
F
Chondrocyte Cell Death
Sham DMM
Average % Chondrocyte Cell Death
(wks)
G
Osteophyte Maturity
Sham DMM
Osteophyte Maturity Score
(wks)
H
Articular Damage
Average Cartilage Structure Score
DMM/Sham Total NIRF Ratio
Loss of GAG Content
Average Safranin O Score
DMM/Sham Total NIRF Ratio
Chondrocyte Cell Death
Average % Chondrocyte Cell Death
DMM/Sham Total NIRF Ratio
Osteophyte Maturity
Osteophyte Maturity Score
DMM/Sham Total NIRF Ratio

Figure 2.6. Histological analysis of OA severity over the course of OA progression in DMM mice. A. Representative histologic appearance of safranin O/hematoxylin stained sagittally sectioned mouse knees 1-8 weeks post DMM surgery. Scale bars = 250 μm. Arrows indicate cartilage damage. **B.** Representative images of tibial articular damage in fast green/safranin O stained sagittally sectioned mouse knees 1-8 weeks post DMM surgery. Scale bars = 25 μm. Arrows indicate cartilage damage. **C.** Representative images of osteophyte formation in safranin O/hematoxylin stained sagittally sectioned mouse knees 1-8 weeks post DMM surgery. Scale bars = 100 μm. Arrows indicate osteophytes. **D.** Cartilage structure scoring of OA severity in mice 1-8 weeks post DMM. **E.** Safranin O scoring of OA severity in mice 1-8 weeks post DMM. **F.** Tibial chondrocyte cell death scoring of OA severity in mice 1-8 weeks post DMM. **G.** Scoring of osteophyte maturity in mice 1-8 weeks post DMM. **H.** Correlation analyses between histological parameters and NIRF DMM:sham total signal intensity ratio results. * = $p < 0.05$ for indicated groups. # = $p<0.05$ for indicated sample compared to all other samples. At each time point, comparison of DMM and sham score has $p<0.05$.

Chapter 3: The Effect of Wnt7a on IL-1β Induced Catabolic Gene Expression *In Vitro* and Articular Cartilage Damage in Experimental Osteoarthritis *In Vivo*

3.1 Materials and Methods

Normal and OA Human Cartilage Tissue Samples. All human samples were de-identified and classified as exempt by the Institutional Review Board at Tufts University. Normal and human OA samples were isolated and characterized as previously described [140]. Normal cartilage samples were obtained from the tibial plateaus of cadaveric joints from patients without history or radiographic signs of OA from the National Disease Research Interchange and Articular Engineering (age/sex: 84/M, 75/M, 65/F, and 49/F). OA cartilage samples were obtained from tibial plateaus of patients undergoing total knee replacement surgery for OA at Tufts Medical Center (age/sex: 53/F, 63/F, 65/F, 72/M, 73/F, 73/M). Gene expression was analyzed using qPCR and TATA binding protein (TBP) used as a reference gene.

***In Vitro* Human Chondrocyte Cultures.** Primary normal human articular chondrocytes (nHACs, Lonza) were redifferentiated in alginate beads according to Lonza's established protocol using chondrogenic differentiation media (Lonza), as previously described [140]. For viral infection, redifferentiated nHACs were infected with lentiviral human Wnt7a-GFP (lenti-Wnt7a-GFP) or lentiviral GFP (lenti-GFP) (Open Biosystems) with a titer of $5x10^7$ IFU for two days before additional treatments were applied. For IL-1β treatment, redifferentiated nHACs were cultured in chondrogenic differentiation media

that contained 0 or 5 ng/mL IL-1β (Peprotech). For qPCR analysis, cells were lysed after 4 days of IL-1β treatment, unless otherwise specified. For Western blot analysis, cells were lysed after 1 hour of IL-1β treatment. In the DKK-1 study, 250 or 500 ng/mL recombinant human DKK-1 (R&D Systems) was also added to the media. For Akt inhibition, 1 or 10 μM of AZD5363 (Selleckchem) was used. For NFAT inhibition, 20 μM of INCA-6 (Tocris) in 0.2% DMSO was used, with 0.2% DMSO alone serving as a control. For all signal inhibition experiments, compounds were added to the media for 48 hours. For Tcf4 inhibition, lentiviral dominant-negative Tcf4 (lenti-dnTcf4, Addgene plasmid #24310) was used to perform a simultaneous double transfection with the lenti-Wnt7a-GFP and lenti-GFP for two days before IL-1β was added. For the control experiment using Wnt3a, Wnt3a conditioned medium was collected from L cells stably expressing Wnt3a (ATCC CRL-2647) and control conditioned medium was collected from the L cell parental line (ATCC CRL-2648) per the manufacturers recommend protocol.

In Vitro **Murine Chondrocyte Cultures.** Primary murine articular chondrocytes were harvested from the articular knee cartilage of 6-day old mice as described [141] and expanded in DMEM (Gibco) with 10% heat-inactivated fetal bovine serum, 1% penicillin/streptomycin, and 2% glutamine. For viral infection, primary murine articular chondrocytes were infected with lenti-Wnt7a-GFP or lenti-GFP (Open Biosystems) with a titer of $5x10^7$ IFU for two days. Then, 0 or 5 ng/mL IL-1β (Peprotech) was added for 2 days before samples were collected for qPCR analysis.

RNA isolation and real- time polymerase chain reaction (qPCR). Total RNA was isolated with the Qiagen RNeasy Mini Kit (Qiagen) and cDNA was generated using M-MLV Reverse Transcriptase (Invitrogen). qPCR was performed using the iQ5 Real-Time PCR Detection System (Bio-Rad). All qPCR analyses were normalized to GAPDH expression unless otherwise noted [131]. Primer sequences are available upon request.

Western blots. Cells were lysed with RIPA buffer. Nuclear and cytoplasmic fractions were isolated using NE-PER Nuclear and Cytoplasmic extraction reagents (Pierce). Protein concentrations were determined using the DC^{TM} Protein Assay (Bio-Rad). Equal concentrations of protein were loaded and separated using sodium dodecyl sulfate polyacrylamide gel electrophoresis (SDS-PAGE; 10% polyacrylamide). The following primary antibodies were used at a concentration recommended by the manufacturer: β-catenin (Millipore), NFAT1 (Cell Signaling), pan-Akt (Cell Signaling), phospho-Akt (Ser473, Cell Signaling), TATA-binding protein (TBP, Abcam), and α-tubulin (Developmental Studies Hybridoma Bank). Horseradish peroxidase-conjugated secondary antibodies (Millipore) were used and chemiluminescence (Pierce) visualized the immunoreactive proteins.

Luciferase Assay. For the NF-κB luciferase assay, cultured nHACs were infected with lenti-Wnt7a-GFP or lenti-GFP (control) as described above. Three days later, the cells were co-transfected with a six-copy NF-κB element-driven luciferase reporter construct (Dr. Gail Sonenshein, Tufts University) and a Renilla luciferase internal control using X-tremeGENE HP (Roche). Twenty-four hours after transfection, the chondrocytes were

treated with 0 or 5 ng/mL IL-1β (Peprotech) for 16 hours. For the NFAT luciferase assay, 293T cells were co-transfected with an NFAT luciferase reporter construct (Dr. Chi-Wing Chow, Albert Einstein College) and a Renilla luciferase internal control using X-tremeGENE HP (Roche). Twenty-four hours after transfection, the cells were treated with 0 or 2 μM ionomycin (Sigma) (as a positive control for inducing the NFAT luciferase reporter) and 0, 4, or 20 μM INCA-6 (Tocris) for 16 hours. For both experiments, luciferase activity was then measured using the Dual-Glo Luciferase Assay System (Promega) and a 1450 MicroBeta Trilux Luminescence Counter (PerkinElmer). Firefly luciferase activity was normalized to the Renilla luciferase activity to calculate the relative luciferase units (RLUs).

Experimental Animals. All animal care and experimental procedures were approved by the Institutional Animal Care and Use Committees at Tufts University. Wild-type CD1 male mice were purchased from Charles River Laboratories. All mice were caged in groups under standard conditions.

Surgical Model of OA in Mice. Destabilization of the medial meniscus (DMM) surgery was performed on 7 week old CD1 male mice according to the established protocol [64, 77]. Briefly, under isoflurane anesthesia, the right knee joint was opened along the medial border of the patellar ligament and the medial meniscotibial ligament (MMTL) was severed. Sham surgery, where the MMTL was visualized but not severed, was performed on the left knee of the same mice as an internal control. Mice were allowed unrestricted cage exercise post surgery.

***In Vivo* Lentiviral Treatment.** On days 7 and 14 post DMM surgery, 5 μL of lenti-Wnt7a-GFP or lenti-GFP with a titer of $5x10^7$ IFU was directly injected through the patellar ligament into the mouse knee joint cavity using a 30G needle. Both knee joints of each mouse were injected with the same lentivirus.

Murine Tissue Samples for RNA Analysis. Wild type mice were euthanized 8 weeks after DMM surgery for articular cartilage qPCR mRNA analysis and mice with lenti-Wnt7a-GFP and lenti-GFP injected knees were euthanized 4 weeks after DMM surgery for articular cartilage microarray mRNA analysis. Immediately after euthanasia, the knee joints were opened and the soft tissue surrounding the joints was removed. Articular cartilage from the tibial plateau was detached using a scalpel and immediately placed into lysis buffer (Qiagen). Three mice per group were used.

Histological Analysis. Mice treated with lenti-Wnt7a-GFP or lenti-GFP after DMM surgery were then euthanized at 5 or 7 weeks post DMM surgery. For histological joint analysis, 6 mice/group were used for a total of 24 mice. Knee joints were isolated and fixed in 4% paraformaldehyde for 24 hours, decalcified in 10% EDTA for 1 week, and then embedded in paraffin. 5 μm serial sections were cut sagittally across the femorotibial joint. Sections every 40 μm were stained with 0.1% safranin O and counterstained with hematoxylin for examination of articular cartilage damage and other joint changes after DMM surgery. Safranin O histology of sham surgery samples was also analyzed to confirm that none of the groups had increased joint damage at baseline. To quantify observed cartilage damage, 9 stained sections from each sample were pooled, randomized

and blindly scored for cartilage damage using the established Articular Cartilage Structure (ACS) scoring system [129]. The femur and tibia were scored separately and added together to calculate a total joint score for each section. The sections were blindly analyzed for three additional OA histological parameters, tibial chondrocyte cell loss, tibial chondrocyte cell number, and osteophyte maturity, according to established methods [43, 129, 130]. Additional serial sagittal sections were stained using 0.1% sirius red diluted in saturated picric acid (i.e. picrosirius red staining) to evaluate ECM collagen fibril thickness and orientation.

Light Microscopy. Bright field and fluorescent images were taken using an Olympus IX-71 microscope and an Olympus DP70 digital camera. Polarized light images were taken using an Axioscope 2 plus microscope (Zeiss) equipped with a polarizer and the Axio Imager system (Zeiss). The optical parameters for each microscope and the camera exposure time were kept constant between samples of the same experiment.

Picrosirius Red Quantification. Using the images of the picrosirius red stained joints, the center 20% of the tibial articular cartilage surface was segmented out using ImageJ (NIH) and placed on to a white background for analysis. A program developed by Dr. Ming Zhang from the Department of Rheumatology at Tufts Medical Center was used to determine the number of black, yellow, and green pixels in the segmented area, as well as the total number of pixels. These values were used to calculate what percentage of the segmented area contained black, yellow, and green stained collagen fibers. The percentage of black fibers was defined as the amount of unorganized or absent collagen

fibers in the center of the tibial articular cartilage, while the percentage of yellow and green fibers was defined as the amount of organized collagen fibers in the center of the tibial articular cartilage.

Immunohistochemistry. For immunohistochemistry (IHC) analysis of Wnt7a and GFP expression, heat-induced antigen retrieval in 10mM citric acid buffer was performed. For Collagen II IHC analysis, enzymatic antigen retrieval was performed using 0.3% hyaluronidase and 0.15% trypsin (Invitrogen) at 37°C. Sections were incubated with the following primary antibodies overnight at 4°C: Wnt7a (Santa Cruz), GFP (Abcam), Collagen II (Abcam). After washing, sections were treated with the following secondary antibodies: Wnt7a staining – donkey anti-goat IgG (H+L) secondary antibody Texas Red conjugate (Jackson) or a biotin-conjugated secondary antibody (Vector) for chromogenic staining; Collagen II staining - goat anti-rabbit IgG (H+L) secondary antibody, Alexa Fluor® 594 conjugate (Invitrogen); GFP - goat anti-chicken IgY (H+L) secondary antibody, Alexa Fluor® 488 conjugate (Invitrogen). Fluorescent sections were counterstained with DAPI. The Vectastain Elite ABC Kit (Vector) was used for chromogenic staining. Sections incubated without the primary antibody served as negative controls for each round of staining.

Near Infrared Fluorescence (NIRF) *In Vivo* Imaging and Data Analysis. For *in vivo* NIRF imaging, 7 mice/group were imaged at 5 and 7 weeks post DMM. To begin, the hair of the mouse hind limb was removed to reduce autofluorescence. Immediately prior to probe injection, the mice were anesthetized and imaged using the IVIS-200 Imaging

System (PerkinElmer) with the Cy5.5 filter set (excitation: 615-665 nm, emission: 695-770) for a background reading. Then, under isoflurane anesthesia, 4 μL of 13.3 nmol MMPSense680 (PerkinElmer) was directly injected through the patellar ligament into the knee joint cavity using a 30G needle. The mice were then allowed unrestricted cage exercise for two hours. After two hours, mice were again anesthetized with isoflurane and an approximately 1.5 cm skin incision was created directly over the patellar ligament of each knee to allow imaging without skin overlying the joint. Fluorescence images were then acquired again using the IVIS-200 Imaging System with the Cy5.5 filter set [77].

Fluorescence signal intensity of the NIRF data was measured using Living Image software (PerkinElmer). A region of interest (ROI) was drawn over each knee joint to quantify the average fluorescent signal intensity, measured in radiance efficiency, collected over each knee joint in the raw image. The size and shape of the region of interest was kept constant for all knees analyzed. The background fluorescence signal intensity of each mouse knee was measured from the background image taken immediately prior to probe injection and subtracted from the raw data for each knee joint to calculate the average radiance efficiency for each knee. The measured average radiance efficiency of the DMM knee was divided by the measured average radiance efficiency of the sham knee to internally calibrate each image.

Micro-Computed Tomography (Micro-CT). For micro-CT analysis, 6 mice/group were scanned using the Skyscan 1176 micro-CT scanner (Bruker) at 7 weeks post DMM. The x-ray source was set to a voxel size of 9 μM at 50 kV and 200μA. A beam filtration

0.5mm aluminum filter was used and data was recorded every 1° for a total of 180°. Images slices were reconstructed using NRecon software (Bruker) and the 3D data analysis was performed using CTAnalyzer software (Bruker).

The epiphysis of the tibia was manually chosen as the ROI for 3D analysis of the subchondral bone. For subchondral trabeculae, the following parameters were calculated: trabecular bone volume fraction (BV/TV), which represents the ratio of the trabecular bone volume (BV) to the endocortical tissue volume (TV), subchondral bone tissue volume, trabecular thickness, and trabecular separation. The osteophytes were then manually chosen as an ROI to measure osteophyte volume. Thickness of the medial and lateral subchondral bone plates was determined using the same algorithm used for analyzing trabecular thickness.

Microarray Data and Analysis. RNA samples were isolated from the tibial articular cartilage of lenti-Wnt7a-GFP and lenti-GFP infected DMM knee joints 4 weeks after DMM surgery. RNA samples from 3 mice per group were pooled for microarray analysis. The amount and quality of the RNA from the pooled samples was determined using the 2100 Bioanalyzer system (Agilent). The RNA integrity numbers obtained were 7.1 (lenti-GFP) and 6.7 (lenti-Wnt7a-GFP). RNA-seq libraries were then prepared, sequenced, and analyzed by the Tufts University Genomics Core Facility. Library preparation was performed using the Ovation RNA-Seq system (NuGen) and single-end sequencing was accomplished using a HiSeq 2500 (Illumina). An average of 150 million 50 base reads was obtained per sample. Sequencing reports were generated with FastQC. Biological

network and functional analyses were performed using Ingenuity Pathway Analysis (IPA, Qiagen).

Statistical Analysis. Data are shown as mean ± standard error of the mean (SEM). The semiquantitative histological scoring systems were evaluated using nonparametric statistical analyses. All other experiments were evaluated with a Student's t-test or analysis of variance (ANOVA) with post-hoc tests for pairwise comparisons. Spearman correlation was used for correlation analyses. Outliers were only removed when statistical significance was acquired using the Grubb's test. A p value of less than 0.05 was considered significant in all cases.

3.2 Results

3.2.1 Wnt7a is downregulated in human OA cartilage and inversely correlated with catabolic gene expression

To establish the relevancy of Wnt7a in OA, I first tested Wnt7a gene expression in human OA cartilage samples from joint replacement surgeries and non-OA cadaveric controls. In a prior study using these specimens, our lab has demonstrated higher levels of catabolic genes and lower levels of anabolic genes in the OA samples [140]. Here, when I analyzed Wnt7a gene expression, I found that Wnt7a was significantly reduced in the

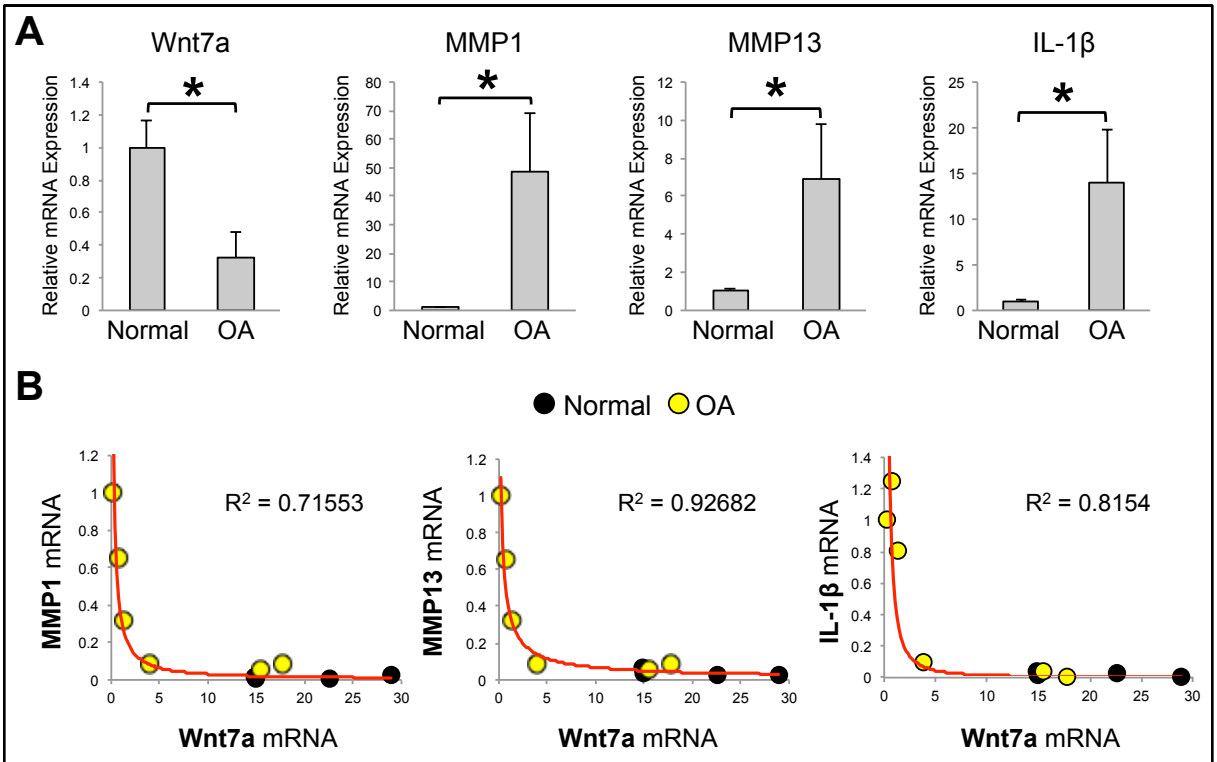

Figure 3.1. Wnt7a mRNA expression is reduced in human OA and inversely correlated with catabolic gene expression. A. RT-PCR analysis of Wnt7a and MMP1, MMP3 and IL-1β gene expression in tibial cartilage specimens isolated from normal cadaveric and OA patients with the following age/sex. Normal: 84/M, 75/M, 65/F, and 49/F. OA: 53/F, 63/F, 65/F, 72/M, 73/F, 73/M. **B.** Correlation analysis of Wnt7a mRNA expression with catabolic gene expression in normal cadaveric and OA patient samples. Data points from the six OA samples scatter toward the left of the graphs (yellow dots), and those from the four normal samples are scattered to the right of the graphs (black dots), with two of the normal sample points overlapping with one another. All correlation analyses were statistically significant.

human OA samples compared to healthy controls, thus exhibiting an opposite trend from MMP1, MMP13, and IL-1β expression (Fig. 3.1A). When the expression of Wnt7a was compared to that of catabolic genes in each sample, including both the normal and OA cartilage specimens, a striking inverse correlation emerged (Fig. 3.1B). I found that the higher the expression of Wnt7a, the lower the expression of MMP1, MMP13, and IL-1β. Vice versa, the lower the expression of Wnt7a, the higher the expression of MMP1, MMP13, and IL-1β. Interestingly, this correlation was not linear. Apparently, when

Wnt7a expression surpassed a certain level, it was correlated with a dramatic decrease in the catabolic gene expression, and these samples tended to be the normal cartilage specimens. When Wnt7a expression fell below this level, it was correlated with a dramatic increase in catabolic gene expression, and these samples tended to be the OA specimens (Fig. 3.1B). More specimens, especially those representing early to moderate OA, are needed to elucidate whether Wnt7a expression is correlated with the extent of OA severity.

3.2.2 Wnt7a inhibits IL-1β induced catabolic gene expression in human articular chondrocytes in vitro

Because of the inverse correlation between Wnt7a and the catabolic genes MMP1, MMP13, and IL-1β in human cartilage, I directly tested the role of Wnt7a in an established *in vitro* system where the pro-inflammatory cytokine IL-1β is used to induce chondrocyte catabolic gene expression *in vitro* [128, 140, 142]. Wnt7a was introduced to cultured normal primary human articular chondrocytes (nHACs) by viral expression. A commercially available lentivirus encoding human Wnt7a with a separate GFP module (lenti-Wnt7a-GFP) was used, and a lentivirus encoding GFP alone (lenti-GFP) served as a control. I first confirmed that these viruses resulted in Wnt7a and GFP ectopic expression in chondrocytes *in vitro* (Fig. 3.2A). I then analyzed gene expression upon Wnt7a and IL-1β treatment. IL-1β induced the expression of multiple MMPs, inducible nitric oxide synthase (iNOS), collagen X, and IL-1β itself. Significantly, Wnt7a ectopic expression led to a dramatic inhibition of the IL-1β-induced upregulation of all these

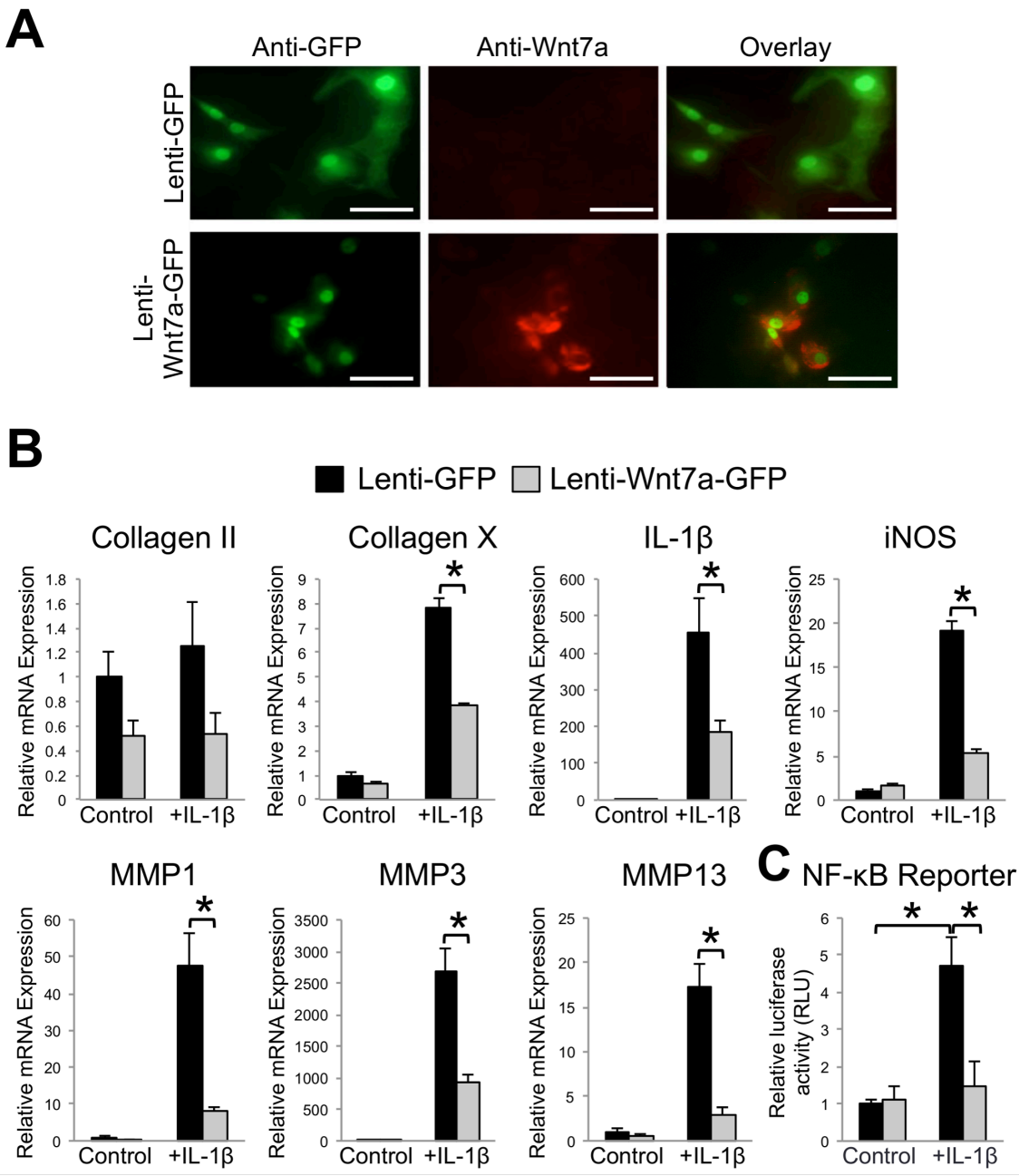

Figure 3.2. Wnt7a ectopic expression reduces IL-1β induced upregulation of OA-related genes and NF-κB activity in human chondrocytes *in vitro*. A. Representative images of Wnt7a IF analysis of normal human articular chondrocytes (nHACs) after infection with lenti-GFP or lenti-Wnt7a-GFP. Wnt7a immunofluorescence images were overlaid with GFP expression. Scale bars = 100 μm. **B.** RT-PCR analysis of nHACs gene expression after infection with lenti-GFP or lenti-Wnt7a-GFP with or without IL-1β (5 ng/mL). Lenti-Wnt7a-GFP viral infection significantly reduced IL-1β upregulation of Collagen X, IL-1β, iNOS, and several MMPs. **C.** NF-κB luciferase assay of NF-κB activity after infection with lenti-GFP or lenti-Wnt7a-GFP and treatment with or without IL-1β (5 ng/mL). Relative luciferase activity in reference to Renilla luciferase internal control is shown. * = $p < 0.05$.

genes (Fig. 3.2B). There was no significant effect on collagen II mRNA expression by IL-1β or Wnt7a.

To investigate how Wnt7a was inhibiting the IL-1β induction of these genes, I examined NF-κB activation in these samples by evaluating an NF-κB luciferase reporter, as NF-κB is a key mediator of IL-1β activity [143-145]. As expected, IL-1β activated the NF-κB reporter (Fig. 3.2C) [128, 140]. However, treatment with the Wnt7a lentivirus inhibited IL-1β-induced NF-κB reporter activity, indicating that Wnt7a inhibited NF-κB activity.

3.2.3 Wnt7a inhibits joint cartilage destruction in vivo

To test whether Wnt7a can inhibit joint damage *in vivo*, I utilized the destabilization of the medial meniscus (DMM) model, which is a well established joint-injury OA mouse model [64, 77]. I first evaluated Wnt7a mRNA expression in the DMM cartilage vs. the sham joint and found that Wnt7a was decreased upon DMM surgery (Fig. 3.3A), which is consistent with my observation using human OA cartilage specimens. Furthermore, I also observed that treatment with lentiviral Wnt7a (i.e. lenti-Wnt7a-GFP) inhibited IL-1β-induced MMPs and iNOS in murine chondrocytes (Fig. 3.3B), which is also consistent with my data using human articular chondrocytes.

Having observed consistent effects of Wnt7a on human and mouse chondrocytes *in vitro*, I evaluated the effect of Wnt7a *in vivo* by intraarticularly injecting lenti-Wnt7a-GFP or lenti-GFP at 1 and 2 weeks post DMM surgery. When their expression was evaluated at

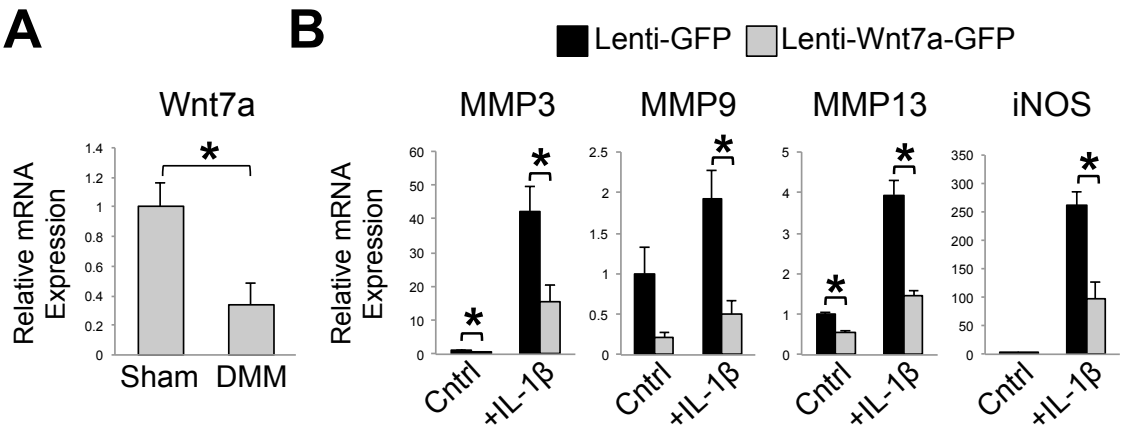

Figure 3.3. Wnt7a ectopic expression reduces IL-1β induced upregulation of OA-related genes in murine chondrocytes *in vitro*. A. RT-PCR analysis of Wnt7a gene expression in tibial cartilage specimens isolated from mouse knees 8 weeks post DMM or sham surgery. A reduced Wnt7a gene expression was observed in the DMM knees compared to sham controls. **B.** RT-PCR analysis of MMP3, MMP9, MMP13 and iNOS gene expression in murine chondrocytes infected with lenti-GFP or lenti-Wnt7a-GFP and cultured with or without IL-1β (5ng/mL). * = $p < 0.05$.

five weeks post surgery, I found that lenti-GFP had infected chondrocytes in the superficial and deeper zones of the articular cartilage, as well in the meniscus (Fig. 3.4A). No evidence of viral infection of the subchondral bone was seen. Additionally, Wnt7a IHC indicated that while endogenous Wnt7a is present in the articular cartilage and meniscus, lenti-Wnt7a-GFP treatment resulted in significantly higher Wnt7a protein expression in the joint cartilage (Fig. 3.4B).

Safranin O staining revealed that articular cartilage damage was evident in lenti-GFP-infected joints at both 5 and 7 weeks post surgery. Strikingly, the damage was greatly diminished in lenti-Wnt7a-GFP infected knees (Fig. 3.4C). This was further confirmed by blinded quantification of the observed histological damage using the articular cartilage structure (ACS) scoring system (Fig. 3.4D). My histological analysis also revealed that

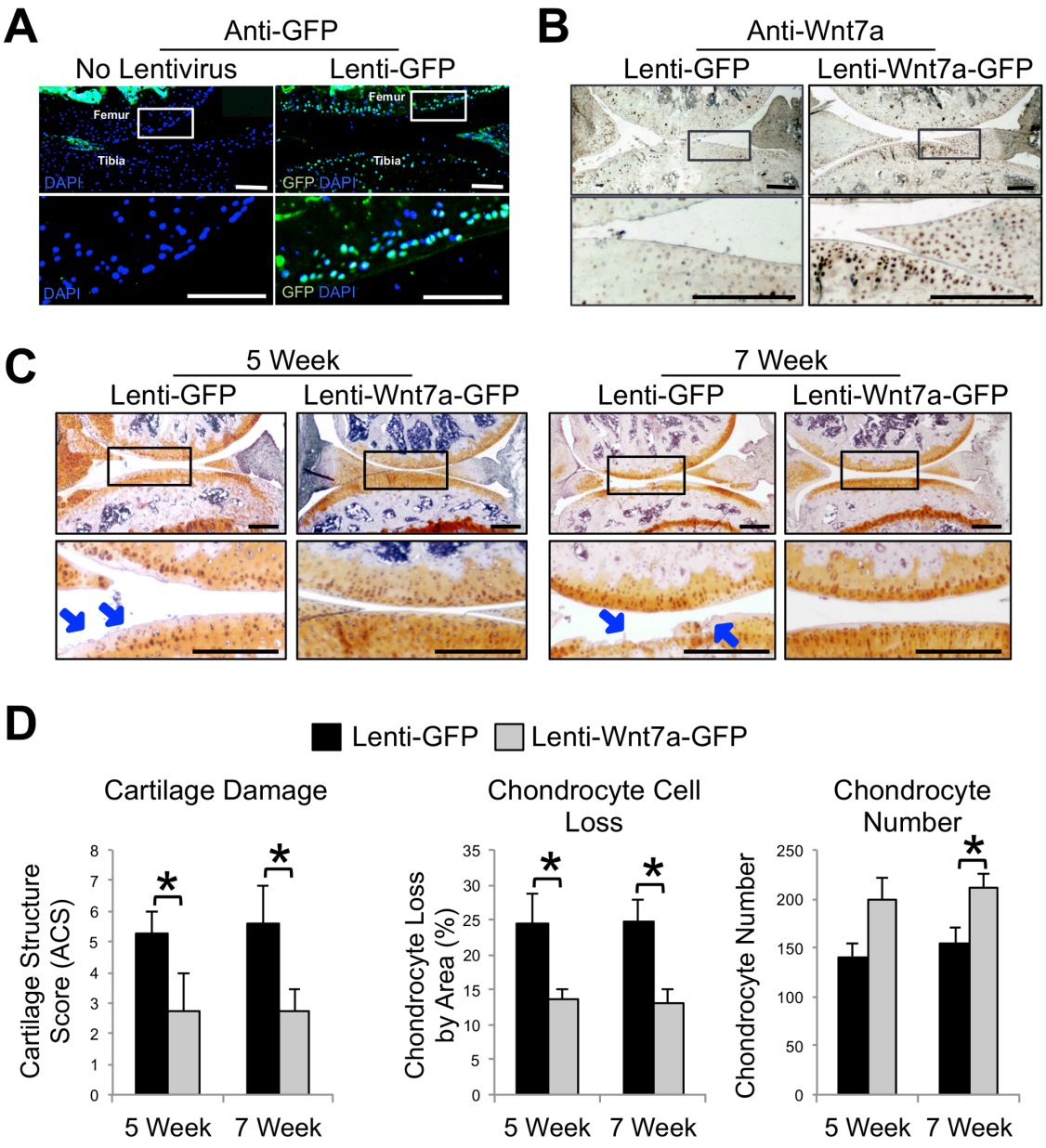

Figure 3.4. Wnt7a ectopic expression prevents cartilage damage in the DMM OA model *in vivo*. A. Representative images of GFP immunofluorescence (IF) analysis of mouse knee joints 5 weeks post DMM surgery with or without lenti-GFP joint infection. Rectangles denote areas shown in higher magnification. Both the superficial and deeper zones of the articular cartilage were infected. **B.** Representative images of Wnt7a IF analysis in mouse knees injected with lenti-GFP or lenti-Wnt7a-GFP at 5 weeks post DMM surgery. Rectangles denote areas shown in higher magnification. Wnt7a IF confirmed ectopic expression of Wnt7a. **Continued on next page.**

Figure 3.4 continued. C. Representative images showing safranin O/hematoxylin stained joint sections at 5 or 7 weeks post DMM surgery in mouse knees injected with lenti-GFP or lenti-Wnt7a-GFP. Rectangles denote areas shown in higher magnification. Arrows denote areas of articular cartilage damage. Lenti-GFP control knees showed significantly more cartilage damage compared to knees ectopically expressing Wnt7a. **D.** Cartilage structure scoring (ACS), chondrocyte loss and chondrocyte numbers in the tibia were quantified at 5 or 7 weeks post DMM in mouse knees injected with lenti-GFP or lenti-Wnt7a-GFP. Scale bars = 250 μm. * = $p < 0.05$.

the Wnt7a knee joints had a significant reduction in chondrocyte cell loss, and subsequently a higher chondrocyte number, compared to GFP controls [43, 129] (Fig. 3.4D). These results strongly indicate that Wnt7a treatment after the onset of OA can preserve articular cartilage against cartilage matrix damage and cell loss.

As the basic dye safranin O does not reflect changes in the principle collagen in cartilage (collagen II), I performed collagen II IHC on the Wnt7a and GFP DMM samples. However, no differences were found among the treatment groups (Fig. 3.5A). In addition, no reduction of collagen II staining was observed in the DMM vs. sham samples, which is not unexpected as significant changes in collagen II protein expression at early time points in the DMM model are rarely reported. It is possible that collagen II fibers had started the degradation process, but IHC is not sensitive enough to detect subtle changes in collagen fiber unwinding or organization that occur at early time points.

I then used picrosirius red staining to determine if subtle differences in collagen fiber architecture were occurring, as picrosirius red staining can be used to detect collagen fiber thickness and orientation when viewed under polarized light. In this staining method, thick organized collagen fibers stain red and thin organized collagen fibers stain yellow

and green, while disorganized collagen fibers of any thickness do not stain at all. I found that picrosirius red staining did potentially indicate a difference between the lenti-GFP and lenti-Wnt7a-GFP groups in collagen fiber organization in the center of the tibia (Fig. 3.5B), however the observable differences were small. To better quantify this potential difference, I performed a semi-quantitative analysis of the picrosirius red stained joint images where pixels were sorted and quantified by color. As disorganized fibers do not show picrosirius red staining under polarized light, the black pixels were defined as disorganized or absent collagen fibers, while the green and yellow pixels were defined as organized collagen fibers. With this semi-quantitative analysis, I found that collagen organization in the center of the tibia in the 5 week GFP and Wnt7a knees was comparable; however, there was significantly more organized collagen in the lenti-Wnt7a-GFP group compared to GFP controls at the 7 week time point (Fig. 3.5B).

As MMP activities have been shown to be upregulated in OA and cause collagen fiber degradation [60, 61, 146], I investigated whether treatment with Wnt7a affected the activities of MMPs in the joint by using near infrared fluorescence (NIRF) live imaging. For NIRF imaging, I used the fluorescent probe MMPSense680, which contains a consensus-MMP cleavage site and is thus activated by multiple MMPs, including MMP13, MMP9 and MMP3 [77, 147]. In the presence of active MMPs, cleavage of this probe causes the emission of fluorescence that falls into the near infrared range [70, 148]. Thus the intensity of the collected fluorescence image is a real-time read out of overall MMP activity. I have previously shown that the DMM/sham MMPSense680 fluorescence emission ratio reflects the trajectory of joint destruction in the DMM OA model [77].

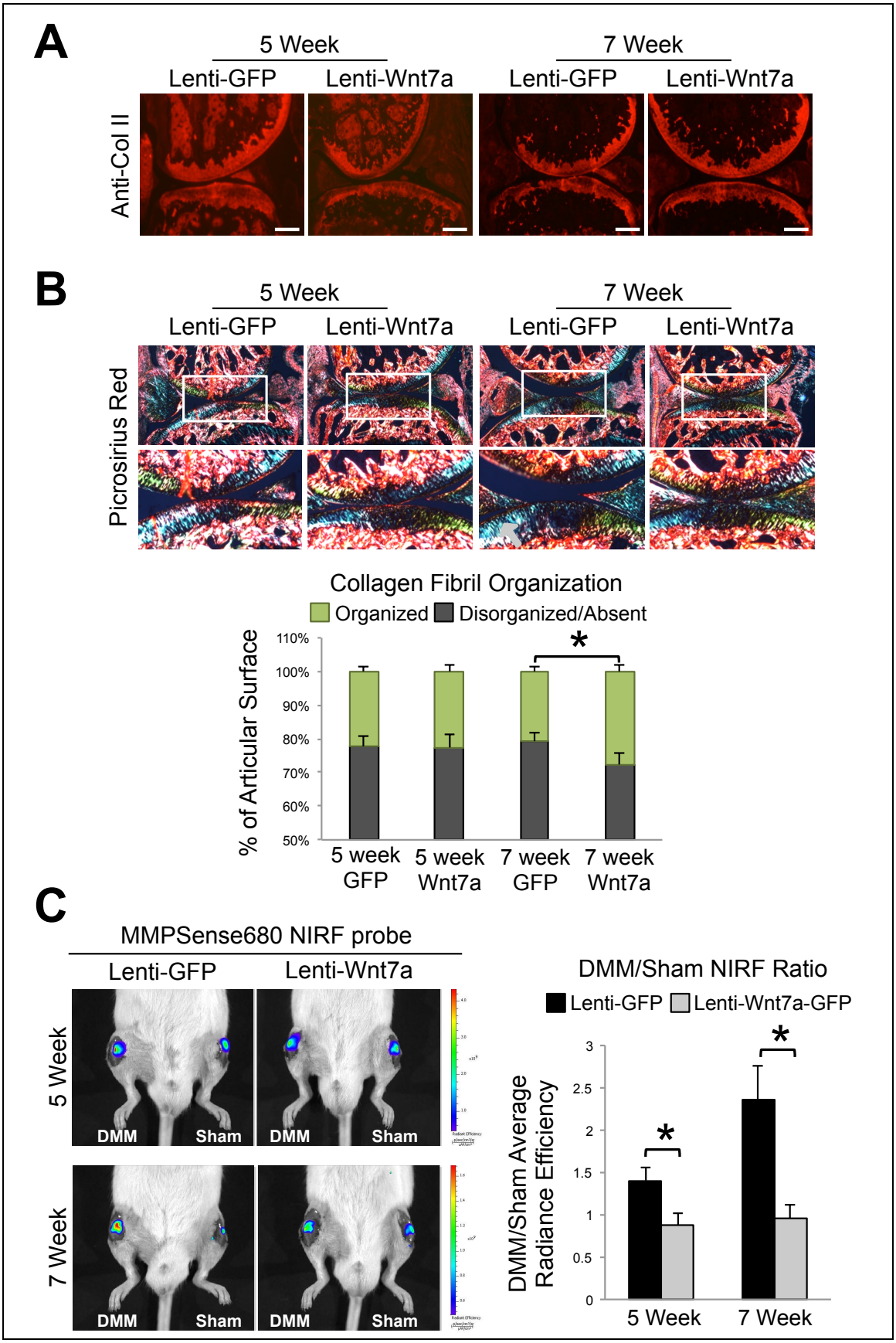
A
5 Week
7 Week
Lenti-GFP
Lenti-Wnt7a
Lenti-GFP
Lenti-Wnt7a
Anti-Col II
B
5 Week
7 Week
Lenti-GFP
Lenti-Wnt7a
Lenti-GFP
Lenti-Wnt7a
Picrosirius Red
Collagen Fibril Organization
Organized
Disorganized/Absent
% of Articular Surface
110%
100%
90%
80%
70%
60%
50%
*
5 week GFP
5 week Wnt7a
7 week GFP
7 week Wnt7a
C
MMPSense680 NIRF probe
Lenti-GFP
Lenti-Wnt7a
5 Week
7 Week
DMM
Sham
DMM
Sham
DMM
Sham
DMM
Sham
DMM/Sham NIRF Ratio
Lenti-GFP
Lenti-Wnt7a-GFP
DMM/Sham Average Radiance Efficiency
3
2.5
2
1.5
1
0.5
0
*
*
5 Week
7 Week

Figure 3.5. Wnt7a increases tibial collagen fiber organization and reduces joint MMP activity during OA development. A. Representative images of Collagen II IF analysis 5 or 7 weeks post DMM surgery in mouse knees injected with lenti-GFP or lenti-Wnt7a-GFP. No differences were detected among groups. **B.** Representative images and semi-quantitative analysis of picrosirius red staining showing collagen fiber thickness and organization 5 or 7 weeks post DMM surgery in mouse knees injected with lenti-GFP or lenti-Wnt7a-GFP, as viewed under polarized light. Rectangles denote areas shown in higher magnification. Arrow denotes area of decreased collagen fiber organization. Quantification revealed an increase in organized collagen fibers in the central portion of the tibia in lenti-Wnt7a-GFP mice compared to lenti-GFP controls at 7 weeks post DMM. **C.** Representative *in vivo* NIRF images taken two hours after 4 μL intraarticular injection of MMPSense680 in each knee. The average radiance efficiency emitted from each knee was quantified from the collected NIRF images and the DMM average radiance efficiency was divided by the sham average radiance efficiency to internally calibrate each signal. Quantification analysis demonstrated that mice ectopically expressing Wnt7a in the joint have reduced NIRF signals compared to lenti-GFP controls. Scale bars = 250 μm. * = $p < 0.05$.

Here, when I analyzed the images from joints injected with MMPSense680, I found that the DMM/sham signal ratio was significantly reduced in the lenti-Wnt7a-GFP treated joints at 5 weeks compared to the lenti-GFP controls (Fig. 3.5C). At 7 weeks, while the DMM/sham signal ratio in the lenti-GFP control knee joints had increased, the DMM/sham signal ratio in the lenti-Wnt7a-GFP treated joints remained low (Fig. 3.5C). Therefore, Wnt7a ectopic expression in the joint reduced MMP activities *in vivo*, which helps to explain how Wnt7a ectopic expression preserved articular cartilage integrity in OA.

It is interesting to note that while both histology and NIRF imaging revealed that Wnt7a reduced OA activity in the joint, only NIRF imaging was able to detect an increase in the OA phenotype from 5 to 7 weeks post DMM. It has been established that the DMM

model shows progressive histological joint damage over time [43, 149, 150]; however, these studies are typically only able to detect progressive changes at 4 or 8 week increments. This suggests that NIRF imaging of MMP activity may be more sensitive than traditional histology, thus allowing progressive OA joint changes to be detected at smaller time intervals.

While articular cartilage damage is a major component of OA joint degeneration, other joint structures are also affected during OA pathogenesis. For example, osteophyte formation (i.e. ectopic bone formation at the edges of the joint) and subchondral bone sclerosis can occur in OA [43, 151]. As Wnt7a attenuated articular cartilage damage during OA development *in vivo*, I examined if Wnt7a also inhibited OA-induced bone changes in the DMM mouse model. Osteophyte development was observed histologically in both the GFP and Wnt7a groups at 5 and 7 weeks post DMM surgery (Fig. 3.6A). Histological scoring for osteophyte maturity showed no differences in the maturation level of the osteophytes between groups (Fig. 3.6B). Micro-computed tomography (micro-CT) imaging was then performed to collect quantitative data on subchondral bone characteristics and osteophyte size at 7 weeks post DMM surgery (Fig. 3.6C). Multiple aspects of the subchondral bone were analyzed, including subchondral bone tissue volume (BV), subchondral bone fraction, subchondral trabecular characteristics, and medial and lateral tibial subchondral bone plate thickness. However, no significant differences were seen between the Wnt7a and GFP groups in relation to any of these values (Fig. 3.6D – F). Moreover, osteophyte size was also evaluated by micro-CT and demonstrated no difference between the Wnt7a and GFP groups (Fig. 3.6G). Therefore,

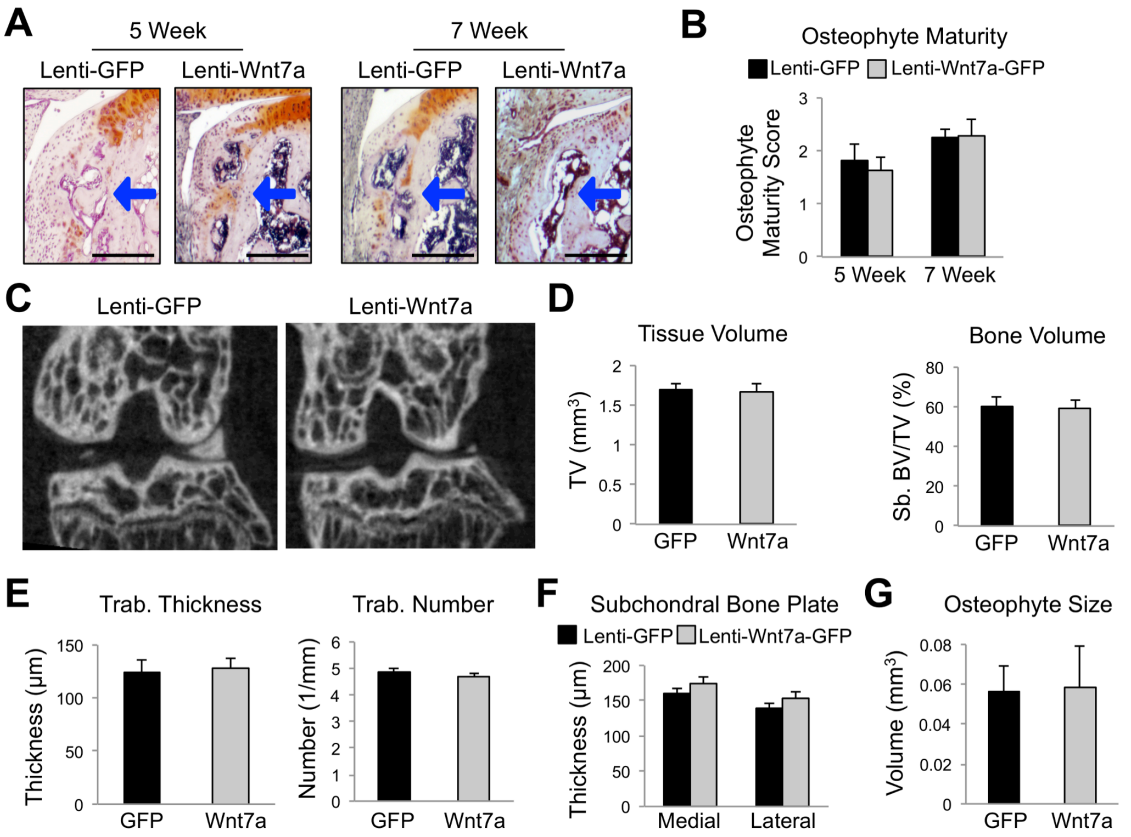

Figure 3.6. Wnt7a ectopic expression has no effect on osteophyte development or the subchondral bone. A. Representative histological images of osteophyte development with safranin O/hematoxylin staining 5 or 7 weeks post DMM surgery in mouse knees injected with lenti-GFP or lenti-Wnt7a-GFP. Arrows indicate osteophytes. Scale bars = 250 μm. **B.** Scoring of osteophyte maturity 5 or 7 weeks post DMM surgery in mouse knees injected with lenti-GFP or lenti-Wnt7a-GFP. Scoring demonstrated no difference between the lenti-GFP and lenti-Wnt7a-GFP groups. **C.** Representative micro-CT cross-sections of the tibia 7 weeks post DMM surgery in mouse knees injected with lenti-GFP or lenti-Wnt7a-GFP. **D–G.** Micro-CT was used 7 weeks post DMM surgery in mouse knees injected with lenti-GFP or lenti-Wnt7a-GFP to quantitatively measure **D.** subchondral tissue volume and bone volume fraction **E.** subchondral trabecular thickness and trabecular number **F.** medial and lateral tibial subchondral bone plate thickness and **G.** osteophyte volume. Micro-CT quantification demonstrated no differences between the lenti-GFP and lenti-Wnt7a-GFP groups.

bone-related analyses did not yield any significant differences between the GFP and Wnt7a treated groups. This could be due to the fact that no Wnt7a ectopic expression was observed in these areas.

3.2.4 Wnt7a activates both canonical and non-canonical pathways in chondrocytes

Next, I investigated the biochemical signaling pathways by which Wnt7a may be exerting its effects. Since Wnt7a has been shown to activate multiple signaling pathways, markers of these pathways were evaluated upon lenti-Wnt7a-GFP infection of human articular chondrocytes (nHACs) to see which were upregulated. I first evaluated Axin2 induction and β-catenin nuclear localization, which are key events in the Wnt canonical pathway [78]. I found that Axin2 mRNA expression and β-catenin nuclear localization were both induced by Wnt7a, suggesting that Wnt7a does activate the Wnt canonical pathway in nHACs (Fig. 3.7A, 3.7B). To determine if Wnt canonical pathway signaling is necessary for the activity of Wnt7a in nHACs, I then added DKK-1 to the nHACs ectopically expressing Wnt7a to inhibit Wnt canonical pathway activation. DKK-1 binds to the LRP co-receptor to inhibit Wnt protein activation of the Wnt canonical pathway specifically [152]. After DKK-1 treatment, I first examined Axin2 mRNA expression to confirm that DKK-1 was blocking Wnt canonical pathway induction by Wnt7a. Unexpectedly, my result demonstrated that DKK-1 treatment at 250ng/mL did not block Wnt7a-induced Axin2 expression (Fig. 3.7C), even though DKK-1 at the same concentration was able to inhibit Wnt3a-induced Axin2 expression in the same cells (Fig. 3.7D) [89, 128]. Accordingly, I found that DKK-1 treatment did not have an effect on the Wnt7a

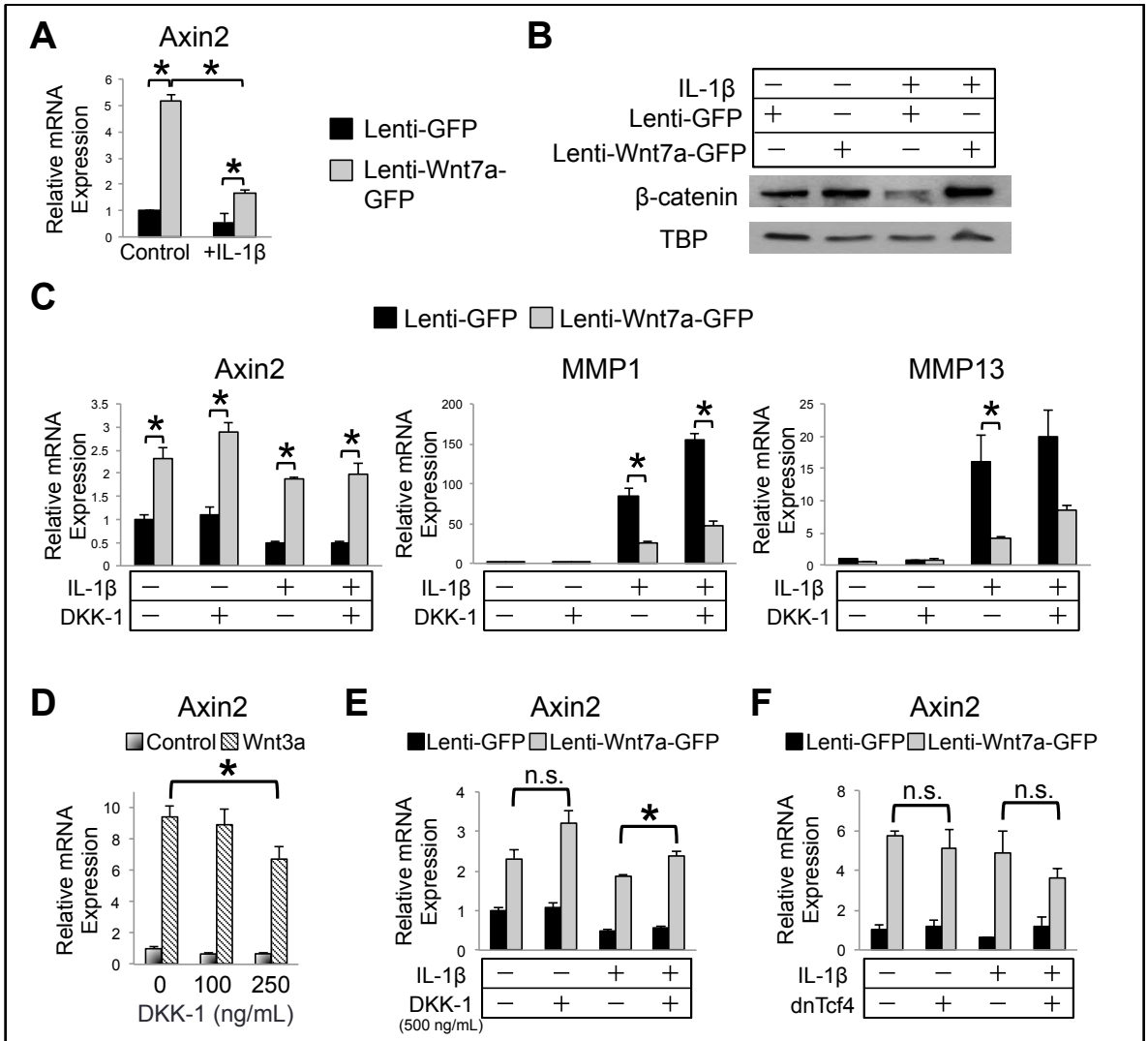

Figure 3.7. Inhibition of canonical Wnt signaling with DKK-1 does not diminish Wnt7a's inhibition of IL-1β activity in human chondrocytes. A. RT-PCR analysis of Axin2 mRNA expression in nHACs after infection with lenti-GFP or lenti-Wnt7a-GFP, and cultured with or without IL-1β (5 ng/mL). **B.** Western blot analysis of nuclear β-catenin in nHACs after infection with lenti-GFP or lenti-Wnt7a-GFP in the presence or absence of IL-1β (5 ng/mL). TATA-binding protein (TBP) served as a loading control. **C.** RT-PCR analysis of Axin2, MMP1 and MMP13 after treatment with DKK-1 (250 ng/mL), on nHACs infected with lenti-GFP or lenti-Wnt7a-GFP, and cultured with or without IL-1β (5 ng/mL). **D.** RT-PCR analysis of Axin2 mRNA expression in nHACs cultured in Wnt3a or control conditioned media, in the presence of 0, 100, or 250 ng/mL DKK-1 for 2 days. Axin2 induction by Wnt3a was inhibited by DKK-1 in a dose-dependent manner. **E.** RT-PCR analysis of Axin2 mRNA expression in nHACs infected with lenti-GFP or lenti-Wnt7a-GFP with or without a higher level of DKK-1 (500 ng/mL) for 2 days. Axin2 induction by Wnt7a was unaffected by DKK-1 when IL-1β was not added, and was even increased when IL-1β (5ng/mL) was added. **Continued on next page.**

Figure 3.7 continued. F. RT-PCR analysis of Axin2 mRNA expression in nHACs infected with lenti-GFP or lenti-Wnt7a-GFP, with or without dominant negative Tcf4 lentivirus (lenti-dnTcf4), and cultured with or without 5 ng/mL IL-1β for 2 days. Lent-dnTcf4 also did not significantly affect the Wnt7a induction of Axin2 mRNA expression. * = $p < 0.05$. n.s. = not significant.

inhibition of IL-1β-induced MMP1 and MMP13 expression (Fig. 3.7C). On the other hand, DKK-1 treatment did enhance overall MMP1 expression under IL-1β treatment (Fig. 3.7C). These results suggest that canonical signaling may be inhibitory towards IL-1β, but it is not essential for Wnt7a-mediated inhibition of catabolic gene expression. In addition, I confirmed that high dose treatment with DKK-1 at 500ng/mL did not have an effect on the Wnt7a upregulation of Axin2 (Fig. 3.7E) and a dominant-negative Tcf4 did not block the Wnt7a upregulation of Axin2 expression either (Fig. 3.7F), suggesting that Wnt7a may induce Axin2 using an alternative mechanism from traditional canonical signaling.

I then tested the non-canonical pathways. Because Wnt7a has been shown to activate the Akt pathway in muscle and rabbit chondrocytes [85, 101], I evaluated Akt phosphorylation by performing Western blot analysis. My data indicated that lenti-Wnt7a-GFP treatment led to Akt phosphorylation in nHACs as well (Fig. 3.8A). To determine whether Wnt7a inhibits IL-1β through the Akt pathway, I used a well-established Akt inhibitor AZD5363 to block Akt signaling in the nHACs ectopically expressing Wnt7a [153, 154]. Similar to the case of DKK-1, administering the Akt inhibitor significantly increased MMP1 and MMP13 expression induced by IL-1β, but it did not block Wnt7a's ability to inhibit IL-1β activity (Fig. 3.8B). Therefore, Akt

signaling may be inhibitory to IL-1β, but it is not required for Wnt7a's ability to inhibit IL-1β induction of MMPs, despite being activated by Wnt7a.

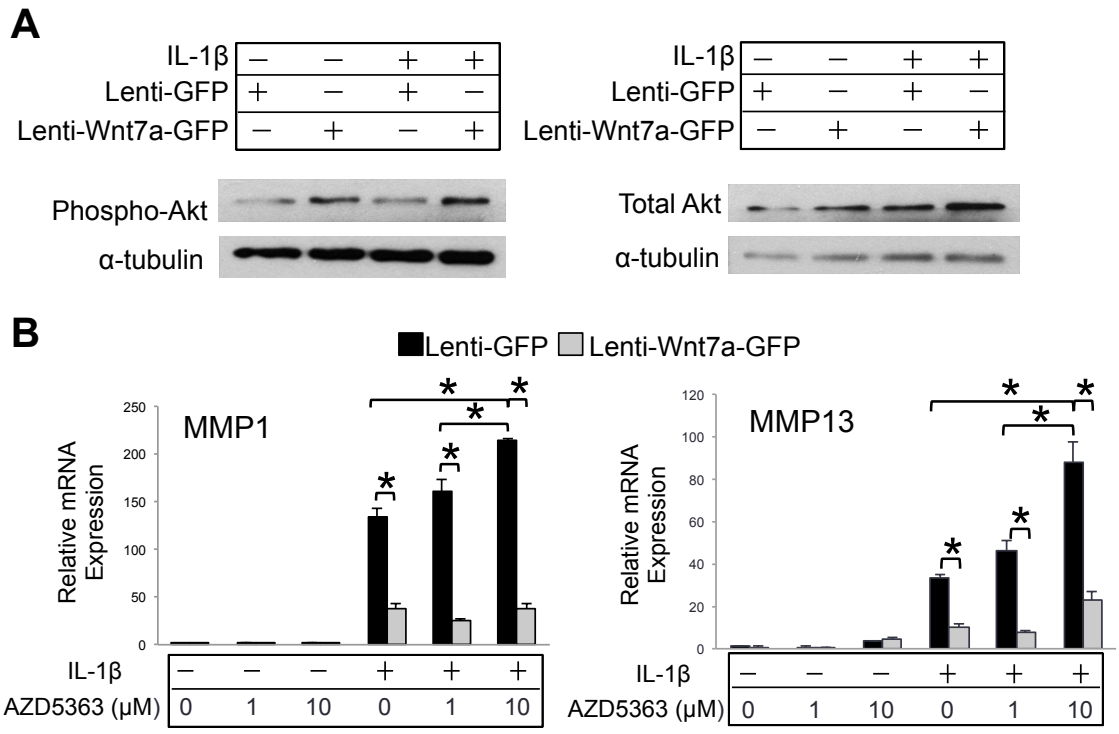

Figure 3.8. Inhibition of Akt signaling does not diminish Wnt7a's inhibition of IL-1β activity in human chondrocytes. A. Western blot analysis of Akt protein expression after nHACs were infected with lenti-GFP or lenti-Wnt7a-GFP and cultured with or without IL-1β (5ng/mL). Results demonstrated that phosphorylated Akt was upregulated with Wnt7a ectopic expression compared to lenti-GFP controls. **B.** RT-PCR analysis of MMP1 and MMP13 gene expression after treatment with Akt inhibitor AZD5363 (1 or 10 μM) on nHACs infected with lenti-GFP or lenti-Wnt7a-GFP and cultured in the presence of absence of IL-1β (5 ng/mL). * = $p < 0.05$.

NFAT signaling is another noted component of Wnt non-canonical signaling, as it one of the mediators of the calcium pathway [86]. I found that Wnt7a induced NFAT1 mRNA expression and NFAT nuclear localization in nHACs (Fig. 3.9A, 3.9B). To determine if NFAT signaling was necessary for Wnt7a action, I applied a well-established NFAT inhibitor INCA-6, which I confirmed to have the ability to inhibit an NFAT luciferase

reporter (Fig. 3.9C), to nHACs ectopically expressing Wnt7a. Significantly, I found that while lenti-Wnt7a-GFP inhibited IL-1β-induced MMP1 expression, it was not able to do so when INCA-6 was added (Fig. 3.9D). In terms of MMP13 expression, in the presence of INCA-6, IL-1β-induced MMP13 expression was much reduced, but Wnt7a did not further inhibit IL-1β-induced MMP13 expression (Fig. 3.9D). Therefore, administration of INCA-6 abolished the differences in MMP1 and MMP13 expression between the lenti-Wnt7a-GFP and lenti-GFP groups under IL-1β treatment (Fig. 3.9D). This data suggests that Wnt7a's inhibition of IL-1β in chondrocytes requires NFAT signaling. It is worth noting that INCA-6 by itself increased basal levels of MMP1 expression in the absence of IL-1β, but inhibited MMP expression in the presence of IL-1β (Fig. 3.9). It is unclear why this is the case, but perhaps a moderate level of NFAT signaling is optimal for chondrocytes.

3.2.5 NFAT and Wnt canonical signaling act synergistically in chondrocytes treated with IL-1β

Since the canonical and non-canonical Wnt signaling pathways are known to crosstalk with one another, and Wnt7a induced both types of pathways, I applied both the NFAT inhibitor INCA-6 and the canonical Wnt pathway inhibitor DKK-1 to the nHACs ectopically expressing Wnt7a. As expected, INCA-6 prevented Wnt7a's ability to inhibit IL-1β-induced MMP1 expression (Fig. 3.9E). Significantly, combinatorial treatment of INCA-6 and DKK-1 resulted in an additional increase in MMP1 expression compared with INCA-6 treatment alone (Fig. 3.9E). Therefore while DKK-1 alone is not sufficient

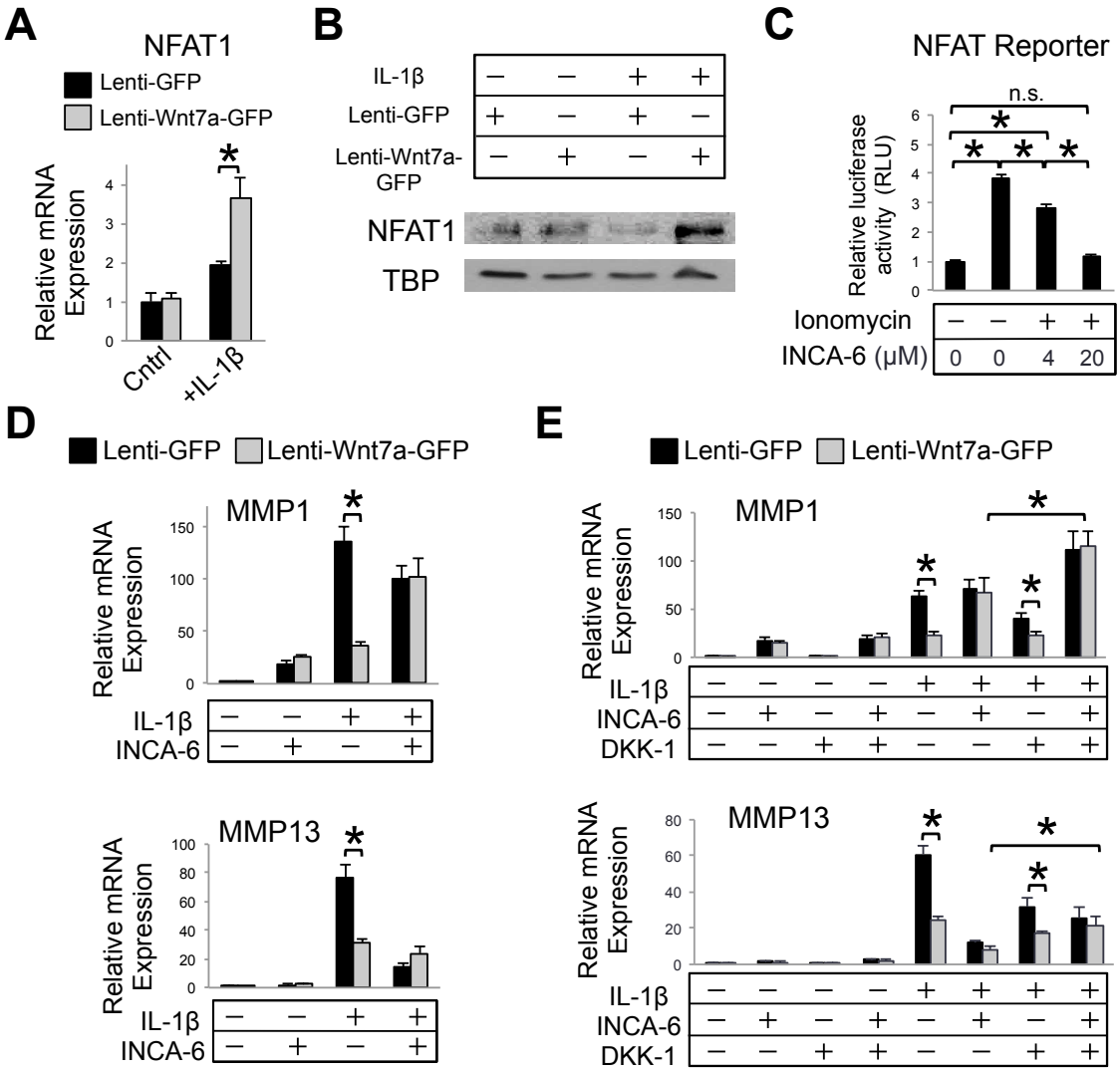

Figure 3.9. Inhibition of NFAT signaling attenuates the effect of Wnt7a on MMP inhibition in human chondrocytes. A. RT-PCR analysis of NFAT1 gene expression in nHACs after infection with lenti-GFP or lenti-Wnt7a-GFP, and cultured with or without IL-1β (5 ng/mL). NFAT1 expression was upregulated with Wnt7a ectopic expression in the IL-1β group only. **B.** Western blot analysis of nuclear NFAT1 protein expression after nHACs were infected with lenti-GFP or lenti-Wnt7a-GFP and cultured with or without IL-1β (5ng/mL). TBP served as a loading control. **C.** NFAT luciferase reporter assay in 293T cells at 16 hours after treatment with or without 2 μM of ionomycin and 0, 4, or 20 μM of INCA-6. INCA-6 significantly reduced ionomycin activation of NFAT luciferase activity in a dose dependent manner. **D.** RT-PCR analysis of MMP1 and MMP13 after treatment with 20 μM of INCA-6, on nHACs infected with lenti-GFP or lenti-Wnt7a-GFP and treated with or without 5 ng/mL IL-1β for 2 days. INCA-6 treatment completely eliminated the difference in MMP expression between the Wnt7a and GFP groups after IL-1β treatment. **E.** RT-PCR analysis of MMP1 and MMP13 gene expression after treatment with 20 μM of INCA-6 and/or 250 ng/mL DKK-1 on nHACs infected with lenti-GFP or lenti-Wnt7a-GFP and cultured in the presence of absence of IL-1β (5 ng/mL). * = $p < 0.05$. n.s. = not significant.

to block Wnt7a's inhibition of IL-1β-induced MMP1 expression, it augmented the effect of INCA-6. Similarly, co-treatment of DKK-1 and INCA-6 increased MMP13 expression in the lenti-Wnt7a-infected chondrocytes, as compared to the same lenti-Wnt7a-infected chondrocytes treated with INCA-6 alone. These results suggest that NFAT signaling and Wnt canonical signaling may act cooperatively to mediate MMP expression in chondrocytes under inflammatory conditions.

3.2.6 Wnt7a may signal through similar pathways in chondrocytes in vitro and in vivo

To begin investigating if Wnt7a signals through similar pathways *in vivo*, I performed a preliminary microarray analysis on *in vivo* tibial cartilage samples from lenti-Wnt7a-GFP and lenti-GFP treated mice 4 weeks after DMM surgery. Samples from three mice per group were pooled together for this preliminary analysis and alterations in gene expression with Wnt7a treatment were examined with the microarray. As the n was very small, only a small number of genes were significantly differentially expressed between the two groups. There were 531 genes with a p value of < 0.05; however, only 21 genes reached significance with both a p and a q value of less than 0.05 (Table 3.1). These 21 significantly differentially expressed genes included several genes involved in inflammation and arthritis including Gadd45a and the chemokines Ccl2 (monocyte chemotactic protein 1, MCP1) and Cxcl9 (monokine induced by gamma interferon, MIG) [155-158]. In addition, Gadd45a and another differentially expressed gene, Klhl31, have been shown to downregulate Wnt canonical signaling in keratinocytes and embryonic

myogenesis respectively [159, 160]. Interestingly, Wnt7a treatment of the joint upregulated expression of both Gadd54a and Klhl31.

For a more in depth analysis of the preliminary microarray data, I performed biological network and functional pathway analyses with Ingenuity Pathway Analysis (IPA) using the 531 differentially expressed genes with a p value < 0.05. IPA canonical pathway analysis consistently predicted an effect of Wnt7a on inflammation based on the microarray data, as three of the top four canonical pathways predicted to be affected by Wnt7a were related to inflammation. Specifically, these pathways were "agranulocyte adhesion and diapedesis", "granulocyte adhesion and diapedesis", and "role of osteoblasts, osteoclasts, and chondrocytes in rheumatoid arthritis" (Table 3.2). IPA canonical pathway analysis also predicted that Wnt7a treatment increased calcium signaling with a z score of 1.89 and inhibited MMPs (Table 2). Therefore, as both the predicted effect on inflammation and the predicted increase in calcium signaling are in line with my previous *in vitro* results, this *in vivo* data suggests that Wnt7a may act similarly on chondrocytes *in vitro* and *in vivo*. However, it is impossible to definitely assess how Wnt7a is altering signaling in the articular cartilage during OA development *in vivo* when using such a small number of significantly differentially expressed genes. While this preliminary microarray data is promising, a larger n is greatly needed in an effort to expand the number of significantly differentially expressed genes and more precisely evaluate how Wnt7a affects signaling in chondrocytes *in vivo* in OA.

Gene	GFP Sample Expression	Wnt7a Sample Expression	Fold Change	Increased or Decreased
1700016C15Rik	6.13456	0		
A530046M15	1.98386	0		
Cap2	13.0247	47.1086	1.85474	
Ccl2	3.7024	0		
Ckm	50.8387	185.292	1.8658	
Clec2e	0	1.83243		
Cxcl9	59.0437	4.93606	-3.58035	
Fbxo32	2.83438	12.9625	2.19324	
Gadd45a	18.9819	154.931	3.02893	
Gdf6	13.9364	78.5735	2.49519	
H2-Ea-ps	8.66138	0		
H2-K1	43.9497	9.35112	-2.23264	
Klhl31	32.5127	140.712	2.11367	
Mafb	12.5943	51.1826	2.02289	
Mylpf	54.3569	205.981	1.92198	
Nox4	10.0903	38.7136	1.93987	
Npy2r	1.92759	0		
Olfr798	4.75744	0		
Ptprd	8.03126	27.5132	1.77643	
Pydc4	1.72376	0		

Table 3.1. Significantly differentially expressed genes in tibial chondrocytes from lenti-Wnt7a-GFP and lenti-GFP treated mice 4 weeks after DMM surgery. This table lists all of the genes identified through preliminary microarray analysis as being significantly differentially expressed after *in vivo* Wnt7a treatment during OA development. These 21 genes all had p values and q values of < 0.05. An additional 510 genes had p values of < 0.05, but had q values > 0.05. A red box represents that the gene was upregulated by Wnt7a treatment and a blue box represents that the gene was downregulated by Wnt7a treatment.

Ingenuity Canonical Pathways	p Value	% Overlap	z-score
Agranulocyte Adhesion and Diapedesis	1.51356E-06	8.99%	
Hepatic Fibrosis / Hepatic Stellate Cell Activation	1.20226E-05	8.08%	
Granulocyte Adhesion and Diapedesis	1.28825E-05	8.47%	
Role of Osteoblasts, Osteoclasts and Chondrocytes in Rheumatoid Arthritis	4.16869E-05	7.31%	
Axonal Guidance Signaling	5.62341E-05	5.54%	
Atherosclerosis Signaling	0.000120226	8.87%	
Adipogenesis pathway	0.000147911	8.66%	
Chondroitin Sulfate Biosynthesis	0.000204174	1.30%	
Dermatan Sulfate Biosynthesis	0.000288403	1.23%	
LXR/RXR Activation	0.000436516	8.26%	1.667
Airway Pathology in Chronic Obstructive Pulmonary Disease	0.000588844	37.50%	
Leukocyte Extravasation Signaling	0.00060256	6.57%	2.530
Calcium Signaling	0.000776247	6.74%	1.890
Bladder Cancer Signaling	0.000794328	9.20%	
Glycogen Degradation II	0.001230269	30%	
Protein Kinase A Signaling	0.001318257	4.94%	
Actin Cytoskeleton Signaling	0.001412538	5.99%	
Inhibition of Matrix Metalloproteinases	0.001778279	12.80%	
VDR/RXR Activation	0.001949845	8.97%	
Glycogen Degradation III	0.002187762	25%	

Table 3.2. The top 20 predicted canonical pathways affected by Wnt7a treatment in chondrocytes *in vivo*. Canonical pathway analysis by Ingenuity Pathway Analysis (IPA) predicted that 71 canonical pathways were significantly affected by Wnt7a treatment based on the provided preliminary microarray data set containing 531 differentially expressed genes with p values < 0.05 after Wnt7a treatment during OA development *in vivo*. The top 20 affected canonical pathways predicted by IPA are listed here. The % overlap denotes the number of genes differentially affected by Wnt7a treatment that are

part of the listed canonical pathway divided by the total number of genes in that pathway. The z-score represents the IPA predicted degree of upregulation or downregulation in pathway activity with Wnt7a treatment. The p value, % overlap, and z-score were all generated by IPA. Pathways associated with inflammation or Wnt signaling have been bolded.

Chapter 4: Discussion

4.1 Near Infrared Fluorescence (NIRF) Imaging of MMP Activities in a Mouse Model of Osteoarthritis

Real-time imaging of the metabolic status of tissues has been increasingly explored as a method for monitoring a diverse array of diseases including cancer, cardiovascular disease, and inflammatory conditions such as colitis [69, 161]. However, it has not been successfully used to monitor different stages of OA progression, which typically occur over a long time period and have been challenging to visualize due to the relative magnitude of changes that occur at any given time. This study demonstrates that an MMP sensitive NIRF probe, whose fluorescence intensity indicates tissue MMP activity, can be used for *in vitro* detection of MMP activity in chondrocytes treated with IL-1β. This suggests that this method could potentially be used for high throughput *in vitro* screening for compounds that can decrease MMP activity in chondrocytes under inflammatory conditions. *In vivo,* I also establish that the fluorescence signal intensity of this same MMP sensitive NIRF probe steadily increases as joint damage progresses from 2 to 8 weeks post DMM surgery. These results suggest that MMP activity may mark the stage of joint degeneration and that NIRF imaging may be used for *in vivo* tracking of OA joint destruction in DMM mice. Given the current lack of detection and monitoring methods for early OA, the fact that this increase in MMP activity starts as early as 2 weeks post DMM is particularly promising. This study differs from mRNA and protein analysis of MMPs in some prior reports which do not show a change in MMP levels over OA

progression [43, 66], and indicates that the net MMP activity may serve as a more sensitive measure of the cartilage destruction during OA progression in DMM mice.

NIRF probes have been used previously to detect increased MMP activity in OA joints. For example, MMPSense680 has been used to compare different regions of cartilage in late stage human OA specimens [147]. However, for moderate human OA, while one report suggested a correlation of NIRF signal with OA severity, another indicated a complete lack of correlation [62, 162]. In terms of *in vivo* preclinical animal models of OA, an MMP activatable NIRF probe was used following total joint destruction in the rat to successfully detect increased MMP activity in the OA knee compared to controls [163, 164]. In mice, MMPSense680 was also able to distinguish between DMM knees and sham controls based on increased MMP activity at a moderate stage of OA joint damage [165]. However, my work differed from these studies in that I continuously imaged mice starting from the very beginning of OA to the later stages to analyze the trajectory of MMP activity in OA *over time*. The non-toxic nature and short half-lives of the NIRF probes allow current MMP activity to be measured at multiple time points and eliminates the need to sacrifice the animals to assess MMP activities [166]. To address concerns related to the effect of repeated skin incisions and intraarticular injections, DMM results were always compared to sham controls, which received the same incisions and injections. In addition, the same trajectory for MMP activity was seen from mice imaged at multiple and single time points, arguing against the possibility that the increase in fluorescence signal was alone due to the repeated incisions and/or injections.

While my manuscript for this study was in the process of being published, another study was published by Lim et al. that used an MMP13-specific NIRF probe to follow MMP13 activity after DMM surgery [167]. NIRF imaging was performed at 4, 6 and 8 weeks post DMM. Interestingly, they found that their MMP13 NIRF imaging was only able to distinguish between MMP13 activity in the DMM and sham knees at 8 weeks post DMM. Additionally, they found their fluorescent signal peaked at 6 weeks post DMM, as opposed to at their latest time point of 8 weeks. This is in contrast with my data, which showed that NIRF imaging of MMP activity with MMPSense680 was able to distinguish between the DMM and sham knees as early as 4 weeks post DMM and that the detected MMP activity increased steadily from 2 to 8 weeks post DMM. However, MMPSense680 measures MMP activity from multiple MMPs, as demonstrated in Figure 2.1, as opposed to just measuring the activity of MMP13. As several MMPs have been shown to be upregulated in OA, it makes sense that measuring activity from multiple MMPs would be more sensitive and therefore able to detect a difference between the DMM and sham knees at an earlier time point. This data also suggests that the trajectory of MMP activation during OA development may differ between specific MMP proteins. Therefore, while the total MMP activity detected with MMPSense680 may increase up to 8 weeks post DMM, the respective contribution of MMP13 may start decreasing before that time, as seen in the Lim et al. study. Additional studies would be needed to investigate what proportion specific MMPs contribute to the NIRF signal generated by MMPSense680 *in vivo* and how the trajectory of specific MMPs differs over time during OA development.

Additionally, in the same month that my manuscript was accepted for publication, Satkunananthan et al. published a study examining changes in MMPSense680 signal over time following a more severe joint injury OA mouse model [168]. This model is a post-traumatic injury model of OA that uses a one-time tibial compression injury to cause an avulsion fracture and ACL rupture. The Satkunananthan et al. study showed that in this OA mouse model, MMP activity detected by MMPSense680 was elevated for 14 days post-injury, but then decreased at later time points. As the histology presented at 8 weeks post injury in this study showed very advanced articular cartilage damage, compared to my 8 week DMM histology showing much more moderate OA development, it appears that the time course of disease development in these two models is very different. This makes it difficult to accurately compare the MMPSense680 trajectories observed by Satkunananthan et al. and myself. It would be interesting to compare collected NIRF signals at time points which show similar histological joint damage between the DMM and tibial compression models. It would also be interesting to determine if other *in vivo* injury induced OA models, or other categories of *in vivo* OA models such as spontaneous or obesity related models, demonstrate similar MMPSense680 trajectories over OA development. Furthermore, the authors of the Satkunananthan et al. study remarked on several issues they had related to variability with their NIRF imaging. It is possible that further optimization of their imaging technique would have revealed differences between time points that they were not able to discern in their current data.

NIRF probes targeting other markers of OA joint damage have also been explored in regards to OA imaging. For example, a cathepsin sensitive NIRF probe was able to detect

increased activity in the OA knee compared to normal controls in the collagenase and partial medial meniscectomy (PMM) OA mouse models [169, 170]. In another study, which used a cathepsin sensitive NIRF probe to track protease activity over time after PMM, cathepsin activity appeared to peak 2 days post PMM and then taper off at later time points [134]. However, their NIRF imaging of cathepsin activity was only performed at 2, 7, and 63 days post PMM in this study; thus, the trajectory of cathepsin activity during the bulk of disease development is still unclear. In addition, a study published after my manuscript used a NIRF probe called ApoPep-1, which targets histone H1, to image cell death over time after DMM surgery [171]. Che et al. measured ApoPep-1 fluorescence at 1, 2, 4, and 8 weeks post DMM and found that the ApoPep-1 *in vivo* signal increased from 1 to 4 weeks post DMM, but then dropped from 4 to 8 weeks. This suggests that cell death may have a different time course than MMP activity in the joint during OA development. This would need to be confirmed by imaging with both ApoPep-1 and MMPSense680 in the same set of mice, as my study was performed in CD1 mice and the Che et al. study was performed in C57BL/6 mice. It would be interesting to determine if imaging with multiple NIRF probes showing slightly different trajectories over disease progression could help to more accurately pinpoint the stage of disease development.

Currently, monitoring OA progression in animals relies largely on histological analysis of structural changes to the joint, for which several comprehensive histopathological scoring systems have been developed [64, 138, 139]. My results demonstrated significantly more structural damage to the articular cartilage in the DMM joint compared to sham controls.

The severity of this structural damage increased over time, following the same trend as chondrocyte cell loss and osteophyte maturation. These data demonstrate the validity of this OA model in my hands and are consistent with published studies [43, 129, 138]. I also found that the safranin O score did not increase over time, which corresponds to a previous study that also did not show a change in safranin O score over time after DMM surgery [43]. This suggests that singular analysis of GAG content with safranin O staining is not a reliable method to use for analysis of DMM damage over time, even though it does reliably indicate the presence or absence of OA cartilage damage. Unexpectedly, I consistently observed increased articular cartilage surface damage in the first week post DMM in all mice examined, which had decreased by two weeks post DMM. Articular cartilage damage then again significantly increased from 2 weeks until the 8 week time point. This phenomenon has not been reported and it is unclear how it took place. It is possible that the sudden change in mechanical loading of the joint could lead to articular surface damage, which was to some extent repaired in the subsequent weeks. Over the long term however, the cartilage may be unable to compensate for the altered loading caused by the DMM surgery, leading to increased structural damage. It would be interesting to determine if similar structural changes occur at such early time points in other injury-induced OA models. Despite the fact that histology is the current gold standard for confirming OA joint changes in *in vivo* OA models, the differences I observed in articular cartilage damage were small and not significantly different from week to week [43, 115, 149]. On the other hand, I demonstrated that NIRF imaging of MMP activity is able to detect larger differences between weekly time points than

histology, at least at early time points, suggesting that this could be a more sensitive approach for monitoring disease progression in OA.

Further investigations would be required to assess whether similar trends in MMP activity exist in other types of animal models or in human OA, which can be associated with aging, injury or obesity. It would also be interesting to determine if the increase in MMP activity continues until very late stage OA in the DMM model, or if MMP activity eventually begins to drop. It will be important to correlate NIRF imaging with biochemical biomarkers, such as the cartilage degradation products CTX-II, C2C, C1, 2C, CPII, and Comp [59, 172], as well as other imaging modalities such as MRI and micro-CT, which would provide higher resolution images than NIRF images. Advanced imaging techniques (such as T1Rho weighted MRI imaging) can even inform us of structural changes at a microscopic level, including GAG content or collagen integrity[173-175]. Thus, NIRF imaging can provide complementary information to structural imaging modalities already currently available.

4.2 The Effect of Wnt7a on IL-1β Induced Catabolic Gene Expression *In Vitro* and Articular Cartilage Damage in Experimental Osteoarthritis *In Vivo*

Human Wnt7a deficiency results in severe birth defects with limb patterning abnormalities [176]. However, whether Wnt7a affects joints health or articular cartilage maintenance in OA conditions in humans is not known. I have shown a striking non-linear inverse correlation of Wnt7a mRNA expression and the catabolic genes MMP1,

MMP13, and IL-1β in human OA samples, which propelled me to investigate the effect of Wnt7a treatment on chondrocytes under pathological conditions. My study constitutes the first study to investigate the effect of Wnt7a on chondrocytes under pathological conditions *in vivo* and *in vitro* and demonstrates that Wnt7a ectopic expression during OA development *in vivo* strikingly reduces OA articular cartilage damage. Importantly, ectopic expression of Wnt7a *in vivo* began at one week post surgery; therefore, Wnt7a protected articular cartilage against OA-related damage even when OA development had already begun, suggesting my result is promising from a therapeutic standpoint.

Prior to my work, an *in vitro* analysis indicated that Wnt7a could delay chondrogenic differentiation in chick limb bud micromass cultures and led to the expression of AP-1 [177, 178]. I did not observe a significant change in collagen II expression upon Wnt7a expression in human articular chondrocyte cultures, but did find that Wnt7a inhibited chondrocyte maturation marker collagen X, which suggests that Wnt7a may inhibit hypertrophic differentiation *in vitro.* In addition to the chicken system, Wnt7a has also been tested using rabbit articular chondrocytes under control, non-pathological conditions [101]. In this report by Hwang et al., Wnt7a promoted chondrogenic dedifferentiation through the Wnt canonical pathway, but enhanced chondrocyte survival through phosphatidylinositol 3-kinase (PI3K) and Akt [101]. While Wnt7a did induce Wnt canonical signaling and Akt phosphorylation in my experiments, inhibiting either the canonical pathway or Akt signaling did not attenuate the activity of Wnt7a on Axin2 induction or MMP inhibition. These differences could be due to the fact that human

articular chondrocytes were used in my study and rabbit articular chondrocytes were used in the prior study.

While Wnt7a has not been investigated under inflammatory conditions in chondrocytes, several other Wnt molecules have been tested on chondrocytes treated with the pro-inflammatory cytokine IL-1β. A report by Ma et al. showed that Wnt3a and Wnt7b inhibited IL-1β-induced MMPs in human articular chondrocytes specifically through the canonical Wnt pathway [128]. An additional study demonstrated that Wnt3a in chondrocytes could activate both the canonical and non-canonical signaling pathways, which regulated cell proliferation and cell differentiation respectively; but it was performed exclusively under control conditions, without IL-1β treatment [89]. Interestingly however, Wnt3a has been shown to exhibit an opposite effect on mouse chondrocytes as in human chondrocytes [128]. Therefore, the activity of Wnts apparently depends on whether a normal or pathological condition was used, as well as the species from which chondrocytes are isolated. This highlights the importance of comprehensively investigating individual Wnt ligands, as studies focusing only on the downstream signaling components may not capture this level of complexity.

Wnts that utilize non-canonical Wnt pathways have not been investigated in human articular chondrocytes under IL-1β treatment. However, using rabbit fibrocartilage cells from the temporal mandibular joint (TMJ), Ge et al. showed that Wnt5a promoted IL-1β-induced MMP expression through activating c-Jun N-terminal kinase (JNK) signaling [125]. My work constitutes the first report on the effect of non-canonical Wnt signaling

under IL-1β treatment using human chondrocytes. What is intriguing from my observations is that Wnt7a can activate both canonical and non-canonical pathways in chondrocytes, which is consistent with prior reports using other cell types [85, 99, 100]. However, since I found that the addition of DKK-1 or dominant-negative Tcf4 did not block Wnt7a's ability to inhibit MMPs, it suggests that Wnt7a does not require the canonical pathway to exert this activity. Therefore, Wnt7a acts in a different manner than the canonical pathway activators Wnt3a and Wnt7b to antagonize IL-1β in human articular chondrocytes. Since Wnt7a inhibited rather than promoted MMP expression, it apparently may also act differently than the non-canonical pathway inducer Wnt5a; however, it is possible that a study on Wnt5a under IL-1β treatment might yield a different result in human articular chondrocytes [128].

My data using an established NFAT inhibitor suggests that Wnt7a requires the NFAT pathway to exert this activity, although additional manipulation of the NFAT pathway is required to further investigate the specific mechanisms. Interestingly, since DKK-1 further augmented IL-1β-induced MMP expression when combined with the NFAT inhibitor in Wnt7a-treated cells, it suggests that even though the canonical Wnt pathway alone is not required for Wnt7a to function, it cooperates with the non-canonical Wnt pathway to mediate MMP expression in chondrocytes. As the canonical and non-canonical Wnt pathways have been mostly viewed to be antagonistic of each other in chondrocytes [179], my study suggests that these pathways may also work together in chondrocytes in certain circumstances. Future studies will involve the evaluation of an

additional non-canonical Wnt pathway, the planar polarity pathway, and the investigation of whether the Akt pathway also crosstalks with these other pathways.

My results suggest that Wnt7a ectopic expression led to the inhibition of IL-1β-induced NF-κB activity, which is similar to what was observed for Wnt3a [128]. It has been previously demonstrated that during chondrogenic differentiation in the mouse limb bud, Wnt5a activated NFAT signaling, which in turn reduced NF-κB activity [180]. Since Wnt7a induced NFAT1 phosphorylation and its activity in nHACs is blocked by an NFAT inhibitor, future studies will involve the determination of whether Wnt7a requires NFAT to prevent NF-κB activation. Apparently Ma et al. showed that Wnt3a relied on an inhibitory interaction between β-catenin and the NF-κB p65 subunit to downregulate NF-κB activity [128]. Since Wnt7a also induced β-catenin nuclear localization, and the addition of DKK-1 together with NFAT inhibitor INCA-6 did further enhance MMP expression, it is possible that the physical interaction of β-catenin and p65 contributed to Wnt7a's activity as well. This possibility will be tested in further experiments. Nevertheless, by inhibiting NF-κB activity, Wnt7a has made the chondrocytes less competent to respond to IL-1β, which had led to a reduction in MMP levels.

It is also interesting to note that while Wnt7a treatment of nHACs completely inhibited the IL-1β induction of NF-κB activity, Wnt7a only partially blocked the IL-1β induction of catabolic genes, including several MMPs and iNOS. It has been shown that in chondrocytes, the effects of IL-1β are mediated by NF-κB, JNK, and p38 mitogen-activated protein kinase (MAPK) signaling [142, 143, 181, 182], suggesting that Wnt7a

may have a differential effect on these signaling pathways. Further studies are necessary to explore the effect of Wnt7a treatment on JNK and p38 MAPK signaling in chondrocytes and how this relates to IL-1β signaling. The relationship between JNK signaling and Wnt7a is further complicated by the fact that JNK signaling can also be activated by Wnt non-canonical signaling and has been shown to be specifically activated by Wnt7a in human mesenchymal stem cells (hMSCs) and endometrial cancer cells [99, 183]. However, Wnt7a signaling has been shown to be very cell-type specific, thus additional experiments would be needed to determine if this is also the case in chondrocytes.

Interestingly, a study by Mengshol et al. demonstrated that the downstream mediators of the IL-1β induction of specific MMPs in chondrocytes may be more complex than originally thought [142]. This report demonstrated that in a chondrosarcoma cell line the IL-1β induction of MMP13 relied on NF-κB, JNK, and p38 MAPK signaling as expected; however, the IL-1β induction of MMP1 instead required p38 and MAPK kinase of the extracellular signal-related kinase (MEK) signaling. Surprisingly, knockdown of NF-κB and JNK signaling had no effect on MMP1 induction in this cell line. This is in contrast to a previous study showing that NF-κB signaling was necessary for the IL-1β induction of MMP1 expression in synovial tissue from patients with rheumatoid arthritis [184]. This suggests that the regulation of MMP1 may be cell type specific, which is further supported by additional experiments performed by Mengshol et al. showing that MEK signaling was instead not necessary for MMP1 induction in rabbit articular chondrocytes, in contrast to their earlier results using a chondrosarcoma cell line.

These results demonstrate that IL-1β induction of MMP1 and MMP13 may involve different signaling pathways and may be regulated in a cell type specific manner. This may help to explain why in my study MMP1 and MMP13 showed differential responses to IL-1β with INCA-6 treatment.

Despite my *in vitro* studies using the pro-inflammatory cytokine IL-1β and the knowledge that inflammation is an important component in OA pathogenesis [144, 185], it is critical to evaluate the effect of Wnt treatment on OA progression *in vivo*, which is much more complex. Prior to my study, Wnt7a has been only been manipulated *in vivo* during embryogenesis, where it was shown to be critical for limb bud patterning [176]. None of the above-discussed Wnt molecules have been reported to be directly evaluated *in vivo* under OA conditions. The only experiments involving introducing Wnts into the joint were performed under normal conditions. In the report by Van Den Bosch et al., adenoviral injection of Wnt8a and Wnt16 into the normal joint resulted in OA-like damage to the articular cartilage. As this activity could be blocked by DKK-1, these Wnts acted through the canonical Wnt pathway [186]. However, because both DKK-1 overexpression and anti-sense knockdown reduced joint damage in experimental OA [115, 116], whether the canonical Wnt pathway has a similar effect in control as in OA conditions is still unclear. In addition, Van Den Bosch et al. also showed that adenoviral injection of Wnt5a had no effect on normal joint cartilage and did not activate β-catenin. Based on this data, they concluded that only Wnts activating canonical signaling had a detrimental effect on the joint. This is a somewhat surprising result, as Wnt5a has been shown to upregulate inflammation in several other disease processes including

atherosclerosis, cancer, and sepsis [187-190], and is thought to play a pro-inflammatory role in rheumatoid arthritis [191]. Perhaps Wnt5a may act differently in the joint during disease processes, including potentially OA development. It is not possible to compare the results of this study with my own, as these specific Wnts were only tested *in vivo* under normal conditions, and not during OA development. In addition, ectopic expression of Wnt5a, Wnt8a, and Wnt16 was performed using an adenovirus that only caused ectopic expression in the synovium, as opposed to my lentiviral system that caused ectopic expression in the joint cartilage. It would be interesting to determine what effect Wnt5a has during OA pathogenesis *in vivo* and if this is similar to my results or those of other Wnts.

While I observed striking differences in relation to the effect of Wnt7a on articular cartilage and joint MMP activity during OA development *in vivo*, I observed no bone related differences with Wnt7a treatment. I have demonstrated in my NIRF imaging study that in CD1 mice, osteophyte formation had clearly begun at 1 week post DMM surgery [77] and in this study, I did not start administering the lentiviruses until 1 week post DMM. It is possible that this timeline was too late to see an effect on osteophyte formation. Additionally, none of my data showed any evidence that the lentiviruses were able to cause ectopic expression in the subchondral bone or osteophytes. Therefore, it is still unclear as to if I would have seen an effect on OA-related bone changes if the virus had been administered earlier or if Wnt7a ectopic expression had occurred specifically in the boney structures. Several papers have shown that ectopic expression of certain proteins specifically in the articular cartilage can have an independent effect on the bone;

however, these studies are typically based on histological analyses [115, 140, 192]. It is possible that micro-CT analysis, which analyzes the bone from a 3D perspective, may reveal different results than what is typically seen with the somewhat limited 2D analysis of histology.

It is still not clear how Wnt7a inhibits matrix loss and chondrocyte survival in OA animals. Based on my *in vitro* study and my preliminary *in vivo* microarray data, future experiments would involve the investigation of whether the Wnt canonical and/or non-canonical pathways, especially NFAT signaling, mediate Wnt7a's activity *in vivo*. While NFAT itself has not been directly studied under OA conditions, it was shown to be beneficial to the joint under control conditions. Loss of NFAT1 resulted in the spontaneous development of OA-like joint damage in mice [119]. An NFAT1 and NFAT2 double knockout also caused spontaneous articular cartilage damage [120]. In addition, overexpression of NFAT1 increased collagen gene expression and decreased IL-1β and TNFα gene expression in chondrocytes from aged mice [193]. In contrast, inhibition of calcineurin signaling by cyclosporine A, which would inhibit NFAT signaling, reduced cartilage damage in the collagenase mouse model of OA, suggesting that NFAT signaling may instead exacerbate damage in OA [121]. However, cyclosporine A treatment does not only affect NFAT signaling. Calcineurin has been shown to activate NF-κB activity independent of NFAT signaling [194], suggesting that cyclosporine A may also inhibit the calcineurin activation of NF-κB and that these differing phenotypes may be due to calcineurin's effects on other pathways outside of NFAT signaling. In addition, cyclosporine A treatment was given systemically while the

NFAT knockout studies used a cartilage specific ablation. As NFAT and calcium signaling have been shown to activate cytokine production in certain inflammatory cells, which would possibly be present in the synovium of the joint during OA development, it is possible that cyclosporine A had an effect on multiple cell types in the joint with differing cell type specific effects. This picture is further complicated by the fact that NFAT has been shown to have differing effects on the same cell type depending on the cellular context. For example, NFAT signaling can have pro-inflammatory or anti-inflammatory effects on T cells depending on what other signaling molecules it interacts with [195]. Therefore, it is still unclear if NFAT ectopic expression would be protective against OA joint damage. It is also worth noting that inflammation is only one aspect of OA development *in vivo*. Other factors such as mechanical stress also cause cell death and matrix damage and contribute to OA, especially in the DMM joint destabilization model [196-198]. Thus, it is also possible that Wnt7a inhibits OA by modulating other aspects of OA joint damage as well.

4.3 Conclusion

My NIRF imaging study demonstrates that molecular imaging of catabolic activity using MMPSense680, a NIRF probe which specifically measures MMP activity, allows us to directly examine the metabolic state of the joint and the microenvironment of the cells within the joint during the course of OA development *in vivo* in real time. As a minimally invasive and sensitive approach, it represents an important step towards incorporating metabolic imaging into various aspects of OA research, such as to facilitate high

throughput *in vitro* screening and serial *in vivo* OA assessment aimed at understanding OA pathogenesis or drug development in a time and cost-effective way. The feasibility of this approach is further supported by data in my Wnt7a project demonstrating that MMPSense680 NIRF imaging is sensitive enough to detect changes in joint MMP activity with Wnt7a treatment in a preclinical *in vivo* OA model. Additionally, there is the long-term potential for the use of NIRF imaging in clinical OA detection and monitoring. NIRF probes have been shown to be safe for patient use and are already being used in several clinical trials for detecting other diseases, such as cancer [69]. Overall, the use of NIRF probes for OA detection and monitoring has the potential for broad scientific and clinical implications.

My Wnt7a study demonstrates that Wnt7a is a molecule whose expression is reduced in OA cartilage and inversely correlated with catabolic gene expression. Wnt7a inhibits pro-inflammatory cytokine IL-1β-induced gene expression in human chondrocytes *in vitro* and preserves articular cartilage integrity in experimental OA *in vivo*. Furthermore, while Wnt7a activates multiple Wnt signaling pathways in articular chondrocytes, my results indicate that the NFAT pathway is required for the activity of Wnt7a and may also collaborate with the canonical Wnt pathway. Thus, this study helps identify new potential therapeutic targets for OA treatment and offers a new perspective on how Wnt signaling affects OA development *in vivo*. Given the current controversial reports on the effect of downstream Wnt components on cartilage regulation, further studies on the mechanism by which Wnt7a is preserving articular cartilage will help to clarify the role of Wnt signaling in OA progression.

In summary, these independent but inter-related projects address important aspects that are still lacking in our knowledge of OA pathogenesis. This combination of studies was able to identify and validate the use of NIRF imaging for evaluating the course of OA joint degeneration and therapeutic treatment in an *in vivo* OA model. In addition, a better understanding of MMP trajectory and Wnt signaling during OA development helps to provide further insight into the control of cartilage homeostasis under pathological conditions and identify new disease-modifying therapeutic targets for OA.

References

1. Horvai A: **Joints**. In: *Robbins and Cotran Pathologic Basis of Disease.* Edited by Kumar V, Abbas A, Aster J, Ninth Edition edn: Saunders; 2015: 1207-1219.
2. Felson DT: **Osteoarthritis**. In: *Harrison's Principles of Internal Medicine.* Edited by Longo DL, Fauci AS, Kasper DL, Hauser SL, Jameson JL, vol. 13, 18 edn. New York: McGraw-Hill; 2012.
3. Poole AR, Kobayashi M, Yasuda T, Laverty S, Mwale F, Kojima T, Sakai T, Wahl C, El-Maadawy S, Webb G *et al*: **Type II collagen degradation and its regulation in articular cartilage in osteoarthritis**. *Ann Rheum Dis* 2002, **61 Suppl 2**:ii78-81.
4. Verzijl N, DeGroot J, Thorpe SR, Bank RA, Shaw JN, Lyons TJ, Bijlsma JW, Lafeber FP, Baynes JW, TeKoppele JM: **Effect of collagen turnover on the accumulation of advanced glycation end products**. *J Biol Chem* 2000, **275**(50):39027-39031.
5. Maroudas A, Bayliss MT, Uchitel-Kaushansky N, Schneiderman R, Gilav E: **Aggrecan turnover in human articular cartilage: use of aspartic acid racemization as a marker of molecular age**. *Arch Biochem Biophys* 1998, **350**(1):61-71.
6. Dillon CF, Rasch EK, Gu Q, Hirsch R: **Prevalence of knee osteoarthritis in the United States: arthritis data from the Third National Health and Nutrition Examination Survey 1991-94**. *J Rheumatol* 2006, **33**(11):2271-2279.
7. Lawrence RC, Felson DT, Helmick CG, Arnold LM, Choi H, Deyo RA, Gabriel S, Hirsch R, Hochberg MC, Hunder GG *et al*: **Estimates of the prevalence of arthritis and other rheumatic conditions in the United States. Part II**. *Arthritis Rheum* 2008, **58**(1):26-35.
8. Cross M, Smith E, Hoy D, Nolte S, Ackerman I, Fransen M, Bridgett L, Williams S, Guillemin F, Hill CL *et al*: **The global burden of hip and knee osteoarthritis: estimates from the global burden of disease 2010 study**. *Ann Rheum Dis* 2014, **73**(7):1323-1330.
9. Guccione AA, Felson DT, Anderson JJ, Anthony JM, Zhang Y, Wilson PW, Kelly-Hayes M, Wolf PA, Kreger BE, Kannel WB: **The effects of specific medical conditions on the functional limitations of elders in the Framingham Study**. *Am J Public Health* 1994, **84**(3):351-358.
10. Srikanth VK, Fryer JL, Zhai G, Winzenberg TM, Hosmer D, Jones G: **A meta-analysis of sex differences prevalence, incidence and severity of osteoarthritis**. *Osteoarthritis Cartilage* 2005, **13**(9):769-781.
11. Lohmander LS, Gerhardsson de Verdier M, Rollof J, Nilsson PM, Engstrom G: **Incidence of severe knee and hip osteoarthritis in relation to different measures of body mass: a population-based prospective cohort study**. *Ann Rheum Dis* 2009, **68**(4):490-496.
12. Muthuri SG, Hui M, Doherty M, Zhang W: **What if we prevent obesity? Risk reduction in knee osteoarthritis estimated through a meta-analysis of observational studies**. *Arthritis Care Res (Hoboken)* 2011, **63**(7):982-990.

13. Zhou ZY, Liu YK, Chen HL, Liu F: **Body mass index and knee osteoarthritis risk: a dose-response meta-analysis**. *Obesity (Silver Spring)* 2014, **22**(10):2180-2185.
14. Richter M, Trzeciak T, Owecki M, Pucher A, Kaczmarczyk J: **The role of adipocytokines in the pathogenesis of knee joint osteoarthritis**. *Int Orthop* 2015, **39**(6):1211-1217.
15. Gelber AC, Hochberg MC, Mead LA, Wang NY, Wigley FM, Klag MJ: **Joint injury in young adults and risk for subsequent knee and hip osteoarthritis**. *Ann Intern Med* 2000, **133**(5):321-328.
16. Lohmander LS, Ostenberg A, Englund M, Roos H: **High prevalence of knee osteoarthritis, pain, and functional limitations in female soccer players twelve years after anterior cruciate ligament injury**. *Arthritis Rheum* 2004, **50**(10):3145-3152.
17. Riordan EA, Little C, Hunter D: **Pathogenesis of post-traumatic OA with a view to intervention**. *Best Pract Res Clin Rheumatol* 2014, **28**(1):17-30.
18. Sharma L, Song J, Dunlop D, Felson D, Lewis CE, Segal N, Torner J, Cooke TD, Hietpas J, Lynch J *et al*: **Varus and valgus alignment and incident and progressive knee osteoarthritis**. *Ann Rheum Dis* 2010, **69**(11):1940-1945.
19. Terjesen T: **Residual hip dysplasia as a risk factor for osteoarthritis in 45 years follow-up of late-detected hip dislocation**. *J Child Orthop* 2011, **5**(6):425-431.
20. Onishi E, Ikeda N, Ueo T: **Degenerative osteoarthritis after Perthes' disease: a 36-year follow-up**. *Arch Orthop Trauma Surg* 2011, **131**(5):701-707.
21. Spector TD, MacGregor AJ: **Risk factors for osteoarthritis: genetics**. *Osteoarthritis Cartilage* 2004, **12 Suppl A**:S39-44.
22. Eyre DR, Weis MA, Moskowitz RW: **Cartilage expression of a type II collagen mutation in an inherited form of osteoarthritis associated with a mild chondrodysplasia**. *J Clin Invest* 1991, **87**(1):357-361.
23. Zhang R, Yao J, Xu P, Ji B, Luck JV, Chin B, Lu S, Kelsoe JR, Ma J: **A comprehensive meta-analysis of association between genetic variants of GDF5 and osteoarthritis of the knee, hip and hand**. *Inflamm Res* 2015, **64**(6):405-414.
24. Miyamoto Y, Shi D, Nakajima M, Ozaki K, Sudo A, Kotani A, Uchida A, Tanaka T, Fukui N, Tsunoda T *et al*: **Common variants in DVWA on chromosome 3p24.3 are associated with susceptibility to knee osteoarthritis**. *Nat Genet* 2008, **40**(8):994-998.
25. Nakajima M, Takahashi A, Kou I, Rodriguez-Fontenla C, Gomez-Reino JJ, Furuichi T, Dai J, Sudo A, Uchida A, Fukui N *et al*: **New sequence variants in HLA class II/III region associated with susceptibility to knee osteoarthritis identified by genome-wide association study**. *PLoS One* 2010, **5**(3):e9723.
26. Kerkhof HJ, Lories RJ, Meulenbelt I, Jonsdottir I, Valdes AM, Arp P, Ingvarsson T, Jhamai M, Jonsson H, Stolk L *et al*: **A genome-wide association study identifies an osteoarthritis susceptibility locus on chromosome 7q22**. *Arthritis Rheum* 2010, **62**(2):499-510.
27. Evangelou E, Valdes AM, Kerkhof HJ, Styrkarsdottir U, Zhu Y, Meulenbelt I, Lories RJ, Karassa FB, Tylzanowski P, Bos SD *et al*: **Meta-analysis of genome-**

wide association studies confirms a susceptibility locus for knee osteoarthritis on chromosome 7q22. *Ann Rheum Dis* 2011, **70**(2):349-355.
28. Castano Betancourt MC, Cailotto F, Kerkhof HJ, Cornelis FM, Doherty SA, Hart DJ, Hofman A, Luyten FP, Maciewicz RA, Mangino M *et al*: **Genome-wide association and functional studies identify the DOT1L gene to be involved in cartilage thickness and hip osteoarthritis**. *Proc Natl Acad Sci U S A* 2012, **109**(21):8218-8223.
29. Evangelou E, Kerkhof HJ, Styrkarsdottir U, Ntzani EE, Bos SD, Esko T, Evans DS, Metrustry S, Panoutsopoulou K, Ramos YF *et al*: **A meta-analysis of genome-wide association studies identifies novel variants associated with osteoarthritis of the hip**. *Ann Rheum Dis* 2014, **73**(12):2130-2136.
30. Day-Williams AG, Southam L, Panoutsopoulou K, Rayner NW, Esko T, Estrada K, Helgadottir HT, Hofman A, Ingvarsson T, Jonsson H *et al*: **A variant in MCF2L is associated with osteoarthritis**. *Am J Hum Genet* 2011, **89**(3):446-450.
31. arc OC, arc OC, Zeggini E, Panoutsopoulou K, Southam L, Rayner NW, Day-Williams AG, Lopes MC, Boraska V, Esko T *et al*: **Identification of new susceptibility loci for osteoarthritis (arcOGEN): a genome-wide association study**. *Lancet* 2012, **380**(9844):815-823.
32. Southam L, Rodriguez-Lopez J, Wilkins JM, Pombo-Suarez M, Snelling S, Gomez-Reino JJ, Chapman K, Gonzalez A, Loughlin J: **An SNP in the 5'-UTR of GDF5 is associated with osteoarthritis susceptibility in Europeans and with in vivo differences in allelic expression in articular cartilage**. *Hum Mol Genet* 2007, **16**(18):2226-2232.
33. Miyamoto Y, Mabuchi A, Shi D, Kubo T, Takatori Y, Saito S, Fujioka M, Sudo A, Uchida A, Yamamoto S *et al*: **A functional polymorphism in the 5' UTR of GDF5 is associated with susceptibility to osteoarthritis**. *Nat Genet* 2007, **39**(4):529-533.
34. Reynard LN, Loughlin J: **The genetics and functional analysis of primary osteoarthritis susceptibility**. *Expert Rev Mol Med* 2013, **15**:e2.
35. Zengini E, Finan C, Wilkinson JM: **The Genetic Epidemiological Landscape of Hip and Knee Osteoarthritis: Where Are We Now and Where Are We Going?** *J Rheumatol* 2016, **43**(2):260-266.
36. Sandell LJ, Aigner T: **Articular cartilage and changes in arthritis. An introduction: cell biology of osteoarthritis**. *Arthritis Res* 2001, **3**(2):107-113.
37. van der Kraan PM, van den Berg WB: **Chondrocyte hypertrophy and osteoarthritis: role in initiation and progression of cartilage degeneration?** *Osteoarthritis Cartilage* 2012, **20**(3):223-232.
38. Felson DT: **Clinical practice. Osteoarthritis of the knee**. *N Engl J Med* 2006, **354**(8):841-848.
39. Homandberg GA, Hui F: **Association of proteoglycan degradation with catabolic cytokine and stromelysin release from cartilage cultured with fibronectin fragments**. *Arch Biochem Biophys* 1996, **334**(2):325-331.
40. Midwood K, Sacre S, Piccinini AM, Inglis J, Trebaul A, Chan E, Drexler S, Sofat N, Kashiwagi M, Orend G *et al*: **Tenascin-C is an endogenous activator of Toll-like receptor 4 that is essential for maintaining inflammation in arthritic joint disease**. *Nat Med* 2009, **15**(7):774-780.

41. Liu-Bryan R, Terkeltaub R: **Chondrocyte innate immune myeloid differentiation factor 88-dependent signaling drives procatabolic effects of the endogenous Toll-like receptor 2/Toll-like receptor 4 ligands low molecular weight hyaluronan and high mobility group box chromosomal protein 1 in mice**. *Arthritis Rheum* 2010, **62**(7):2004-2012.
42. Poole AR: **Osteoarthritis as a whole joint disease**. *HSS journal : the musculoskeletal journal of Hospital for Special Surgery* 2012, **8**(1):4-6.
43. Loeser RF, Olex AL, McNulty MA, Carlson CS, Callahan M, Ferguson C, Fetrow JS: **Disease progression and phasic changes in gene expression in a mouse model of osteoarthritis**. *PLoS One* 2013, **8**(1):e54633.
44. Zhen G, Wen C, Jia X, Li Y, Crane JL, Mears SC, Askin FB, Frassica FJ, Chang W, Yao J *et al*: **Inhibition of TGF-beta signaling in mesenchymal stem cells of subchondral bone attenuates osteoarthritis**. *Nature medicine* 2013, **19**(6):704-712.
45. Funck-Brentano T, Bouaziz W, Marty C, Geoffroy V, Hay E, Cohen-Solal M: **Dkk-1-mediated inhibition of Wnt signaling in bone ameliorates osteoarthritis in mice**. *Arthritis & rheumatology* 2014, **66**(11):3028-3039.
46. Lange AK, Vanwanseele B, Fiatarone Singh MA: **Strength training for treatment of osteoarthritis of the knee: a systematic review**. *Arthritis Rheum* 2008, **59**(10):1488-1494.
47. Caron JP, Fernandes JC, Martel-Pelletier J, Tardif G, Mineau F, Geng C, Pelletier JP: **Chondroprotective effect of intraarticular injections of interleukin-1 receptor antagonist in experimental osteoarthritis. Suppression of collagenase-1 expression**. *Arthritis Rheum* 1996, **39**(9):1535-1544.
48. Furman BD, Mangiapani DS, Zeitler E, Bailey KN, Horne PH, Huebner JL, Kraus VB, Guilak F, Olson SA: **Targeting pro-inflammatory cytokines following joint injury: acute intra-articular inhibition of interleukin-1 following knee injury prevents post-traumatic arthritis**. *Arthritis Res Ther* 2014, **16**(3):R134.
49. Elsaid KA, Zhang L, Shaman Z, Patel C, Schmidt TA, Jay GD: **The impact of early intra-articular administration of interleukin-1 receptor antagonist on lubricin metabolism and cartilage degeneration in an anterior cruciate ligament transection model**. *Osteoarthritis Cartilage* 2015, **23**(1):114-121.
50. Chevalier X, Goupille P, Beaulieu AD, Burch FX, Bensen WG, Conrozier T, Loeuille D, Kivitz AJ, Silver D, Appleton BE: **Intraarticular injection of anakinra in osteoarthritis of the knee: a multicenter, randomized, double-blind, placebo-controlled study**. *Arthritis Rheum* 2009, **61**(3):344-352.
51. Cohen SB, Proudman S, Kivitz AJ, Burch FX, Donohue JP, Burstein D, Sun YN, Banfield C, Vincent MS, Ni L *et al*: **A randomized, double-blind study of AMG 108 (a fully human monoclonal antibody to IL-1R1) in patients with osteoarthritis of the knee**. *Arthritis Res Ther* 2011, **13**(4):R125.
52. Chevalier X, Eymard F, Richette P: **Biologic agents in osteoarthritis: hopes and disappointments**. *Nat Rev Rheumatol* 2013, **9**(7):400-410.
53. Lafeber FP, van Spil EW: **Osteoarthritis year 2013 in review: Biomarkers; reflecting before moving forward, one step at a time**. *Osteoarthritis Cartilage* 2013.

54. Patra D, Sandell LJ: **Evolving biomarkers in osteoarthritis**. *The journal of knee surgery* 2011, **24**(4):241-249.
55. Braun HJ, Gold GE: **Diagnosis of osteoarthritis: imaging**. *Bone* 2012, **51**(2):278-288.
56. Conaghan PG, Hunter DJ, Maillefert JF, Reichmann WM, Losina E: **Summary and recommendations of the OARSI FDA osteoarthritis Assessment of Structural Change Working Group**. *Osteoarthritis Cartilage* 2011, **19**(5):606-610.
57. Hunter DJ, Zhang YQ, Tu X, Lavalley M, Niu JB, Amin S, Guermazi A, Genant H, Gale D, Felson DT: **Change in joint space width: hyaline articular cartilage loss or alteration in meniscus?** *Arthritis Rheum* 2006, **54**(8):2488-2495.
58. Goldring MB, Otero M, Tsuchimochi K, Ijiri K, Li Y: **Defining the roles of inflammatory and anabolic cytokines in cartilage metabolism**. *Ann Rheum Dis* 2008, **67 Suppl 3**:iii75-82.
59. Kraus VB, Burnett B, Coindreau J, Cottrell S, Eyre D, Gendreau M, Gardiner J, Garnero P, Hardin J, Henrotin Y *et al*: **Application of biomarkers in the development of drugs intended for the treatment of osteoarthritis**. *Osteoarthritis Cartilage* 2011, **19**(5):515-542.
60. Goldring MB, Berenbaum F: **The regulation of chondrocyte function by proinflammatory mediators: prostaglandins and nitric oxide**. *Clin Orthop Relat Res* 2004(427 Suppl):S37-46.
61. Leong DJ, Hardin JA, Cobelli NJ, Sun HB: **Mechanotransduction and cartilage integrity**. *Ann N Y Acad Sci* 2011, **1240**:32-37.
62. Ryu JH, Lee A, Huh MS, Chu J, Kim K, Kim BS, Choi K, Kwon IC, Park JW, Youn I: **Measurement of MMP Activity in Synovial Fluid in Cases of Osteoarthritis and Acute Inflammatory Conditions of the Knee Joints Using a Fluorogenic Peptide Probe-Immobilized Diagnostic Kit**. *Theranostics* 2012, **2**(2):198-206.
63. Swingler TE, Waters JG, Davidson RK, Pennington CJ, Puente XS, Darrah C, Cooper A, Donell ST, Guile GR, Wang W *et al*: **Degradome expression profiling in human articular cartilage**. *Arthritis Res Ther* 2009, **11**(3):R96.
64. Glasson SS, Blanchet TJ, Morris EA: **The surgical destabilization of the medial meniscus (DMM) model of osteoarthritis in the 129/SvEv mouse**. *Osteoarthritis Cartilage* 2007, **15**(9):1061-1069.
65. Kim BJ, Choi BH, Jin LH, Park SR, Min BH: **Comparison between Subchondral Bone Change and Cartilage Degeneration in Collagenase- and DMM- induced Osteoarthritis (OA) Models in Mice**. *Tissue Engineering and Regenerative Medicine* 2013, **10**(4):211.
66. Bateman JF, Rowley L, Belluoccio D, Chan B, Bell K, Fosang AJ, Little CB: **Transcriptomics of wild-type mice and mice lacking ADAMTS-5 activity identifies genes involved in osteoarthritis initiation and cartilage destruction**. *Arthritis Rheum* 2013, **65**(6):1547-1560.
67. Funovics M, Weissleder R, Tung CH: **Protease sensors for bioimaging**. *Anal Bioanal Chem* 2003, **377**(6):956-963.

68. He X, Gao J, Gambhir SS, Cheng Z: **Near-infrared fluorescent nanoprobes for cancer molecular imaging: status and challenges**. *Trends Mol Med* 2010, **16**(12):574-583.
69. Sevick-Muraca EM: **Translation of near-infrared fluorescence imaging technologies: emerging clinical applications**. *Annu Rev Med* 2012, **63**:217-231.
70. Wunder A, Tung CH, Muller-Ladner U, Weissleder R, Mahmood U: **In vivo imaging of protease activity in arthritis: a novel approach for monitoring treatment response**. *Arthritis Rheum* 2004, **50**(8):2459-2465.
71. Hansch A, Frey O, Hilger I, Sauner D, Haas M, Schmidt D, Kurrat C, Gajda M, Malich A, Brauer R *et al*: **Diagnosis of arthritis using near-infrared fluorochrome Cy5.5**. *Invest Radiol* 2004, **39**(10):626-632.
72. Hansch A, Frey O, Sauner D, Hilger I, Haas M, Malich A, Brauer R, Kaiser WA: **In vivo imaging of experimental arthritis with near-infrared fluorescence**. *Arthritis Rheum* 2004, **50**(3):961-967.
73. Ryu JH, Lee A, Chu JU, Koo H, Ko CY, Kim HS, Yoon SY, Kim BS, Choi K, Kwon IC *et al*: **Early diagnosis of arthritis in mice with collagen-induced arthritis, using a fluorogenic matrix metalloproteinase 3-specific polymeric probe**. *Arthritis Rheum* 2011, **63**(12):3824-3832.
74. Chen WT, Mahmood U, Weissleder R, Tung CH: **Arthritis imaging using a near-infrared fluorescence folate-targeted probe**. *Arthritis Res Ther* 2005, **7**(2):R310-317.
75. Ibarra JM, Jimenez F, Martinez HG, Clark K, Ahuja SS: **MMP-Activated Fluorescence Imaging Detects Early Joint Inflammation in Collagen-Antibody-Induced Arthritis in CC-Chemokine Receptor-2-Null Mice, In-Vivo**. *International journal of inflammation* 2011, **2011**:691587.
76. Galligan CL, Fish EN: **Circulating fibrocytes contribute to the pathogenesis of collagen antibody-induced arthritis**. *Arthritis Rheum* 2012, **64**(11):3583-3593.
77. Leahy AA, Esfahani SA, Foote AT, Hui CK, Rainbow RS, Nakamura DS, Tracey BH, Mahmood U, Zeng L: **Analysis of the trajectory of osteoarthritis development in a mouse model by serial near-infrared fluorescence imaging of matrix metalloproteinase activities**. *Arthritis & rheumatology* 2015, **67**(2):442-453.
78. Clevers H: **Wnt/beta-catenin signaling in development and disease**. *Cell* 2006, **127**(3):469-480.
79. Regard JB, Zhong Z, Williams BO, Yang Y: **Wnt signaling in bone development and disease: making stronger bone with Wnts**. *Cold Spring Harb Perspect Biol* 2012, **4**(12).
80. Miller JR: **The Wnts**. *Genome Biol* 2002, **3**(1):REVIEWS3001.
81. Staines KA, Macrae VE, Farquharson C: **Cartilage development and degeneration: a Wnt Wnt situation**. *Cell biochemistry and function* 2012, **30**(8):633-642.
82. Florian MC, Nattamai KJ, Dorr K, Marka G, Uberle B, Vas V, Eckl C, Andra I, Schiemann M, Oostendorp RA *et al*: **A canonical to non-canonical Wnt signalling switch in haematopoietic stem-cell ageing**. *Nature* 2013.

83. Yates KE, Shortkroff S, Reish RG: **Wnt influence on chondrocyte differentiation and cartilage function**. *DNA and cell biology* 2005, **24**(7):446-457.
84. Komiya Y, Habas R: **Wnt signal transduction pathways**. *Organogenesis* 2008, **4**(2):68-75.
85. von Maltzahn J, Bentzinger CF, Rudnicki MA: **Wnt7a-Fzd7 signalling directly activates the Akt/mTOR anabolic growth pathway in skeletal muscle**. *Nat Cell Biol* 2012, **14**(2):186-191.
86. De A: **Wnt/Ca2+ signaling pathway: a brief overview**. *Acta Biochim Biophys Sin (Shanghai)* 2011, **43**(10):745-756.
87. Li L, Yuan H, Xie W, Mao J, Caruso AM, McMahon A, Sussman DJ, Wu D: **Dishevelled proteins lead to two signaling pathways. Regulation of LEF-1 and c-Jun N-terminal kinase in mammalian cells**. *J Biol Chem* 1999, **274**(1):129-134.
88. Weber U, Paricio N, Mlodzik M: **Jun mediates Frizzled-induced R3/R4 cell fate distinction and planar polarity determination in the Drosophila eye**. *Development* 2000, **127**(16):3619-3629.
89. Nalesso G, Sherwood J, Bertrand J, Pap T, Ramachandran M, De Bari C, Pitzalis C, Dell'accio F: **WNT-3A modulates articular chondrocyte phenotype by activating both canonical and noncanonical pathways**. *J Cell Biol* 2011, **193**(3):551-564.
90. McMahon AP, Moon RT: **Ectopic expression of the proto-oncogene int-1 in Xenopus embryos leads to duplication of the embryonic axis**. *Cell* 1989, **58**(6):1075-1084.
91. Wong GT, Gavin BJ, McMahon AP: **Differential transformation of mammary epithelial cells by Wnt genes**. *Mol Cell Biol* 1994, **14**(9):6278-6286.
92. Shimizu H, Julius MA, Giarre M, Zheng Z, Brown AM, Kitajewski J: **Transformation by Wnt family proteins correlates with regulation of beta-catenin**. *Cell Growth Differ* 1997, **8**(12):1349-1358.
93. Cha SW, Tadjuidje E, Tao Q, Wylie C, Heasman J: **Wnt5a and Wnt11 interact in a maternal Dkk1-regulated fashion to activate both canonical and non-canonical signaling in Xenopus axis formation**. *Development* 2008, **135**(22):3719-3729.
94. van Amerongen R, Fuerer C, Mizutani M, Nusse R: **Wnt5a can both activate and repress Wnt/beta-catenin signaling during mouse embryonic development**. *Dev Biol* 2012, **369**(1):101-114.
95. Mikels AJ, Nusse R: **Purified Wnt5a protein activates or inhibits beta-catenin-TCF signaling depending on receptor context**. *PLoS Biol* 2006, **4**(4):e115.
96. Tu X, Joeng KS, Nakayama KI, Nakayama K, Rajagopal J, Carroll TJ, McMahon AP, Long F: **Noncanonical Wnt signaling through G protein-linked PKCdelta activation promotes bone formation**. *Dev Cell* 2007, **12**(1):113-127.
97. Moverare-Skrtic S, Henning P, Liu X, Nagano K, Saito H, Borjesson AE, Sjogren K, Windahl SH, Farman H, Kindlund B *et al*: **Osteoblast-derived WNT16 represses osteoclastogenesis and prevents cortical bone fragility fractures**. *Nat Med* 2014, **20**(11):1279-1288.

98. Tao Q, Yokota C, Puck H, Kofron M, Birsoy B, Yan D, Asashima M, Wylie CC, Lin X, Heasman J: **Maternal wnt11 activates the canonical wnt signaling pathway required for axis formation in Xenopus embryos**. *Cell* 2005, **120**(6):857-871.
99. Carmon KS, Loose DS: **Secreted frizzled-related protein 4 regulates two Wnt7a signaling pathways and inhibits proliferation in endometrial cancer cells**. *Molecular cancer research : MCR* 2008, **6**(6):1017-1028.
100. Le Grand F, Jones AE, Seale V, Scime A, Rudnicki MA: **Wnt7a activates the planar cell polarity pathway to drive the symmetric expansion of satellite stem cells**. *Cell Stem Cell* 2009, **4**(6):535-547.
101. Hwang SG, Ryu JH, Kim IC, Jho EH, Jung HC, Kim K, Kim SJ, Chun JS: **Wnt-7a causes loss of differentiated phenotype and inhibits apoptosis of articular chondrocytes via different mechanisms**. *J Biol Chem* 2004, **279**(25):26597-26604.
102. Loughlin J, Dowling B, Chapman K, Marcelline L, Mustafa Z, Southam L, Ferreira A, Ciesielski C, Carson DA, Corr M: **Functional variants within the secreted frizzled-related protein 3 gene are associated with hip osteoarthritis in females**. *Proc Natl Acad Sci U S A* 2004, **101**(26):9757-9762.
103. Cheon H, Boyle DL, Firestein GS: **Wnt1 inducible signaling pathway protein-3 regulation and microsatellite structure in arthritis**. *J Rheumatol* 2004, **31**(11):2106-2114.
104. Nakamura Y, Nawata M, Wakitani S: **Expression profiles and functional analyses of Wnt-related genes in human joint disorders**. *Am J Pathol* 2005, **167**(1):97-105.
105. Lane NE, Lian K, Nevitt MC, Zmuda JM, Lui L, Li J, Wang J, Fontecha M, Umblas N, Rosenbach M *et al*: **Frizzled-related protein variants are risk factors for hip osteoarthritis**. *Arthritis Rheum* 2006, **54**(4):1246-1254.
106. Blom AB, Brockbank SM, van Lent PL, van Beuningen HM, Geurts J, Takahashi N, van der Kraan PM, van de Loo FA, Schreurs BW, Clements K *et al*: **Involvement of the Wnt signaling pathway in experimental and human osteoarthritis: prominent role of Wnt-induced signaling protein 1**. *Arthritis Rheum* 2009, **60**(2):501-512.
107. Velasco J, Zarrabeitia MT, Prieto JR, Perez-Castrillon JL, Perez-Aguilar MD, Perez-Nunez MI, Sanudo C, Hernandez-Elena J, Calvo I, Ortiz F *et al*: **Wnt pathway genes in osteoporosis and osteoarthritis: differential expression and genetic association study**. *Osteoporos Int* 2010, **21**(1):109-118.
108. Abed E, Chan TF, Delalandre A, Martel-Pelletier J, Pelletier JP, Lajeunesse D: **R-spondins are newly recognized players in osteoarthritis that regulate Wnt signaling in osteoblasts**. *Arthritis Rheum* 2011, **63**(12):3865-3875.
109. Valdes AM, Loughlin J, Oene MV, Chapman K, Surdulescu GL, Doherty M, Spector TD: **Sex and ethnic differences in the association of ASPN, CALM1, COL2A1, COMP, and FRZB with genetic susceptibility to osteoarthritis of the knee**. *Arthritis Rheum* 2007, **56**(1):137-146.
110. Lories RJ, Peeters J, Bakker A, Tylzanowski P, Derese I, Schrooten J, Thomas JT, Luyten FP: **Articular cartilage and biomechanical properties of the long bones in Frzb-knockout mice**. *Arthritis Rheum* 2007, **56**(12):4095-4103.

111. Zhu M, Tang D, Wu Q, Hao S, Chen M, Xie C, Rosier RN, O'Keefe RJ, Zuscik M, Chen D: **Activation of beta-catenin signaling in articular chondrocytes leads to osteoarthritis-like phenotype in adult beta-catenin conditional activation mice**. *J Bone Miner Res* 2009, **24**(1):12-21.
112. Yuasa T, Otani T, Koike T, Iwamoto M, Enomoto-Iwamoto M: **Wnt/beta-catenin signaling stimulates matrix catabolic genes and activity in articular chondrocytes: its possible role in joint degeneration**. *Laboratory investigation; a journal of technical methods and pathology* 2008, **88**(3):264-274.
113. Yuasa T, Kondo N, Yasuhara R, Shimono K, Mackem S, Pacifici M, Iwamoto M, Enomoto-Iwamoto M: **Transient activation of Wnt/{beta}-catenin signaling induces abnormal growth plate closure and articular cartilage thickening in postnatal mice**. *Am J Pathol* 2009, **175**(5):1993-2003.
114. Zhu M, Chen M, Zuscik M, Wu Q, Wang YJ, Rosier RN, O'Keefe RJ, Chen D: **Inhibition of beta-catenin signaling in articular chondrocytes results in articular cartilage destruction**. *Arthritis Rheum* 2008, **58**(7):2053-2064.
115. Oh H, Chun CH, Chun JS: **Dkk-1 expression in chondrocytes inhibits experimental osteoarthritic cartilage destruction in mice**. *Arthritis Rheum* 2012, **64**(8):2568-2578.
116. Weng LH, Wang CJ, Ko JY, Sun YC, Wang FS: **Control of Dkk-1 ameliorates chondrocyte apoptosis, cartilage destruction, and subchondral bone deterioration in osteoarthritic knees**. *Arthritis Rheum* 2010, **62**(5):1393-1402.
117. Kerkhof JM, Uitterlinden AG, Valdes AM, Hart DJ, Rivadeneira F, Jhamai M, Hofman A, Pols HA, Bierma-Zeinstra SM, Spector TD *et al*: **Radiographic osteoarthritis at three joint sites and FRZB, LRP5, and LRP6 polymorphisms in two population-based cohorts**. *Osteoarthritis Cartilage* 2008, **16**(10):1141-1149.
118. Evangelou E, Chapman K, Meulenbelt I, Karassa FB, Loughlin J, Carr A, Doherty M, Doherty S, Gomez-Reino JJ, Gonzalez A *et al*: **Large-scale analysis of association between GDF5 and FRZB variants and osteoarthritis of the hip, knee, and hand**. *Arthritis Rheum* 2009, **60**(6):1710-1721.
119. Wang J, Gardner BM, Lu Q, Rodova M, Woodbury BG, Yost JG, Roby KF, Pinson DM, Tawfik O, Anderson HC: **Transcription factor Nfat1 deficiency causes osteoarthritis through dysfunction of adult articular chondrocytes**. *J Pathol* 2009, **219**(2):163-172.
120. Greenblatt MB, Ritter SY, Wright J, Tsang K, Hu D, Glimcher LH, Aliprantis AO: **NFATc1 and NFATc2 repress spontaneous osteoarthritis**. *Proc Natl Acad Sci U S A* 2013, **110**(49):19914-19919.
121. Yoo SA, Park BH, Yoon HJ, Lee JY, Song JH, Kim HA, Cho CS, Kim WU: **Calcineurin modulates the catabolic and anabolic activity of chondrocytes and participates in the progression of experimental osteoarthritis**. *Arthritis Rheum* 2007, **56**(7):2299-2311.
122. Sitara D, Aliprantis AO: **Transcriptional regulation of bone and joint remodeling by NFAT**. *Immunol Rev* 2010, **233**(1):286-300.
123. Yasuhara R, Yuasa T, Williams JA, Byers SW, Shah S, Pacifici M, Iwamoto M, Enomoto-Iwamoto M: **Wnt/beta-catenin and retinoic acid receptor signaling**

pathways interact to regulate chondrocyte function and matrix turnover. *J Biol Chem* 2010, **285**(1):317-327.
124. Bouaziz W, Funck-Brentano T, Lin H, Marty C, Ea HK, Hay E, Cohen-Solal M: **Loss of sclerostin promotes osteoarthritis in mice via beta-catenin-dependent and -independent Wnt pathways**. *Arthritis Res Ther* 2015, **17**:24.
125. Ge X, Ma X, Meng J, Zhang C, Ma K, Zhou C: **Role of Wnt-5A in interleukin-1beta-induced matrix metalloproteinase expression in rabbit temporomandibular joint condylar chondrocytes**. *Arthritis Rheum* 2009, **60**(9):2714-2722.
126. Shin Y, Huh YH, Kim K, Kim S, Park KH, Koh JT, Chun JS, Ryu JH: **Low-density lipoprotein receptor-related protein 5 governs Wnt-mediated osteoarthritic cartilage destruction**. *Arthritis Res Ther* 2014, **16**(1):R37.
127. Wang X, Zhang H, Zheng J, Zheng Y, Cao Y, Zhan H, Shi Y, Ding D: **Establishment of a chondrocyte degeneration model by over-expression of human Wnt7b gene in 293ft cell line**. *Nan Fang Yi Ke Da Xue Xue Bao* 2015, **35**(3):370-374.
128. Ma B, van Blitterswijk CA, Karperien M: **A Wnt/beta-catenin negative feedback loop inhibits interleukin-1-induced matrix metalloproteinase expression in human articular chondrocytes**. *Arthritis Rheum* 2012, **64**(8):2589-2600.
129. McNulty MA, Loeser RF, Davey C, Callahan M, Ferguson C, Carlson CS: **A Comprehensive Histological Assessment of Osteoarthritis Lesions in Mice**. *Cartilage* 2011, **2**(4):354-363.
130. Little CB, Barai A, Burkhardt D, Smith SM, Fosang AJ, Werb Z, Shah M, Thompson EW: **Matrix metalloproteinase 13-deficient mice are resistant to osteoarthritic cartilage erosion but not chondrocyte hypertrophy or osteophyte development**. *Arthritis Rheum* 2009, **60**(12):3723-3733.
131. Livak KJ, Schmittgen TD: **Analysis of relative gene expression data using real-time quantitative PCR and the 2(-Delta Delta C(T)) Method**. *Methods* 2001, **25**(4):402-408.
132. Galazka G, Windsor LJ, Birkedal-Hansen H, Engler JA: **APMA (4-aminophenylmercuric acetate) activation of stromelysin-1 involves protein interactions in addition to those with cysteine-75 in the propeptide**. *Biochemistry* 1996, **35**(34):11221-11227.
133. Cortial D, Gouttenoire J, Rousseau CF, Ronziere MC, Piccardi N, Msika P, Herbage D, Mallein-Gerin F, Freyria AM: **Activation by IL-1 of bovine articular chondrocytes in culture within a 3D collagen-based scaffold. An in vitro model to address the effect of compounds with therapeutic potential in osteoarthritis**. *Osteoarthritis Cartilage* 2006, **14**(7):631-640.
134. Wang S, Wei X, Zhou J, Zhang J, Li K, Chen Q, Terek R, Fleming BC, Goldring MB, Ehrlich MG *et al*: **Identification of alpha2 -Macroglobulin as a Master Inhibitor of Cartilage-Degrading Factors That Attenuates the Progression of Posttraumatic Osteoarthritis**. *Arthritis & rheumatology* 2014, **66**(7):1843-1853.
135. Freemont AJ, Byers RJ, Taiwo YO, Hoyland JA: **In situ zymographic localisation of type II collagen degrading activity in osteoarthritic human articular cartilage**. *Ann Rheum Dis* 1999, **58**(6):357-365.

136. Quillard T, Tesmenitsky Y, Croce K, Travers R, Shvartz E, Koskinas KC, Sukhova GK, Aikawa E, Aikawa M, Libby P: **Selective inhibition of matrix metalloproteinase-13 increases collagen content of established mouse atherosclerosis**. *Arterioscler Thromb Vasc Biol* 2011, **31**(11):2464-2472.
137. Klohs J, Baeva N, Steinbrink J, Bourayou R, Boettcher C, Royl G, Megow D, Dirnagl U, Priller J, Wunder A: **In vivo near-infrared fluorescence imaging of matrix metalloproteinase activity after cerebral ischemia**. *Journal of cerebral blood flow and metabolism : official journal of the International Society of Cerebral Blood Flow and Metabolism* 2009, **29**(7):1284-1292.
138. McNulty MA, Loeser RF, Davey C, Callahan MF, Ferguson CM, Carlson CS: **Histopathology of naturally occurring and surgically induced osteoarthritis in mice**. *Osteoarthritis Cartilage* 2012, **20**(8):949-956.
139. Glasson SS, Chambers MG, Van Den Berg WB, Little CB: **The OARSI histopathology initiative - recommendations for histological assessments of osteoarthritis in the mouse**. *Osteoarthritis Cartilage* 2010, **18 Suppl 3**:S17-23.
140. Uchimura T, Foote AT, Smith EL, Matzkin EG, Zeng L: **Insulin-Like Growth Factor II (IGF-II) Inhibits IL-1beta-Induced Cartilage Matrix Loss and Promotes Cartilage Integrity in Experimental Osteoarthritis**. *J Cell Biochem* 2015.
141. Gosset M, Berenbaum F, Thirion S, Jacques C: **Primary culture and phenotyping of murine chondrocytes**. *Nat Protoc* 2008, **3**(8):1253-1260.
142. Mengshol JA, Vincenti MP, Coon CI, Barchowsky A, Brinckerhoff CE: **Interleukin-1 induction of collagenase 3 (matrix metalloproteinase 13) gene expression in chondrocytes requires p38, c-Jun N-terminal kinase, and nuclear factor kappaB: differential regulation of collagenase 1 and collagenase 3**. *Arthritis Rheum* 2000, **43**(4):801-811.
143. Liacini A, Sylvester J, Li WQ, Zafarullah M: **Inhibition of interleukin-1-stimulated MAP kinases, activating protein-1 (AP-1) and nuclear factor kappa B (NF-kappa B) transcription factors down-regulates matrix metalloproteinase gene expression in articular chondrocytes**. *Matrix Biol* 2002, **21**(3):251-262.
144. Goldring MB, Otero M: **Inflammation in osteoarthritis**. *Curr Opin Rheumatol* 2011, **23**(5):471-478.
145. Rigoglou S, Papavassiliou AG: **The NF-kappaB signalling pathway in osteoarthritis**. *Int J Biochem Cell Biol* 2013, **45**(11):2580-2584.
146. Wang M, Sampson ER, Jin H, Li J, Ke QH, Im HJ, Chen D: **MMP13 is a critical target gene during the progression of osteoarthritis**. *Arthritis Res Ther* 2013, **15**(1):R5.
147. Jones EF, Schooler J, Miller DC, Drake CR, Wahnishe H, Siddiqui S, Li X, Majumdar S: **Characterization of human osteoarthritic cartilage using optical and magnetic resonance imaging**. *Mol Imaging Biol* 2012, **14**(1):32-39.
148. Mahmood U, Tung CH, Bogdanov A, Jr., Weissleder R: **Near-infrared optical imaging of protease activity for tumor detection**. *Radiology* 1999, **213**(3):866-870.

149. Ma HL, Blanchet TJ, Peluso D, Hopkins B, Morris EA, Glasson SS: **Osteoarthritis severity is sex dependent in a surgical mouse model**. *Osteoarthritis Cartilage* 2007, **15**(6):695-700.
150. Hashimoto S, Rai MF, Janiszak KL, Cheverud JM, Sandell LJ: **Cartilage and bone changes during development of post-traumatic osteoarthritis in selected LGXSM recombinant inbred mice**. *Osteoarthritis Cartilage* 2012, **20**(6):562-571.
151. Botter SM, van Osch GJ, Clockaerts S, Waarsing JH, Weinans H, van Leeuwen JP: **Osteoarthritis induction leads to early and temporal subchondral plate porosity in the tibial plateau of mice: an in vivo microfocal computed tomography study**. *Arthritis Rheum* 2011, **63**(9):2690-2699.
152. Kawano Y, Kypta R: **Secreted antagonists of the Wnt signalling pathway**. *J Cell Sci* 2003, **116**(Pt 13):2627-2634.
153. Davies BR, Greenwood H, Dudley P, Crafter C, Yu DH, Zhang J, Li J, Gao B, Ji Q, Maynard J *et al*: **Preclinical pharmacology of AZD5363, an inhibitor of AKT: pharmacodynamics, antitumor activity, and correlation of monotherapy activity with genetic background**. *Mol Cancer Ther* 2012, **11**(4):873-887.
154. Toren P, Kim S, Cordonnier T, Crafter C, Davies BR, Fazli L, Gleave ME, Zoubeidi A: **Combination AZD5363 with Enzalutamide Significantly Delays Enzalutamide-resistant Prostate Cancer in Preclinical Models**. *Eur Urol* 2015, **67**(6):986-990.
155. Meyer NJ, Huang Y, Singleton PA, Sammani S, Moitra J, Evenoski CL, Husain AN, Mitra S, Moreno-Vinasco L, Jacobson JR *et al*: **GADD45a is a novel candidate gene in inflammatory lung injury via influences on Akt signaling**. *FASEB J* 2009, **23**(5):1325-1337.
156. Lopez-Santalla M, Gonzalez-Alvaro I, Lamana A, Ortiz AM, Castaneda S, Salvador JM: **P38 MAPK Phosphorylation as a Rheumatoid Arthritis Biomarker**. *Annals of the Rheumatic Diseases* 2013, **71**(647).
157. Griffith JW, Sokol CL, Luster AD: **Chemokines and chemokine receptors: positioning cells for host defense and immunity**. *Annu Rev Immunol* 2014, **32**:659-702.
158. Yuan GH, Masuko-Hongo K, Sakata M, Tsuruha J, Onuma H, Nakamura H, Aoki H, Kato T, Nishioka K: **The role of C-C chemokines and their receptors in osteoarthritis**. *Arthritis Rheum* 2001, **44**(5):1056-1070.
159. Hildesheim J, Belova GI, Tyner SD, Zhou X, Vardanian L, Fornace AJ, Jr.: **Gadd45a regulates matrix metalloproteinases by suppressing DeltaNp63alpha and beta-catenin via p38 MAP kinase and APC complex activation**. *Oncogene* 2004, **23**(10):1829-1837.
160. Abou-Elhamd A, Alrefaei AF, Mok GF, Garcia-Morales C, Abu-Elmagd M, Wheeler GN, Munsterberg AE: **Klhl31 attenuates beta-catenin dependent Wnt signaling and regulates embryo myogenesis**. *Dev Biol* 2015, **402**(1):61-71.
161. Gounaris E, Martin J, Ishihara Y, Khan MW, Lee G, Sinh P, Chen EZ, Angarone M, Weissleder R, Khazaie K *et al*: **Fluorescence endoscopy of cathepsin activity discriminates dysplasia from colitis**. *Inflamm Bowel Dis* 2013, **19**(7):1339-1345.

162. Ryu JH, Lee A, Lee S, Ahn CH, Park JW, Leary JF, Park S, Kim K, Kwon IC, Youn IC *et al*: **"One-step" detection of matrix metalloproteinase activity using a fluorogenic peptide probe-immobilized diagnostic kit**. *Bioconjug Chem* 2010, **21**(7):1378-1384.
163. Ryu JH, Lee A, Na JH, Lee S, Ahn HJ, Park JW, Ahn CH, Kim BS, Kwon IC, Choi K *et al*: **Optimization of matrix metalloproteinase fluorogenic probes for osteoarthritis imaging**. *Amino Acids* 2011, **41**(5):1113-1122.
164. Lee S, Park K, Lee SY, Ryu JH, Park JW, Ahn HJ, Kwon IC, Youn IC, Kim K, Choi K: **Dark quenched matrix metalloproteinase fluorogenic probe for imaging osteoarthritis development in vivo**. *Bioconjug Chem* 2008, **19**(9):1743-1747.
165. Vermeij EA, Koenders MI, Blom AB, Arntz OJ, Bennink MB, van den Berg WB, van Lent PL, van de Loo FA: **In vivo molecular imaging of cathepsin and matrix metalloproteinase activity discriminates between arthritic and osteoarthritic processes in mice**. *Mol Imaging* 2014, **13**(2):1-10.
166. Frangioni JV: **In vivo near-infrared fluorescence imaging**. *Curr Opin Chem Biol* 2003, **7**(5):626-634.
167. Lim NH, Meinjohanns E, Meldal M, Bou-Gharios G, Nagase H: **In vivo imaging of MMP-13 activity in the murine destabilised medial meniscus surgical model of osteoarthritis**. *Osteoarthritis Cartilage* 2014, **22**(6):862-868.
168. Satkunananthan PB, Anderson MJ, De Jesus NM, Haudenschild DR, Ripplinger CM, Christiansen BA: **In vivo fluorescence reflectance imaging of protease activity in a mouse model of post-traumatic osteoarthritis**. *Osteoarthritis Cartilage* 2014, **22**(10):1461-1469.
169. Lai WF, Chang CH, Tang Y, Bronson R, Tung CH: **Early diagnosis of osteoarthritis using cathepsin B sensitive near-infrared fluorescent probes**. *Osteoarthritis Cartilage* 2004, **12**(3):239-244.
170. Zhou J, Chen Q, Lanske B, Fleming BC, Terek R, Wei X, Zhang G, Wang S, Li K, Wei L: **Disrupting the Indian hedgehog signaling pathway in vivo attenuates surgically induced osteoarthritis progression in Col2a1-CreERT2; Ihhfl/fl mice**. *Arthritis Res Ther* 2014, **16**(1):R11.
171. Che X, Chi L, Park CY, Cho GH, Park N, Kim SG, Lee BH, Choi JY: **A novel method to detect articular chondrocyte death during early stages of osteoarthritis using a non-invasive ApoPep-1 probe**. *Arthritis Res Ther* 2015, **17**:309.
172. Cibere J, Zhang H, Garnero P, Poole AR, Lobanok T, Saxne T, Kraus VB, Way A, Thorne A, Wong H *et al*: **Association of biomarkers with pre-radiographically defined and radiographically defined knee osteoarthritis in a population-based study**. *Arthritis Rheum* 2009, **60**(5):1372-1380.
173. Buck RJ, Wyman BT, Le Graverand MP, Hudelmaier M, Wirth W, Eckstein F: **Does the use of ordered values of subregional change in cartilage thickness improve the detection of disease progression in longitudinal studies of osteoarthritis?** *Arthritis Rheum* 2009, **61**(7):917-924.
174. Hayashi D, Guermazi A, Hunter DJ: **Osteoarthritis year 2010 in review: imaging**. *Osteoarthritis Cartilage* 2011, **19**(4):354-360.

175. Lakin BA, Grasso DJ, Stewart RC, Freedman JD, Snyder BD, Grinstaff MW: **Contrast enhanced CT attenuation correlates with the GAG content of bovine meniscus**. *J Orthop Res* 2013.
176. Woods CG, Stricker S, Seemann P, Stern R, Cox J, Sherridan E, Roberts E, Springell K, Scott S, Karbani G *et al*: **Mutations in WNT7A cause a range of limb malformations, including Fuhrmann syndrome and Al-Awadi/Raas-Rothschild/Schinzel phocomelia syndrome**. *Am J Hum Genet* 2006, **79**(2):402-408.
177. Tufan AC, Tuan RS: **Wnt regulation of limb mesenchymal chondrogenesis is accompanied by altered N-cadherin-related functions**. *FASEB J* 2001, **15**(8):1436-1438.
178. Tufan AC, Daumer KM, DeLise AM, Tuan RS: **AP-1 transcription factor complex is a target of signals from both WnT-7a and N-cadherin-dependent cell-cell adhesion complex during the regulation of limb mesenchymal chondrogenesis**. *Exp Cell Res* 2002, **273**(2):197-203.
179. Rybchyn MS, Slater M, Conigrave AD, Mason RS: **An Akt-dependent increase in canonical Wnt signaling and a decrease in sclerostin protein levels are involved in strontium ranelate-induced osteogenic effects in human osteoblasts**. *J Biol Chem* 2011, **286**(27):23771-23779.
180. Bradley EW, Drissi MH: **WNT5A regulates chondrocyte differentiation through differential use of the CaN/NFAT and IKK/NF-kappaB pathways**. *Molecular endocrinology* 2010, **24**(8):1581-1593.
181. Chowdhury TT, Arghandawi S, Brand J, Akanji OO, Bader DL, Salter DM, Lee DA: **Dynamic compression counteracts IL-1beta induced inducible nitric oxide synthase and cyclo-oxygenase-2 expression in chondrocyte/agarose constructs**. *Arthritis Res Ther* 2008, **10**(2):R35.
182. Kapoor M, Martel-Pelletier J, Lajeunesse D, Pelletier JP, Fahmi H: **Role of proinflammatory cytokines in the pathophysiology of osteoarthritis**. *Nat Rev Rheumatol* 2011, **7**(1):33-42.
183. Tsai HL, Deng WP, Lai WF, Chiu WT, Yang CB, Tsai YH, Hwang SM, Renshaw PF: **Wnts enhance neurotrophin-induced neuronal differentiation in adult bone-marrow-derived mesenchymal stem cells via canonical and noncanonical signaling pathways**. *PLoS One* 2014, **9**(8):e104937.
184. Bondeson J, Foxwell B, Brennan F, Feldmann M: **Defining therapeutic targets by using adenovirus: blocking NF-kappaB inhibits both inflammatory and destructive mechanisms in rheumatoid synovium but spares anti-inflammatory mediators**. *Proc Natl Acad Sci U S A* 1999, **96**(10):5668-5673.
185. Daghestani HN, Pieper CF, Kraus VB: **Soluble macrophage biomarkers indicate inflammatory phenotypes in patients with knee osteoarthritis**. *Arthritis & rheumatology* 2015, **67**(4):956-965.
186. van den Bosch MH, Blom AB, Sloetjes AW, Koenders MI, van de Loo FA, van den Berg WB, van Lent PL, van der Kraan PM: **Induction of Canonical Wnt Signaling by Synovial Overexpression of Selected Wnts Leads to Protease Activity and Early Osteoarthritis-Like Cartilage Damage**. *Am J Pathol* 2015, **185**(7):1970-1980.

187. Kim J, Kim J, Kim DW, Ha Y, Ihm MH, Kim H, Song K, Lee I: **Wnt5a induces endothelial inflammation via beta-catenin-independent signaling**. *J Immunol* 2010, **185**(2):1274-1282.
188. Pukrop T, Klemm F, Hagemann T, Gradl D, Schulz M, Siemes S, Trumper L, Binder C: **Wnt 5a signaling is critical for macrophage-induced invasion of breast cancer cell lines**. *Proc Natl Acad Sci U S A* 2006, **103**(14):5454-5459.
189. Pereira C, Schaer DJ, Bachli EB, Kurrer MO, Schoedon G: **Wnt5A/CaMKII signaling contributes to the inflammatory response of macrophages and is a target for the antiinflammatory action of activated protein C and interleukin-10**. *Arterioscler Thromb Vasc Biol* 2008, **28**(3):504-510.
190. Bhatt PM, Malgor R: **Wnt5a: a player in the pathogenesis of atherosclerosis and other inflammatory disorders**. *Atherosclerosis* 2014, **237**(1):155-162.
191. Sen M, Chamorro M, Reifert J, Corr M, Carson DA: **Blockade of Wnt-5A/frizzled 5 signaling inhibits rheumatoid synoviocyte activation**. *Arthritis Rheum* 2001, **44**(4):772-781.
192. Kim JH, Jeon J, Shin M, Won Y, Lee M, Kwak JS, Lee G, Rhee J, Ryu JH, Chun CH *et al*: **Regulation of the catabolic cascade in osteoarthritis by the zinc-ZIP8-MTF1 axis**. *Cell* 2014, **156**(4):730-743.
193. Zhang M, Lu Q, Egan B, Zhong XB, Brandt K, Wang J: **Epigenetically mediated spontaneous reduction of NFAT1 expression causes imbalanced metabolic activities of articular chondrocytes in aged mice**. *Osteoarthritis Cartilage* 2016.
194. Palkowitsch L, Marienfeld U, Brunner C, Eitelhuber A, Krappmann D, Marienfeld RB: **The Ca2+-dependent phosphatase calcineurin controls the formation of the Carma1-Bcl10-Malt1 complex during T cell receptor-induced NF-kappaB activation**. *J Biol Chem* 2011, **286**(9):7522-7534.
195. Macian F, Garcia-Cozar F, Im SH, Horton HF, Byrne MC, Rao A: **Transcriptional mechanisms underlying lymphocyte tolerance**. *Cell* 2002, **109**(6):719-731.
196. Lane Smith R, Trindade MC, Ikenoue T, Mohtai M, Das P, Carter DR, Goodman SB, Schurman DJ: **Effects of shear stress on articular chondrocyte metabolism**. *Biorheology* 2000, **37**(1-2):95-107.
197. Martin JA, McCabe D, Walter M, Buckwalter JA, McKinley TO: **N-acetylcysteine inhibits post-impact chondrocyte death in osteochondral explants**. *J Bone Joint Surg Am* 2009, **91**(8):1890-1897.
198. Ding L, Heying E, Nicholson N, Stroud NJ, Homandberg GA, Buckwalter JA, Guo D, Martin JA: **Mechanical impact induces cartilage degradation via mitogen activated protein kinases**. *Osteoarthritis Cartilage* 2010, **18**(11):1509-1517.